

Drivers of plant nutrient acquisition and allocation strategies and their influence
on plant responses to environmental change

by

Evan A. Perkowski, B.S.

A Dissertation

In

Biological Sciences

Submitted to the Graduate Faculty
of Texas Tech University in
Partial Fulfillment of
the Requirements for
the Degree of

Doctor of Philosophy

Approved

Dr. Nicholas G. Smith
Chair of Committee

Dr. Aimée T. Classen

Dr. Natasja van Gestel

Dr. Lindsey C. Slaughter

Dr. Dylan W. Schwilk

Dr. Mark Sheridan
Dean of the Graduate School

May 2023

Copyright 2023, Evan A. Perkowski

Acknowledgements

Placeholder for text

Table of Contents

Acknowledgements	ii
Abstract	vii
List of Tables	viii
List of Figures	x
1. Introduction	1
2. Structural carbon costs to acquire nitrogen are determined by nitrogen and light availability in two species with different nitrogen acquisition strategies	3
2.1 Introduction	3
2.2 Methods	7
2.2.1 <i>Experiment setup</i>	7
2.2.2 <i>Plant measurements and calculations</i>	8
2.2.3 <i>Statistical analyses</i>	9
2.3 Results	11
2.3.1 <i>Carbon costs to acquire nitrogen</i>	11
2.3.2 <i>Whole plant nitrogen biomass</i>	14
2.3.3 <i>Root carbon biomass</i>	16
2.3.4 <i>Root nodule biomass</i>	18
2.4 Discussion	22
3. Soil nitrogen availability modifies leaf nitrogen economies in mature temperate deciduous forests: a direct test of photosynthetic least-cost theory	30
3.1 Introduction	30
3.2 Methods	34
3.2.1 <i>Study site description</i>	34
3.2.2 <i>Experimental design</i>	35
3.2.3 <i>Leaf gas exchange and trait measurements</i>	35
3.2.4 <i>A_{net}/C_i curve-fitting and parameter estimation</i>	38

3.2.5 <i>Proportion of leaf nitrogen allocated to photosynthesis and structure</i>	40
3.2.6 <i>Tradeoffs between nitrogen and water use</i>	41
3.2.7 <i>Soil nitrogen availability and pH</i>	42
3.2.8 <i>Statistical analyses</i>	44
3.3 Results	46
3.3.1 <i>Leaf N content</i>	46
3.3.2 <i>Net photosynthesis and leaf biochemistry</i>	49
3.3.3 <i>Leaf N allocation</i>	52
3.3.4 <i>Tradeoffs between nitrogen and water use</i>	55
3.4 Discussion	58
3.4.1 <i>Soil nitrogen availability modifies tradeoffs between nitrogen and water use</i>	59
3.4.2 <i>Soil pH did not modify tradeoffs between nitrogen and water usage</i>	61
3.4.3 <i>Species identity explains a large amount of variation in leaf and whole plant traits</i>	62
3.4.4 <i>Implications for photosynthetic least-cost theory model development</i>	63
3.4.5 <i>Conclusions</i>	65
4. The relative cost of resource use for photosynthesis drives variance in leaf nitrogen content across climate and soil resource availability gradients	66
4.1 Introduction	66
4.2 Methods	68
4.2.1 <i>Site descriptions and sampling methodology</i>	68
4.2.2 <i>Leaf trait measurements</i>	68
4.2.3 <i>Site climate data</i>	74
4.2.4 <i>Site edaphic characteristics</i>	74
4.2.5 <i>Plant functional group assignments</i>	76
4.2.6 <i>Data analysis</i>	77

4.3 Results	79
4.3.1 Cost to acquire nitrogen relative to water (β)	79
4.3.2 Leaf $C_i:C_a$	83
4.3.3 Leaf nitrogen content	86
4.3.4 Structural equation model	90
4.4 Discussion	93
5. Optimal resource investment to photosynthetic capacity maximizes nutrient allocation to whole plant growth under elevated CO₂	94
5.1 Introduction	94
5.2 Methods	99
5.2.1 Seed treatments and experimental design	99
5.2.2 Growth chamber conditions	100
5.2.3 Leaf gas exchange measurements	102
5.2.4 Leaf trait measurements	103
5.2.5 A/C_i curve fitting and parameter estimation	105
5.2.6 Stomatal limitation	105
5.2.7 Proportion of leaf nitrogen allocated to photosynthesis and structure	106
5.2.8 Whole plant traits	108
5.2.9 Statistical analyses	110
5.3 Results	112
5.3.1 Leaf nitrogen content, chlorophyll content, and mass per area	112
5.3.2 Leaf biochemistry and stomatal conductance	116
5.3.3 Leaf nitrogen allocation	120
5.3.4 Whole plant growth and total leaf area	124
5.3.5 Carbon costs to acquire nitrogen	124
5.3.6 Nitrogen fixation	128
5.4 Discussion	132

6. Conclusions	134
References	135

Abstract

List of Tables

2.1 Analysis of variance results exploring species-specific effects of light availability, nitrogen fertilization, and their interactions on carbon costs to acquire nitrogen, whole-plant nitrogen biomass, and root carbon biomass	12
2.2 Analysis of variance results exploring effects of light availability, nitrogen fertilization, and their interactions on <i>G. max</i> root nodule biomass and the ratio of root nodule biomass to root biomass*	19
2.3 Slopes of the regression line describing the relationship between each dependent variable and nitrogen fertilization at each light level*	20
3.1 Effects of soil N availability, soil pH, and species on leaf N content per unit leaf area (N_{area}), leaf N content per unit leaf mass (N_{mass}), and leaf mass per unit leaf area (M_{area})	47
3.2 Effects of soil N availability, soil pH, species, and N_{area} on leaf biochemistry	50
3.3 Effects of soil N availability, soil pH, and species on the proportion of leaf nitrogen content allocated to photosynthesis, Rubisco, bioenergetics, and structure	53
3.4 Effects of soil N availability, soil pH, species, and N_{area} on tradeoffs between nitrogen and water use	56

5.1 Effects of soil nitrogen fertilization, inoculation, and CO ₂ treatments on N_{area} , N_{mass} , M_{area} , and Chl_{area}	114
5.2 Effects of soil nitrogen fertilization, inoculation, and CO ₂ on leaf biochemistry	118
5.3 Effects of soil N availability, soil pH, species, and N_{area} on leaf nitrogen allocation	122
5.4 Effects of soil N availability, soil pH, species, and N_{area} on total leaf area, whole plant biomass, and costs of nitrogen acquisition	126
5.5 Effects of soil N availability, soil pH, species, and N_{area} on leaf biochemistry	130

List of Figures

2.1 Relationships between soil nitrogen fertilization and light availability on carbon costs to acquire nitrogen in <i>G. hirsutum</i> and <i>G. max</i>	13
2.2 Relationships between soil nitrogen fertilization and light availability on whole-plant nitrogen biomass in <i>G. hirsutum</i> and <i>G. max</i>	15
2.3 Relationships between soil nitrogen fertilization and light availability on root carbon biomass in <i>G. hirsutum</i> and <i>G. max</i>	17
2.4 Effects of shade cover and nitrogen fertilization on root nodule biomass and the ratio of root nodule biomass to root biomass in <i>G. max</i>	21
3.1 Effects of soil N availability and species on leaf N content per unit leaf area, leaf nitrogen content per unit leaf biomass, and leaf mass per leaf area	48
3.2 Effects of soil N availability, species, and leaf N content leaf biochemistry	51
3.3 Effects of soil N availability, species, and leaf N content on the fraction of leaf nitrogen allocated to photosynthesis and structure	54
3.4 Effects of soil N availability, species, and leaf N content on tradeoffs between nitrogen and water use	57

4.1	Maps that detail site locations along 2006-2020 mean annual precipitation (panel A) and mean annual temperature (panel B) gradients in Texas, USA.	73
4.2	Effects of soil nitrogen availability and soil moisture on the unit cost ratio β	82
4.3	Effects of 4-day mean vapor pressure deficit, 2-day soil moisture (per water holding capacity), and soil nitrogen availability on χ	85
4.4	Effects of χ , soil nitrogen availability, and soil moisture on leaf nitrogen content per unit leaf area, leaf nitrogen content per unit leaf biomass, and leaf mass per area.	89
4.5	Structural equation model results exploring direct and indirect drivers of N_{area}	92
5.1	Effects of CO_2 , fertilization, and inoculation on leaf nitrogen per unit leaf area, leaf nitrogen content, leaf mass per unit leaf area, and chlorophyll content per unit leaf area.	115
5.2	Effects of CO_2 , fertilization, and inoculation on maximum rate of Rubisco carboxylation, the maximum rate of RuBP regeneration, and the ratio of the maximum rate of RuBP regeneration to the maximum rate of Rubisco carboxylation leaf mass per unit leaf area, dark respiration, stomatal conductance, and stomatal limitation. . .	119
5.3	Effects of CO_2 , fertilization, and inoculation on the relative fraction of leaf nitrogen allocated to photosynthesis and the fraction of leaf nitrogen allocated to structure.	123

5.4 Effects of CO ₂ , fertilization, and inoculation on total leaf area, total biomass, and structural carbon costs to acquire nitrogen.	127
5.5 Effects of CO ₂ , fertilization, and inoculation on nodule biomass, nodule: root biomass, and percent nitrogen fixed from the atmosphere.	131

1 Chapter 1

2 Introduction

Terrestrial ecosystems are regulated by complex carbon and nutrient cycles. As a result, terrestrial biosphere models, which are beginning to include linked carbon and nutrient cycles (Shi et al. 2016; Davies-Barnard et al. 2020; Braghieri et al. 2022), must accurately represent these cycles under different environmental scenarios to reliably simulate carbon and nitrogen fluxes between the atmosphere and terrestrial biosphere fluxes (Oreskes et al. 1994; Hungate et al. 2003; Prentice et al. 2015). While the inclusion of coupled carbon and nitrogen cycles tends to reduce model uncertainty (Arora et al. 2020), carbon and nutrient flux simulations across terrestrial biosphere models tends to diverge under future environmental scenarios (Friedlingstein et al. 2014; Meyerholt et al. 2020). The widespread divergence of terrestrial biosphere model simulations may be driven by uncertainty in the response of photosynthetic processes across resource availability gradients and in response to environmental change. This is because photosynthesis is the largest carbon flux between the atmosphere and terrestrial biosphere, and is constrained by ecosystem carbon and nutrient cycles (Hungate et al. 2003; IPCC 2021; LeBauer and Treseder 2008; Fay et al. 2015). Yet, open questions remain regarding the influence of soil resource availability and climate on plant nutrient acquisition, plant nutrient allocation, photosynthetic processes, and whole plant growth.

22 Here, I conduct a nitrogen-by-light manipulative greenhouse experiment, a
23 nitrogen-by-sulfur manipulative field experiment, a soil resource availability and

24 climate environmental gradient field experiment, and a CO₂-by-inoculation-by-
25 nitrogen manipulative growth chamber experiment to test underlying assumptions
26 of photosynthetic least-cost theory. Specifically, these experiments

27 test effects of soil resource availability and aboveground climate on plant
28 nutrient acquisition, plant nutrient allocation, photosynthetic processes, and whole
29 plant growth

30 In this dissertation, I test underlying assumptions of photosynthetic least-
31 cost theory. Using a greenhouse nitrogen-by-light manipulation experiment, I
32 show that

33 conducted a series of experiments to quantify effects of aboveground cli-
34 mate and soil resource availability on nutrient acquisition and alloc

35 Here, I propose a series of experiments to quantify nutrient acquisition
36 and allocaton responses to resource availability gradients dissertation designed to
37 quantify nutrient acquisition and allocation responses to varying environmental
38 conditions and resource availability gradients through the lens of the least-cost
39 theory. Specifically, I will address five main questions:

40

Chapter 2

41

Structural carbon costs to acquire nitrogen are determined by
42 nitrogen and light availability in two species with different nitrogen
43 acquisition strategies

44 2.1 Introduction

45 Carbon and nitrogen cycles are tightly coupled in terrestrial ecosystems.
46 This tight coupling influences photosynthesis (Walker et al. 2014; Rogers et al.
47 2017), net primary productivity (LeBauer and Treseder 2008; Thomas et al. 2013),
48 decomposition (Cornwell et al. 2008; Bonan et al. 2013; Sulman et al. 2019), and
49 plant resource competition (Gill and Finzi 2016; Xu-Ri and Prentice 2017). Ter-
50 restrial biosphere models are beginning to include connected carbon and nitrogen
51 cycles to improve the realism of their simulations (Fisher et al. 2010; Brzostek
52 et al. 2014; Wieder et al. 2015; Shi et al. 2016; Zhu et al. 2019). Simula-
53 tions from these models indicate that coupling carbon and nitrogen cycles can
54 drastically influence future biosphere-atmosphere feedbacks under global change,
55 such as elevated carbon dioxide or nitrogen deposition (Thornton et al. 2007;
56 Goll et al. 2012; Wieder et al. 2015; Wieder et al. 2019). Nonetheless, there
57 are still limitations in our quantitative understanding of connected carbon and
58 nitrogen dynamics (Thomas et al. 2015; Meyerholt et al. 2016; Rogers et al.
59 2017; Exbrayat et al. 2018; Shi et al. 2019), forcing models to make potentially
60 unreliable assumptions.

61

Plant nitrogen acquisition is a process in terrestrial ecosystems by which
62 carbon and nitrogen are tightly coupled (Vitousek and Howarth 1991; Delaire
63 et al. 2005; Brzostek et al. 2014). Plants must allocate photosynthetically de-

64 rived carbon belowground to produce and maintain root systems or exchange with
65 symbiotic soil microbes in order to acquire nitrogen (Högberg et al. 2008; Hög-
66 berg et al. 2010). Thus, plants have an inherent carbon cost associated with
67 acquiring nitrogen, which can include both direct energetic costs associated with
68 nitrogen acquisition and indirect costs associated with building structures that
69 support nitrogen acquisition (Gutschick 1981; Rastetter et al. 2001; Vitousek
70 et al. 2002; Menge et al. 2008). Model simulations (Fisher et al. 2010; Brzostek
71 et al. 2014; Shi et al. 2016; Allen et al. 2020) and meta-analyses (Terrer et al.
72 2018) suggest that these carbon costs vary between species, particularly those
73 with different nitrogen acquisition strategies. For example, simulations using iter-
74 ations of the Fixation and Uptake of Nitrogen (FUN) model indicate that species
75 that acquire nitrogen from non-symbiotic active uptake pathways (e.g. mass flow)
76 generally have larger carbon costs to acquire nitrogen than species that acquire
77 nitrogen through symbiotic associations with nitrogen-fixing bacteria (Brzostek
78 et al. 2014; Allen et al. 2020).

79 Carbon costs to acquire nitrogen likely vary in response to changes in soil
80 nitrogen availability. For example, if the primary mode of nitrogen acquisition
81 is through non-symbiotic active uptake, then nitrogen availability could decrease
82 carbon costs to acquire nitrogen as a result of increased per-root nitrogen up-
83 take (Franklin et al. 2009; Wang et al. 2018). However, if the primary mode of
84 nitrogen acquisition is through symbiotic active uptake, then nitrogen availabil-
85 ity may incur additional carbon costs to acquire nitrogen if it causes microbial
86 symbionts to shift toward parasitism along the parasitism–mutualism continuum
87 (Johnson et al. 1997; Hoek et al. 2016; Friel and Friesen 2019) or if it reduces

88 the nitrogen acquisition capacity of a microbial symbiont (van Diepen et al. 2007;
89 Soudzilovskaia et al. 2015; Muñoz et al. 2016). Species may respond to shifts in
90 soil nitrogen availability by switching their primary mode of nitrogen acquisition
91 to a strategy with lower carbon costs to acquire nitrogen in order to maximize
92 the magnitude of nitrogen acquired from a belowground carbon investment and
93 outcompete other individuals for soil resources (Rastetter et al. 2001; Menge et al.
94 2008).

95 Environmental conditions that affect demand to acquire nitrogen to sup-
96 port new and existing tissues could also be a source of variance in plant carbon
97 costs to acquire nitrogen. For example, an increase in plant nitrogen demand could
98 increase carbon costs to acquire nitrogen if this increases the carbon that must be
99 allocated belowground to acquire a proportional amount of nitrogen (Kulmatiski
100 et al. 2017; Noyce et al. 2019). This could be driven by a temporary state of
101 diminishing return associated with investing carbon toward building and main-
102 taining structures that are necessary to support enhanced nitrogen uptake, such
103 as fine roots (Matamala and Schlesinger 2000; Norby et al. 2004; Arndal et al.
104 2018), mycorrhizal hyphae (Saleh et al. 2020), or root nodules (Parvin et al. 2020).
105 Alternatively, if the environmental factor that increases plant nitrogen demand
106 causes nitrogen to become more limiting in the system (e.g. atmospheric CO₂;
107 Luo et al. (2004), LeBauer and Treseder (2008), Vitousek et al. (2010), Liang
108 et al. (2016)), species might switch their primary mode of nitrogen acquisition to
109 a strategy with lower relative carbon costs to acquire nitrogen in order to gain a
110 competitive advantage over species with either different or more limited modes of
111 nitrogen acquisition (Ainsworth and Long 2005; Taylor and Menge 2018).

112 Using a plant economics approach, we examined the influence of plant
113 nitrogen demand and soil nitrogen availability on plant carbon costs to acquire
114 nitrogen. This was done by growing a species capable of forming associations
115 with nitrogen-fixing bacteria (*Glycine max* L. (Merr)) and a species not capable
116 of forming these associations (*Gossypium hirsutum* L.) under four levels of light
117 availability (plant nitrogen demand proxy) and four levels of soil nitrogen fertil-
118 ization (soil nitrogen availability proxy) in a full-factorial, controlled greenhouse
119 experiment. We used this experimental set-up to test the following hypotheses:

- 120 1. An increase in plant nitrogen demand due to increasing light availability will
121 increase carbon costs to acquire nitrogen through a proportionally larger
122 increase in belowground carbon than whole-plant nitrogen acquisition. This
123 will be the result of an increased investment of carbon toward belowground
124 structures that support enhanced nitrogen uptake, but at a lower nitrogen
125 return.
- 126 2. An increase in soil nitrogen availability will decrease carbon costs to acquire
127 nitrogen as a result of increased per root nitrogen uptake in *G. hirsutum*.
128 However, soil nitrogen availability will not affect carbon costs to acquire
129 nitrogen in *G. max* because of the already high return of nitrogen supplied
130 through nitrogen fixation.

131 2.2 Methods

132 2.2.1 *Experiment setup*

133 *Gossypium hirsutum* and *G. max* were planted in individual 3 liter pots
134 (NS-300; Nursery Supplies, Orange, CA, USA) containing a 3:1 mix of unfertil-
135 ized potting mix (Sungro Sunshine Mix #2, Agawam, MA, USA) to native soil
136 extracted from an agricultural field most recently planted with *G. max* at the
137 USDA-ARS Laboratory in Lubbock, TX, USA (33.59°N, -101.90°W). The field
138 soil was classified as Amarillo fine sandy loam (75% sand, 10% silt, 15% clay).
139 Upon planting, all *G. max* pots were inoculated with *Bradyrhizobium japonicum*
140 (Verdesian N-Dure™ Soybean, Cary, NC, USA) to stimulate root nodulation. In-
141 dividuals of both species were grown under similar, unshaded, ambient greenhouse
142 conditions for 2 weeks to germinate and begin vegetative growth. Three blocks
143 were set up in the greenhouse, each containing four light treatments created us-
144 ing shade cloth that reduced incoming radiation by either 0 (full sun), 30, 50,
145 or 80%. Two weeks post-germination, individuals were randomly placed in the
146 four light treatments in each block. Individuals received one of four nitrogen fer-
147 tilization doses as 100ml of a modified Hoagland solution (Hoagland and Arnon
148 1950) equivalent to either 0, 70, 210, or 630 ppm N twice per week within each
149 light treatment. Nitrogen fertilization doses were received as topical agents to
150 the soil surface. Each Hoagland solution was modified to keep concentrations of
151 other macro- and micronutrients equivalent (Supplementary Table S1). Plants
152 were routinely well watered to eliminate water stress.

153 2.2.2 *Plant measurements and calculations*

154 Each individual was harvested after 5 weeks of treatment, and biomass
155 was separated by organ type (leaves, stems, and roots). Nodules on *G. max*
156 roots were also harvested. With the exception of the 0% shade cover and 630
157 ppm N treatment combination, all treatment combinations in both species had
158 lower average dry biomass:pot volume ratios than the 1:1 ratio recommended by
159 Poorter et al. (2012) to minimize the likelihood of pot volume-induced growth
160 limitation (Supplementary Tables S2, S3; Supplementary Fig. S1). All harvested
161 material was dried, weighed, and ground by organ type. Carbon and nitrogen
162 content (g g^{-1}) was determined by subsampling from ground and homogenized
163 biomass of each organ type using an elemental analyzer (Costech 4010; Costech,
164 Inc., Valencia, CA, USA). We scaled these values to total leaf, stem, and root
165 carbon and nitrogen biomass (g) by multiplying dry biomass of each organ type
166 by carbon or nitrogen content of each corresponding organ type. Whole-plant
167 nitrogen biomass (g) was calculated as the sum of total leaf (g), stem (g), and
168 root (g) nitrogen biomass. Root nodule carbon biomass was not included in the
169 calculation of root carbon biomass; however, relative plant investment toward root
170 or root nodule standing stock was estimated as the ratio of root biomass to root
171 nodule biomass (g g^{-1}), following similar metrics to those adopted by Dovrat et al.
172 (2018) and Dovrat et al. (2020).

173 Carbon costs to acquire nitrogen (gC gN^{-1}) were estimated as the ratio of
174 total root carbon biomass (gC) to whole-plant nitrogen biomass (gN). This cal-
175 culation quantifies the relationship between carbon spent on nitrogen acquisition
176 and whole-plant nitrogen acquisition by using root carbon biomass as a proxy for

177 estimating the magnitude of carbon allocated toward nitrogen acquisition. This
178 calculation therefore assumes that the magnitude of root carbon standing stock is
179 proportional to carbon transferred to root nodules or mycorrhizae, or lost through
180 root exudation or turnover. This assumption has been supported in species that
181 associate with ectomycorrhizal fungi (Hobbie 2006; Hobbie and Hobbie 2008), but
182 is less clear in species that acquire nitrogen through non-symbiotic active uptake
183 or symbiotic nitrogen fixation. It is also unclear whether relationships between
184 root carbon standing stock and carbon transfer to root nodules are similar in mag-
185 nitude to carbon lost through exudation or when allocated toward other active
186 uptake pathways. Thus, because of the way we performed our measurements, our
187 proximal values of carbon costs to acquire nitrogen are underestimates.

188 2.2.3 *Statistical analyses*

189 We explored the effects of light and nitrogen availability on carbon costs to
190 acquire nitrogen using separate linear mixed-effects models for each species. Mod-
191 els included shade cover, nitrogen fertilization, and interactions between shade
192 cover and nitrogen fertilization as continuous fixed effects, and also included block
193 as a random intercept term. Three separate models for each species were built
194 with this independent variable structure for three different dependent variables: (i)
195 carbon costs to acquire nitrogen (gC gN^{-1}); (ii) whole-plant nitrogen biomass (de-
196 nominator of carbon cost to acquire nitrogen; gN); and (iii) root carbon biomass
197 (numerator of carbon cost to acquire nitrogen; gC). We constructed two additional
198 models for *G. max* with the same model structure described above to investigate
199 the effects of light availability and nitrogen fertilization on root nodule biomass

200 (g) and the ratio of root nodule biomass to root biomass (unitless).

201 We used Shapiro–Wilk tests of normality to determine whether species-
202 specifc linear mixed-effects model residuals followed a normal distribution. None
203 of our models satisfied residual normality assumptions when models were fit using
204 untransformed data (Shapiro–Wilk: $P<0.05$ in all cases). We attempted to satisfy
205 residual normality assumptions by first fitting models using dependent variables
206 that were natural-log transformed. If residual normality assumptions were still
207 not met (Shapiro–Wilk: $P<0.05$), then models were fit using dependent variables
208 that were square root transformed. All residual normality assumptions were satis-
209 fied when models were fit with either a natural-log or square root transformation
210 (Shapiro–Wilk: $P>0.05$ in all cases). Specifically, we natural-log transformed *G.*
211 *hirsutum* carbon costs to acquire nitrogen and *G. hirsutum* whole-plant nitrogen
212 biomass. We also square root transformed *G. max* carbon costs to acquire nitro-
213 gen, *G. max* whole-plant nitrogen biomass, root carbon biomass in both species,
214 *G. max* root nodule biomass, and the *G. max* ratio of root nodule biomass to root
215 biomass. We used the ‘lmer’ function in the ‘lme4’ R package (Bates et al. 2015)
216 to fit each model and the ‘Anova’ function in the ‘car’ R package (Fox and Weis-
217 berg 2019) to calculate Wald’s χ^2 to determine the significance ($\alpha = 0.05$) of each
218 fixed effect coefficient. Finally, we used the ‘emmeans’ R package (Lenth 2019)
219 to conduct post-hoc comparisons of our treatment combinations using Tukey’s
220 tests. Degrees of freedom for all Tukey’s tests were approximated using the Ken-
221 ward–Roger approach (Kenward and Roger 1997). All analyses and plots were
222 conducted in R version 4.0.1 (R Core Team 2021).

223 2.3 Results

224 2.3.1 *Carbon costs to acquire nitrogen*

225 Carbon costs to acquire nitrogen in *G. hirsutum* increased with increasing
226 light availability ($p < 0.001$; Table 2.1; Fig. 2.1) and decreased with increasing
227 nitrogen fertilization ($p < 0.001$; Table 2.1; Fig. 2.1). There was no interaction
228 between light availability and nitrogen fertilization ($p = 0.486$, Table 2.1; Fig.
229 2.1).

230 Carbon costs to acquire nitrogen in *G. max* also increased with increasing
231 light availability ($p < 0.001$, Table 2.1; Fig. 2.1) and decreased with increasing
232 nitrogen fertilization ($p < 0.001$; Table 2.1; Fig. 2.1). There was no interaction
233 between light availability and nitrogen fertilization ($p = 0.261$, Table 2.1; Fig.
234 2.1).

Table 2.1. Analysis of variance results exploring species-specific effects of light availability, nitrogen fertilization, and their interactions on carbon costs to acquire nitrogen, whole-plant nitrogen biomass, and root carbon biomass

	Carbon costs to acquire nitrogen			Whole-plant nitrogen biomass			Root carbon biomass			
	df	Coefficient	χ^2	p	Coefficient	χ^2	p	Coefficient	χ^2	p
<i>G. hirsutum</i>										
Intercept		1.594	-	-	-3.232	-	-	0.432	-	-
Light (L)	1	-1.09E-02	56.494	<0.001	-6.41E-03	91.275	<0.001	-2.62E-03	169.608	<0.001
Nitrogen (N)	1	-1.34E-03	54.925	<0.001	1.83E-03	118.784	<0.001	1.15E-04	2.901	0.089
L*N	1	3.88E-06	0.485	0.486	-1.34E-05	10.721	0.001	-1.67E-06	3.140	0.076
<i>G. max</i>										
Intercept		1.877	-	-	0.239	-	-	0.438	-	-
Light (L)	1	-7.67E-03	174.156	<0.001	-6.72E-04	39.799	<0.001	-2.55E-03	194.548	<0.001
Nitrogen (N)	1	-2.35E-04	21.948	<0.001	1.55E-04	70.771	<0.001	2.52E-04	19.458	<0.001
L*N	1	-2.89E-06	1.262	0.261	-6.32E-07	1.435	0.231	-3.16E-06	10.803	0.001

*Significance determined using Wald's χ^2 tests ($P=0.05$). P -values<0.05 are in bold and p -values between 0.05 and 0.1 are italicized. Negative coefficients for light treatments indicate a positive effect of increasing light availability on all response variables, as light availability is treated as percent shade cover in all linear mixed-effects models.

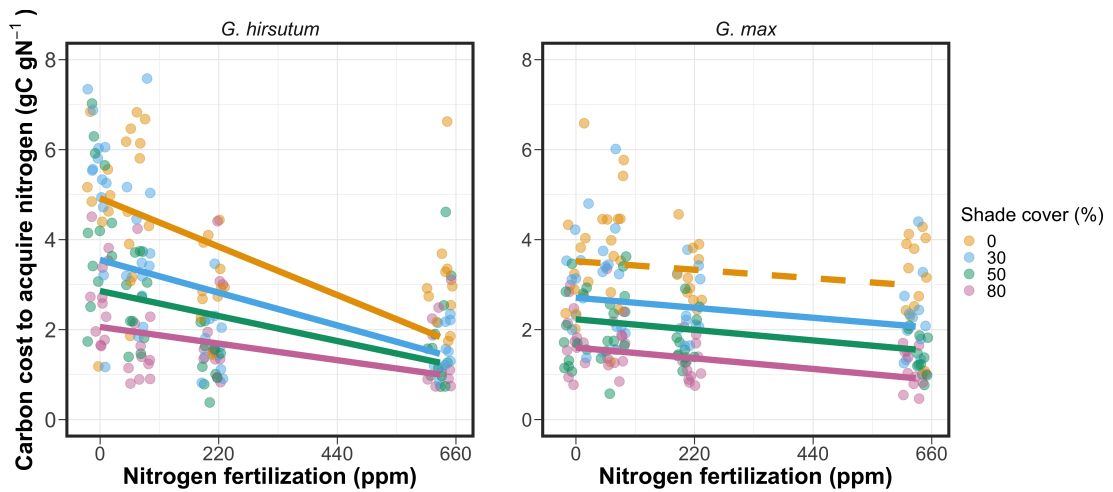


Figure 2.1. Relationships between soil nutrient fertilization and light availability on carbon costs to acquire nitrogen in *G. hirsutum* and *G. max*. Nitrogen fertilization treatments are represented on the x-axis. Shade cover treatments are represented through colored points and trendlines. Trendlines were created by back-transforming marginal mean slopes and intercepts from species-specific linear mixed-effects models. These values were calculated using the ‘emtrends’ and ‘emmeans’ functions in the ‘emmeans’ R package (Lenth, 2019). Points are jittered for visibility. Yellow points and trendlines represent the 0% shade cover treatment, blue points and trendlines represent the 30% shade cover treatment, green points and trendlines represent the 50% shade cover treatment, and purple points and trendlines represent the 80% shade cover treatment. Solid trendlines indicate slopes that are significantly different from zero (Tukey: $p < 0.05$), while dashed trendlines indicate slopes that are not statistically different from zero.

235 2.3.2 *Whole plant nitrogen biomass*

236 Whole-plant nitrogen biomass in *G. hirsutum* was driven by an interaction
237 between light availability and nitrogen fertilization ($p = 0.001$; Table 2.1; Fig.
238 2.2). This interaction indicated a greater stimulation of whole-plant nitrogen
239 biomass by nitrogen fertilization as light levels increased (Table 2.1; Fig. 2.2).

240 Whole-plant nitrogen biomass in *G. max* increased with increasing light
241 availability ($p < 0.001$) and nitrogen fertilization ($p < 0.001$), with no interaction
242 between light availability and nitrogen fertilization ($p = 0.231$; Table 2.1; Fig.
243 2.2).

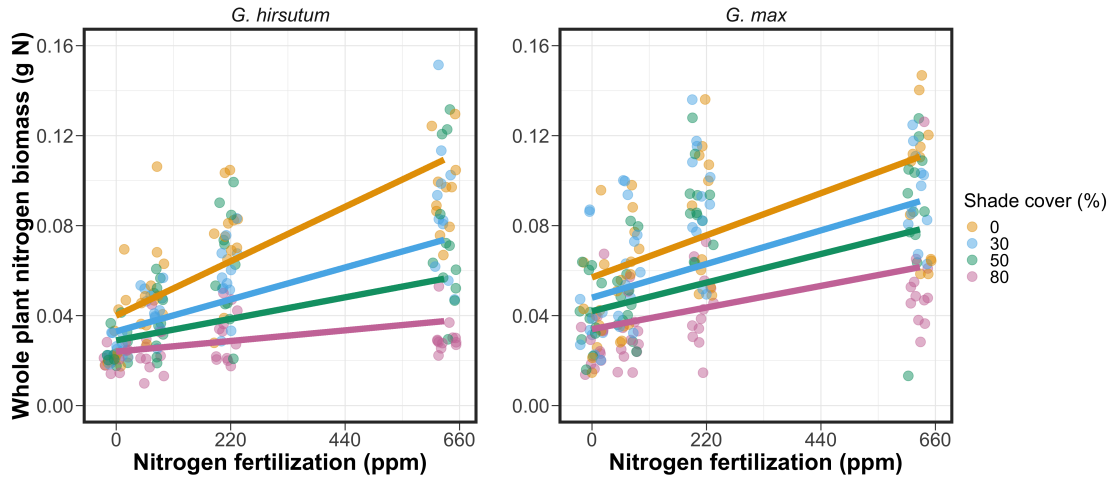


Figure 2.2. Relationships between soil nutrient fertilization and light availability on whole-plant nitrogen biomass in *G. hirsutum* and *G. max*. Whole-plant nitrogen biomass is the denominator of the carbon cost to acquire nitrogen calculation. Nitrogen fertilization treatments are represented on the x-axis. Shade cover treatments are represented through colored points and trendlines. Trendlines were created by back-transforming marginal mean slopes and intercepts from species-specific linear mixed-effects models. These values were calculated using the ‘emtrends’ and ‘emmmeans’ functions in the ‘emmeans’ R package (Lenth 2019). Points are jittered for visibility. Yellow points and trendlines represent the 0% shade cover treatment, blue points and trendlines represent the 30% shade cover treatment, green points and trendlines represent the 50% shade cover treatment, and purple points and trendlines represent the 80% shade cover treatment. Solid trendlines indicate slopes that are significantly different from zero (Tukey: $P < 0.05$), while dashed trendlines indicate slopes that are not statistically different from zero.

244 2.3.3 *Root carbon biomass*

245 Root carbon biomass in *G. hirsutum* significantly increased with increasing
246 light availability ($p < 0.001$; Table 2.1; Fig. 2.3) and marginally increased with
247 nitrogen fertilization ($p = 0.089$; Table 2.1; Fig. 2.3). There was also a marginal
248 interaction between light availability and nitrogen fertilization ($p = 0.076$; Table
249 2.1), driven by an increase in the positive response of root carbon biomass to
250 increasing nitrogen fertilization as light availability increased. This resulted in
251 significantly positive trends between root carbon biomass and nitrogen fertilization
252 in the two highest light treatments (Tukey: $p < 0.05$ in both cases; Table 2.3;
253 Fig. 2.3) and no effect of nitrogen fertilization in the two lowest light treatments
254 (Tukey: $p > 0.05$ in both cases; Table 2.3; Fig. 2.3).

255 There was an interaction between light availability and nitrogen fertiliza-
256 tion on root carbon biomass in *G. max* ($p = 0.001$; Table 2.1; Fig. 2.3). Post-hoc
257 analyses indicated that the positive effects of nitrogen fertilization on *G. max* root
258 carbon biomass increased with increasing light availability (Table 2.3; Fig. 2.3).
259 There were also positive individual effects of increasing nitrogen fertilization ($p <$
260 0.001) and light availability ($p < 0.001$) on *G. max* root carbon biomass (Table
261 2.1; Fig. 2.3).

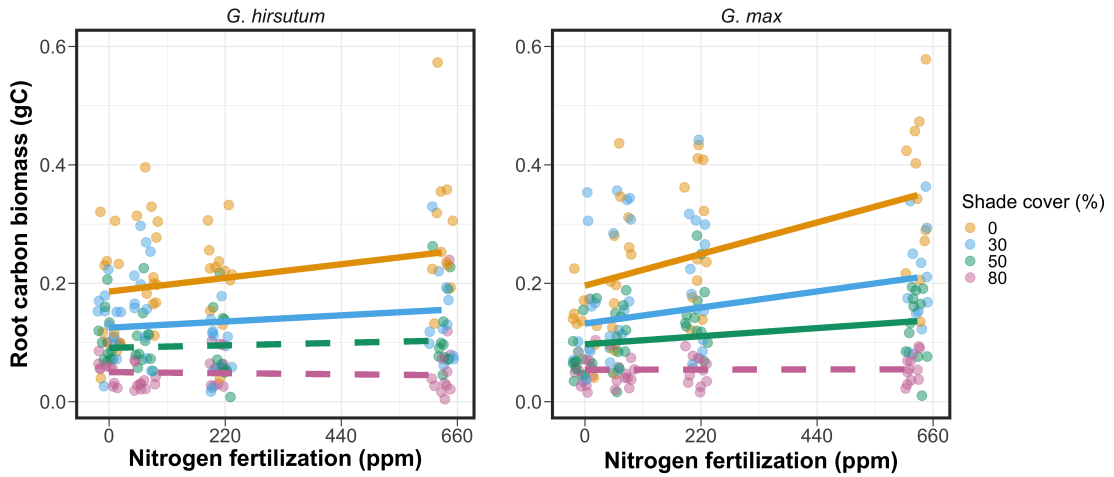


Figure 2.3. Relationships between soil nutrient fertilization and light availability on root carbon biomass in *G. hirsutum* and *G. max*. Root carbon biomass is the numerator of the carbon cost to acquire nitrogen calculation. Nitrogen fertilization treatments are represented on the x-axis. Shade cover treatments are represented through colored points and trendlines. Trendlines were created by back-transforming marginal mean slopes and intercepts from species-specific linear mixed-effects models. These values were calculated using the ‘emtrends’ and ‘emmmeans’ functions in the ‘emmeans’ R package (Lenth 2019). Points are jittered for visibility. Yellow points and trendlines represent the 0% shade cover treatment, blue points and trendlines represent the 30% shade cover treatment, green points and trendlines represent the 50% shade cover treatment, and purple points and trendlines represent the 80% shade cover treatment. Solid trendlines indicate slopes that are significantly different from zero (Tukey: $p < 0.05$), while dashed trendlines indicate slopes that are not statistically different from zero.

262 2.3.4 *Root nodule biomass*

263 Root nodule biomass in *G. max* increased with increasing light availability
264 ($p < 0.001$; Table 2.2; Fig. 2.4A) and decreased with increasing nitrogen fertiliza-
265 tion ($p < 0.001$; Table 2.2; Fig. 2.4A). There was no interaction between nitrogen
266 fertilization and light availability ($p = 0.133$; Table 2.2; Fig. 2.4A). The ratio of
267 root nodule biomass to root biomass did not change in response to light avail-
268 ability ($p = 0.481$; Table 2.2; Fig. 2.4B) but decreased with increasing nitrogen
269 fertilization ($p < 0.001$; Table 2.2; Fig. 2.4B). There was no interaction between
270 nitrogen fertilization and light availability on the ratio of root nodule biomass to
271 root biomass ($p = 0.621$; Table 2.2; Fig. 2.4B).

Table 2.2. Analysis of variance results exploring effects of light availability, nitrogen fertilization, and their interactions on *G. max* root nodule biomass and the ratio of root nodule biomass to root biomass*

	Nodule biomass			Nodule biomass: root biomass			
	df	Coefficient	χ^2	p	coefficient	χ^2	p
(Intercept)		0.302	-	-	0.448	-	-
Light (L)	1	-1.81E-03	72.964	<0.001	-8.76E-05	0.496	0.481
Nitrogen (N)	1	-2.83E-04	115.377	<0.001	-5.09E-04	156.476	<0.001
L*N	1	1.14E-06	2.226	0.133	-7.30E-07	0.244	0.621

*Significance determined using Wald's χ^2 tests ($\alpha = 0.05$). *p*-values less than 0.05 are in bold. Negative coefficients for light treatments indicate a positive effect of increasing light availability on all response variables, as light availability is treated as percent shade cover in all linear mixed-effects models. Root nodule biomass and nodule biomass: root biomass models were only constructed for *G. max* because *G. hirsutum* was not inoculated with *B. japonicum* and is not capable of forming root nodules.

Table 2.3. Slopes of the regression line describing the relationship between each dependent variable and nitrogen fertilization at each light level*

Shade cover	Carbon cost to acquire nitrogen	Whole-plant nitrogen biomass	Root carbon biomass	Root nodule biomass	Nodule biomass root biomass
<i>G. hirsutum</i>					
0%	-1.34E-03^a	1.83E-03^a	1.15E-04^b	-	-
30%	-1.22E-03^a	1.43E-03^a	1.17E-04^b	-	-
50%	-1.14E-03^a	1.17E-03^a	3.12E-05 ^b	-	-
80%	-1.02E-03^a	7.66E-04^a	-1.89E-06 ^b	-	-
<i>G. max</i>					
0%	-2.35E-04 ^b	1.55E-05^b	2.51E-04^b	-2.83E-04^b	-5.09E-04^b
30%	-3.22E-04^b	1.35E-05^b	1.57E-04^b	-2.49E-04^b	-5.31E-04^b
50%	-3.80E-04^b	1.23E-05^b	9.37E-05^b	-2.26E-04^b	-5.45E-04^b
80%	-4.66E-04^b	1.04E-05^b	-9.95E-07 ^b	-1.92E-04^b	-5.67E-04^b

*Slopes represent estimated marginal mean slopes from linear mixed-effects models described in the Methods. Slopes were calculated using the ‘emmeans’ R package (Lenth 2019). Superscripts indicate slopes fit to natural-log (^a) or square root (^b) transformed data. Slopes statistically different from zero (Tukey: $p < 0.05$) are indicated in bold. Marginally significant slopes (Tukey: $0.05 < p < 0.1$) are italicized.

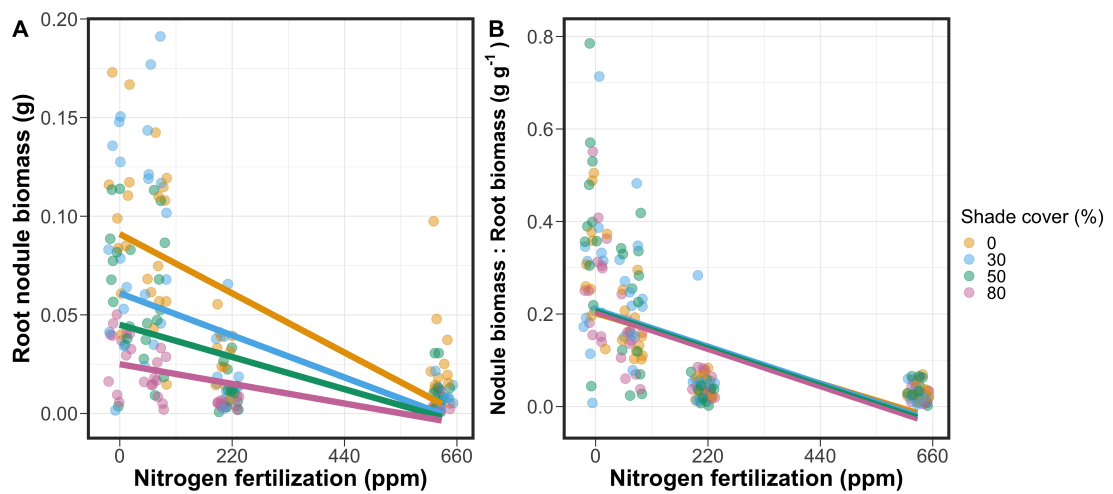


Figure 2.4. Effects of shade cover and nitrogen fertilization on root nodule biomass (A) and the ratio of root nodule biomass to root biomass (B) in *G. max*. Nitrogen fertilization treatments are represented on the x-axis. Shade cover treatments are represented through colored points and trendlines. Trendlines were created by back-transforming marginal mean slopes and intercepts from species-specific linear mixed-effects models. These values were calculated using the ‘emtrends’ and ‘emmeans’ functions in the ‘emmeans’ R package (Lenth 2019). Points are jittered for visibility. Yellow points and trendlines represent the 0% shade cover treatment, blue points and trendlines represent the 30% shade cover treatment, green points and trendlines represent the 50% shade cover treatment, and purple points and trendlines represent the 80% shade cover treatment. Solid trendlines indicate slopes that are significantly different from zero (Tukey: $p < 0.05$), while dashed trendlines indicate slopes that are not statistically different from zero.

272 2.4 Discussion

273 In this chapter, we determined the effects of light availability and soil ni-
274 trogen fertilization on root mass carbon costs to acquire nitrogen in *G. hirsutum*
275 and *G. max*. In support of our hypotheses, we found that carbon costs to acquire
276 nitrogen generally increased with increasing light availability and decreased with
277 increasing soil nitrogen fertilization in both species. These findings suggest that
278 carbon costs to acquire nitrogen are determined by factors that influence plant
279 nitrogen demand and soil nitrogen availability. In contrast to our second hypothe-
280 sis, root nodulation data suggested that *G. max* and *G. hirsutum* achieved similar
281 directional carbon cost responses to nitrogen fertilization despite a likely shift in
282 G.!max allocation from nodulation to root biomass along the nitrogen fertilization
283 gradient (Fig. 2.4B).

284 Both *G. max* and *G. hirsutum* experienced an increase in carbon costs to
285 acquire nitrogen due to increasing light availability. These patterns were driven by
286 a larger increase in root carbon biomass than whole-plant nitrogen biomass. In-
287 creases in root carbon biomass due to factors that increase plant nitrogen demand
288 are a commonly observed pattern, as carbon allocated belowground provides sub-
289 strate needed to produce and maintain structures that satisfy aboveground plant
290 nitrogen demand (Nadelhoffer and Raich 1992; Giardina et al. 2005; Raich et al.
291 2014). Our findings suggest that plants allocate relatively more carbon for acquir-
292 ing nitrogen when demand increases over short temporal scales, which may cause
293 a temporary state of diminishing return due to asynchrony between belowground
294 carbon and whole-plant nitrogen responses to plant nitrogen demand (Kulmatiski
295 et al. 2017; Noyce et al. 2019). These responses might be attributed to a temporal

296 lag associated with producing structures that enhance nitrogen acquisition. For
297 example, fine roots (Matamala and Schlesinger 2000; Norby et al. 2004; Arndal
298 et al. 2018) and root nodules (Parvin et al. 2020) take time to build and first
299 require the construction of coarse roots. Thus, full nitrogen returns from these
300 investments may not occur immediately (Kayler et al. 2010; Kayler et al. 2017),
301 and may vary by species acquisition strategy. We speculate that increases in ni-
302 trogen acquisition from a given carbon investment may occur beyond the 5 week
303 scope of this experiment. A similar study conducted over a longer temporal scale
304 would address this.

305 Increasing soil nitrogen fertilization generally decreased carbon costs to
306 acquire nitrogen in both species. These patterns were driven by a larger increase
307 in whole-plant nitrogen biomass than root carbon biomass. In *G. hirsutum*, re-
308 ductions in carbon costs to acquire nitrogen may have been due to an increase in
309 per-root nitrogen uptake, allowing individuals to maximize the amount of nitro-
310 gen acquired from a belowground carbon investment. Interestingly, increased soil
311 nitrogen fertilization increased whole-plant nitrogen biomass in *G. max* despite
312 reductions in root nodule biomass that likely reduced the nitrogen-fixing capac-
313 ity of *G. max* (Andersen et al. 2005; Muñoz et al. 2016). While reductions in
314 root nodulation due to increased soil nitrogen availability are commonly observed
315 (Gibson and Harper 1985; Fujikake et al. 2003), our responses were observed in
316 tandem with increased root carbon biomass, implying that *G. max* shifted relative
317 carbon allocation from nitrogen fixation to soil nitrogen acquisition (Markham and
318 Zekveld 2007; Dovrat et al. 2020). This was likely because there was a reduction in
319 the carbon cost advantage of acquiring fixed nitrogen relative to soil nitrogen, and

320 suggests that species capable of associating with symbiotic nitrogen-fixing bacte-
321 ria shift their relative nitrogen acquisition pathway to optimize nitrogen uptake
322 (Rastetter et al. 2001). Future studies should further investigate these patterns
323 with a larger quantity of phylogenetically related species, or different varieties
324 of a single species that differ in their ability to form associations with symbiotic
325 nitrogen-fixing bacteria to more directly test the impact of nitrogen fixation on
326 the patterns observed in this study.

327 Carbon costs to acquire nitrogen are subsumed in the general discussion of
328 economic analogies to plant resource uptake (Bloom et al. 1985; Rastetter et al.
329 2001; Vitousek et al. 2002; Phillips et al. 2013; Terrer et al. 2018; Henneron et al.
330 2020). Despite this, terrestrial biosphere models rarely include these carbon costs
331 within their framework for predicting plant nitrogen uptake. There is currently
332 one plant resource uptake model, FUN, that quantitatively predicts carbon costs
333 to acquire nitrogen within a framework for predicting plant nitrogen uptake for
334 different nitrogen acquisition strategies (Fisher et al. 2010; Brzostek et al. 2014)
335 (Fisher et al. 2010; Brzostek et al. 2014). Iterations of FUN are currently
336 coupled to two terrestrial biosphere models: the Community Land Model 5.0 and
337 the Joint UK Land Environment Simulator (Shi et al. 2016; Lawrence et al.
338 2019; Clark et al. 2011). Recent work suggests that coupling FUN to CLM 5.0
339 caused a large overprediction of plant nitrogen uptake associated with nitrogen
340 fixation (Davies-Barnard et al. 2020). Thus, empirical data from manipulative
341 experiments that explicitly quantify carbon costs to acquire nitrogen in species
342 capable of associating with nitrogen-fixing bacteria across different environmental
343 contexts is an important step toward identifying potential biases in models such

344 as FUN.

345 Our findings broadly support the FUN formulation of carbon costs to ac-
346 quire nitrogen in response to soil nitrogen availability. FUN calculates carbon
347 costs to acquire nitrogen based on the sum of carbon costs to acquire nitrogen
348 via nitrogen fixation, mycorrhizal active uptake, non-mycorrhizal active uptake,
349 and retranslocation (Fisher et al. 2010; Brzostek et al. 2014). Carbon costs to
350 acquire nitrogen via mycorrhizal or non-mycorrhizal active uptake pathways are
351 derived as a function of nitrogen availability, root biomass, and two parameterized
352 values based on nitrogen acquisition strategy (Brzostek et al. 2014). Due to this,
353 FUN simulates a net decrease in carbon costs to acquire nitrogen with increasing
354 nitrogen availability for mycorrhizal and non-mycorrhizal active uptake pathways,
355 assuming constant root biomass. This was a pattern we observed in *G. hirsutum*
356 regardless of light availability. In contrast, FUN would not simulate a net change
357 in carbon costs to acquire nitrogen via nitrogen fixation due to nitrogen avail-
358 ability. This is because carbon costs to acquire nitrogen via nitrogen fixation are
359 derived from a well-established function of soil temperature, which is independent
360 of soil nitrogen availability (Houlton et al. 2008; Fisher et al. 2010). We observed
361 a net reduction in carbon costs to acquire nitrogen in *G. max*, except when in-
362 dividuals were grown under 0% shade cover (Fig. 2.1). While a net reduction of
363 carbon costs in response to nitrogen fertilization runs counter to nitrogen fixa-
364 tion carbon costs simulated by FUN, these patterns were likely because *G. max*
365 individuals switched their primary mode of nitrogen acquisition from symbiotic
366 nitrogen fixation to a non-symbiotic active uptake pathway (Fig. 2.4B).

367 It should be noted that the metric used in this study to determine carbon

368 costs to acquire nitrogen has several limitations. Most notably, this metric uses
369 root carbon biomass as a proxy for estimating the amount of carbon spent on
370 nitrogen acquisition. While it is true that most carbon allocated belowground
371 has at least an indirect structural role in acquiring soil resources, it remains un-
372 clear whether this assumption holds true for species that acquire nitrogen via
373 symbiotic nitrogen fixation. We also cannot quantify carbon lost through root
374 exudates or root turnover, which may increase due to factors that increase plant
375 nitrogen demand (Tingey et al. 2000; Phillips et al. 2011), and can increase the
376 magnitude of available nitrogen from soil organic matter through priming effects
377 on soil microbial communities (Uselman et al. 2000; Bengtson et al. 2012). It is
378 also not clear whether these assumptions hold under all environmental conditions,
379 such as those that shift belowground carbon allocation toward a different mode of
380 nitrogen acquisition (Taylor and Menge 2018; Friel and Friesen 2019) or between
381 species with different acquisition strategies. In this study, increasing soil nitrogen
382 fertilization increased carbon investment to roots relative to carbon transferred
383 to root nodules (Fig. 2.4B). By assuming that carbon allocated to root carbon
384 was proportional to carbon allocated to root nodules across all treatment com-
385 binations, these observed responses to soil nitrogen fertilization were likely to be
386 overestimated in *G. max*. We encourage future research to quantify these carbon
387 fates independently.

388 Researchers conducting pot experiments must carefully choose pot volume
389 to minimize the likelihood of pot volume-induced growth limitation (Poorter et al.
390 2012). Poorter et al. (2012) indicate that researchers are likely to avoid growth
391 limitations associated with pot volume if measurements are collected when the

392 plant biomass:pot volume ratio is less than 1 g L^{-1} . In this experiment, all treat-
393 ment combinations in both species had biomass:pot volume ratios less than 1 g
394 L^{-1} except for *G. max* and *G. hirsutum* that were grown under 0% shade cover
395 and had received 630 ppm N. Specifically, *G. max* and *G. hirsutum* had average
396 respective biomass:pot volume ratios of $1.24 \pm 0.07 \text{ g L}^{-1}$ and $1.34 \pm 0.13 \text{ g L}^{-1}$, when
397 grown under 0% shade cover and received 630 ppm N (Supplementary Tables S2,
398 S3; Supplementary Fig. S1). If growth in this treatment combination was limited
399 by pot volume, then individuals may have had larger carbon costs to acquire ni-
400 trogen than would be expected if they were grown in larger pots. This pot volume
401 induced growth limitation could cause a reduction in per-root nitrogen uptake as-
402 sociated with more densely packed roots, which could reduce the positive effect
403 of nitrogen fertilization on whole-plant nitrogen biomass relative to root carbon
404 biomass (Poorter et al. 2012).

405 Growth limitation associated with pot volume provides a possible explana-
406 tion for the marginally insignificant effect of increasing nitrogen fertilization on *G.*
407 *max* carbon costs to acquire nitrogen when grown under 0% shade cover (Table
408 2.3; Fig. 2.1). This is because the regression line describing the relationship be-
409 tween carbon costs to acquire nitrogen and nitrogen fertilization in *G. max* grown
410 under 0% shade cover would have flattened if growth limitation had caused larger
411 than expected carbon costs to acquire nitrogen in the 0% shade cover, 630 ppm
412 N treatment combination. This may have been exacerbated by the fact that *G.*
413 *max* likely shifted relative carbon allocation from nitrogen fixation to soil nitrogen
414 acquisition, which could have increased the negative effect of more densely packed
415 roots on nitrogen uptake. These patterns could have also occurred in *G. hirsutum*

416 grown under 0% shade cover; however, there was no change in the effect of nitro-
417 gen fertilization on *G. hirsutum* carbon costs to acquire nitrogen grown under 0%
418 shade cover relative to other shade cover treatments. Regardless, the possibility
419 of growth limitation due to pot volume suggests that effects of increasing nitro-
420 gen fertilization on carbon costs to acquire nitrogen in both species grown under
421 0% shade cover could have been underestimated. Follow-up studies using a simi-
422 lar experimental design with a larger pot volume would be necessary in order to
423 determine whether these patterns were impacted by pot volume-induced growth
424 limitation.

425 In conclusion, this study provides empirical evidence that carbon costs to
426 acquire nitrogen are influenced by light availability and soil nitrogen fertilization
427 in a species capable of acquiring nitrogen via symbiotic nitrogen fixation and a
428 species not capable of forming such associations. We show that carbon costs to
429 acquire nitrogen generally increase with increasing light availability and decrease
430 with increasing nitrogen fertilization. This study provides important empirical
431 data needed to evaluate the formulation of carbon costs to acquire nitrogen in
432 terrestrial biosphere models, particularly carbon costs to acquire nitrogen that
433 are associated with symbiotic nitrogen fixation. Our findings broadly support
434 the general formulation of these carbon costs in the FUN biogeochemical model
435 in response to shifts in nitrogen availability. However, there is a need for future
436 studies to explicitly quantify carbon costs to acquire nitrogen under different en-
437 vironmental contexts, over longer temporal scales, and using larger selections of
438 phylogenetically related species. In addition, we suggest that future studies mini-
439 mize the limitations associated with the metric used here by explicitly measuring

440 belowground carbon fates independently.

441

Chapter 3

442 Soil nitrogen availability modifies leaf nitrogen economies in mature
443 temperate deciduous forests: a direct test of photosynthetic least-cost
444 theory

445 3.1 Introduction

446 Photosynthesis represents the largest carbon flux between the atmosphere
447 and land surface (IPCC 2021), and plays a central role in biogeochemical cycling
448 at multiple spatial and temporal scales (Vitousek and Howarth 1991; LeBauer and
449 Treseder 2008; Kaiser et al. 2015; Wieder et al. 2015). Therefore, carbon and
450 energy fluxes simulated by terrestrial biosphere models are sensitive to the formu-
451 lation of photosynthetic processes (Ziehn et al. 2011; Bonan et al. 2011; Booth
452 et al. 2012; Smith et al. 2016; Smith et al. 2017) and must be represented using
453 robust, empirically tested processes (Prentice et al. 2015; Wieder et al. 2019).
454 Current formulations of photosynthesis vary across terrestrial biosphere models
455 (Smith and Dukes 2013; Rogers et al. 2017), which causes variation in modeled
456 ecosystem processes (Knorr 2000; Knorr and Heimann 2001; Bonan et al. 2011;
457 Friedlingstein et al. 2014) and casts uncertainty on the ability of these models to
458 accurately predict terrestrial ecosystem responses and feedbacks to global change
459 (Zaehle et al. 2005; Schaefer et al. 2012; Davies-Barnard et al. 2020).

460 Terrestrial biosphere models commonly represent C₃ photosynthesis through
461 variants of the Farquhar et al. (1980) biochemical model (Smith and Dukes 2013;
462 Rogers 2014; Rogers et al. 2017). This well-tested photosynthesis model es-
463 timates leaf-level carbon assimilation, or photosynthetic capacity, as a function
464 of the maximum rate of Ribulose-1,5-bisphosphate carboxylase-oxygenase (Ru-

465 bisco) carboxylation (V_{cmax}) and the maximum rate of Ribulose-1,5-bisphosphate
466 (RuBP) regeneration (J_{max}) (Farquhar et al. 1980). Many terrestrial biosphere
467 models predict these model inputs based on plant functional group specific linear
468 relationships between leaf nutrient content and V_{cmax} (Smith and Dukes 2013;
469 Rogers 2014; Rogers et al. 2017) under the tenet that a large fraction of leaf
470 nutrients, and nitrogen (N) in particular, are partitioned toward building and
471 maintaining enzymes that support photosynthetic capacity, such as Rubisco (Brix
472 1971; Gulmon and Chu 1981; Evans 1989; Kattge et al. 2009; Walker et al. 2014).
473 Terrestrial biosphere models also predict leaf nutrient content from soil nutrient
474 availability based on the assumption that increasing soil nutrients generally in-
475 creases leaf nutrients (Firn et al. 2019; Li et al. 2020; Liang et al. 2020) which, in
476 the case of N, generally corresponds with an increase in photosynthetic processes
477 (Li et al. 2020; Liang et al. 2020).

478 Recent work calls the generality of relationships between soil nutrient avail-
479 ability, leaf nutrient content, and photosynthetic capacity into question, suggest-
480 ing instead that leaf nutrients and photosynthetic capacity are better predicted as
481 an integrated product of aboveground climate, leaf traits, and soil nutrient avail-
482 ability, rather than soil nutrient availability alone (Dong et al. 2017; Dong et al.
483 2020; Dong et al. 2022; Firn et al. 2019; Smith et al. 2019; Peng et al. 2021).
484 It has been reasoned that this result is because plants allocate added nutrients to
485 growth and storage rather than alterations in leaf chemistry (Smith et al. 2019),
486 perhaps as a result of nutrient limitation of primary productivity (LeBauer and
487 Treseder 2008; Fay et al. 2015). Additionally, recent work suggests that relation-
488 ships between leaf nutrient content and photosynthesis vary across environments,

489 and that the proportion of leaf nutrient content allocated to photosynthetic tis-
490 sue varies over space and time with plant acclimation and adaptation responses
491 to light availability, vapor pressure deficit, soil pH, soil nutrient availability, and
492 environmental factors that influence leaf mass per area (Pons and Pearcy 1994;
493 Niinemets and Tenhunen 1997; Evans and Poorter 2001; Hikosaka and Shigeno
494 2009; Ghimire et al. 2017; Onoda et al. 2017; Luo et al. 2021). The use of linear
495 relationships between leaf nutrient content and Vcmax to predict photosynthetic
496 capacity, as commonly used in terrestrial biosphere models (Rogers 2014), is not
497 capable of detecting such responses.

498 Photosynthetic least-cost theory provides an alternative framework for un-
499 derstanding relationships between soil nutrient availability, leaf nutrient content,
500 and photosynthetic capacity (Harrison et al. 2021). Leveraging a two-input mi-
501 croeconomics approach (Wright et al. 2003), the theory posits that plants accli-
502 mate to a given environment by optimizing leaf photosynthesis rates at the lowest
503 summed cost of using nutrients and water (Prentice et al. 2014; Wang et al. 2017;
504 Smith et al. 2019; Paillassa et al. 2020). Across resource availability gradients,
505 the theory predicts that optimal photosynthetic rates can be achieved by trading
506 less efficient use of a resource that is less costly to acquire (or more abundant)
507 for more efficient use of a resource more costly to acquire (or less abundant). For
508 example, an increase in soil nutrient availability should reduce the cost of acquir-
509 ing and using nutrients (Bae et al. 2015; Eastman et al. 2021; Perkowski et al.
510 2021), which could increase leaf nutrient investments in photosynthetic proteins to
511 allow similar photosynthetic rates to be achieved with higher nutrient use (lower
512 nutrient use efficiency) but lower water use (greater water use efficiency). The

513 theory suggests similar tradeoffs in response to increasing soil pH (Paillassa et al.
514 2020), specifically, that increasing soil pH should reduce the cost of acquiring soil
515 nutrients due to an increase in plant-available nutrient concentration (Paillassa
516 et al. 2020; Dong et al. 2022). The theory is also capable of reconciling dynamic
517 leaf nutrient-photosynthesis relationships at global scales (Luo et al. 2021).

518 Patterns expected from photosynthetic least-cost theory have recently re-
519 ceived empirical support both in global environmental gradient (Smith et al.
520 2019; Paillassa et al. 2020; Luo et al. 2021; Querejeta et al. 2022; Wester-
521 band et al. 2023) and local manipulative invasion (Bialic-Murphy et al. 2021)
522 studies. However, nutrient addition experiments that directly examine nutrient-
523 water use tradeoffs expected from the theory are rare (Guerrieri et al. 2011), and
524 only global gradient studies testing the theory have considered soil pH in their
525 analyses. As a result, there is a need to use nutrient addition and soil pH manu-
526 lation experiments to test mechanisms driving responses predicted by the theory.
527 Such experiments would also be useful to detect whether patterns expected from
528 theory translate to finer spatial scales.

529 In this study, we measured leaf responses to soil N availability in five decid-
530 uous tree species growing in the upper canopy of mature closed canopy temperate
531 forests in the northeastern United States. Soil N availability and pH were manip-
532 ulated through a N-by-pH field manipulation experiment with treatments applied
533 since 2011, eight years prior to measurement. Two different soil N treatments were
534 applied to increase N availability with opposing effects on soil pH. An additional
535 N-free acidifying treatment was expected to decrease soil pH. We hypothesized
536 that increased soil N availability would enable plants to increase nutrient uptake

537 and create more photosynthetic enzymes per leaf, allowing similar photosynthetic
538 rates achieved with lower leaf C_i:C_a and increased leaf N content allocated to
539 photosynthetic leaf tissue. We expected that this response would be driven by a
540 reduction in the cost of acquiring N, which would cause trees to sacrifice efficient
541 N use to enable more efficient use of other limiting resources (i.e., water). We
542 hypothesized similar leaf responses to increasing soil pH.

543 3.2 Methods

544 3.2.1 *Study site description*

545 We conducted this study in summer 2019 at three stands located within
546 a 20-km radius of Ithaca, NY, USA (42.444 °N, 76.502 °W). All stands contain
547 mature, closed-canopy forests dominated by deciduous tree species. Stands con-
548 tained abundant sugar maple (*Acer saccharum* Marshall), American beech (*Fagus*
549 *grandifolia* Ehrh.), and white ash (*Fraxinus americana* L.), accounting for 43%,
550 15%, and 17% of the total aboveground biomass across the three stands, respec-
551 tively, with less frequent red maple (*Acer rubrum* L.; 9% of total aboveground
552 biomass) and red oak occurrences (*Quercus rubra* L.; 10% of total aboveground
553 biomass). Soils at each site were broadly classified as a channery silt loam Incep-
554 tisols using the USDA NRCS Web Soil Survey data product (Soil Survey Staff
555 2022). Between 2006 and 2020, study sites averaged 972 mm of precipitation per
556 year and had an average temperature of 7.9 °C per a weather station located near
557 the Cornell University campus (42.449 °N, 76.449 °W) part of the NOAA NCEI
558 Global Historical Climatology Network (Menne et al. 2012).

559 3.2.2 *Experimental design*

560 Four 40 m x 40 m plots were set up at each site in 2009, each with an
561 additional 10 m buffer along plot perimeters (60 m x 60 m total). The plots
562 were set up as a nitrogen-by-pH field manipulation experiment, with one each of
563 four treatments at each site. Two nitrogen treatments were applied, both at 50
564 kg N ha⁻¹ yr⁻¹, as either sodium nitrate (NaNO₃) to raise soil pH, or ammonium
565 sulfate ((NH₄)₂SO₄) to acidify; an elemental sulfur treatment was selected to acid-
566 ify without N, applied at the same rate of S addition (57 kg S ha⁻¹ yr⁻¹); and
567 control plots received no additions. All amendments were added in pelletized form
568 using hand-held fertilizer spreaders to both the main plots and buffers. Amend-
569 ments were divided into three equal doses distributed across the growing season
570 from 2011-2017 and added as a single dose from 2018 onward. During 2019, plots
571 were fertilized during the week of May 20.

572 3.2.3 *Leaf gas exchange and trait measurements*

573 We sampled one leaf each from 6 to 10 individuals per plot between June
574 25 and July 12, 2019 for gas exchange measurements (Table S1). Leaves were
575 collected from deciduous broadleaf trees represented across all sites and plots and
576 were replicated in efforts to mimic the species abundance of each plot at each
577 site. We also attempted to collect leaves from the upper canopy to reduce differ-
578 ential shading effects on leaf physiology. Leaves were accessed by pulling down
579 small branches using an arborist's slingshot and weighted beanbag attached to a
580 throwline. Branches were immediately recut under deionized water and remained
581 submerged to reduce stomatal closure and avoid xylem embolism (as in Smith &

582 Dukes, 2018) until gas exchange data were collected.

583 Randomly selected leaves with little to no visible external damage were
584 attached to a Li-COR LI-6800 (Li-COR Bioscience, Lincoln, Nebraska, USA)
585 portable photosynthesis machine to measure net photosynthesis (A_{net} ; $\mu\text{mol m}^{-2} \text{s}^{-1}$),
586 stomatal conductance (g_{sw} ; $\text{mol m}^{-2} \text{s}^{-1}$), and intercellular CO_2 concentration
587 (C_i ; $\mu\text{mol mol}^{-1}$) at different reference CO_2 concentrations (C_a ; $\mu\text{mol mol}^{-1}$)
588 concentrations (i.e., an A_{net}/C_i curve) under saturating light conditions (2,000
589 $\mu\text{mol m}^{-2} \text{s}^{-1}$). Reference CO_2 concentrations followed the sequence: 400, 300,
590 200, 100, 50, 400, 400, 600, 800, 1000, 1200, 1500, and 2000 $\mu\text{mol mol}^{-1} \text{CO}_2$. Leaf
591 temperatures were not controlled in the cuvette and ranged from 21.8 °C to 31.7
592 °C (mean±SD: 27.2 ± 2.2 °C). A linear and second order log-polynomial nonlinear
593 regression suggested no effect of temperature on stomatal conductance measured
594 at 400 $\mu\text{mol mol}^{-1} \text{CO}_2$ or net photosynthesis measured at $\mu\text{mol mol}^{-1} \text{CO}_2$ (Ta-
595 ble S2-3; Fig. S1). All A_{net}/C_i curves were generated within one hour of branch
596 severance.

597 Leaf morphological and chemical traits were collected on the same leaf used
598 to generate each A_{net}/C_i curve. Images of each leaf were taken using a flat-bed
599 scanner to determine fresh leaf area using the ‘LeafArea’ R package (Katabuchi
600 2015), which automates leaf area calculations using ImageJ software (Schneider
601 et al. 2012). Each leaf was dried at 65°C for at least 48 hours, weighed, and
602 ground using a Retsch MM200 ball mill grinder (Verder Scientific, Inc., Newtown,
603 PA, USA) until homogenized. Leaf mass per area (M_{area} , g m^{-2}) was calculated
604 as the ratio of dry leaf biomass to fresh leaf area. Using a subsample of ground and
605 homogenized leaf biomass, leaf N content (N_{mass} ; gN g^{-1}) and leaf $\delta^{13}\text{C}$ (‰, rela-

606 tive to VPDB) were measured at the Cornell Stable Isotope Lab with an elemental
607 analyzer (NC 2500, CE Instruments, Wigan, UK) interfaced to an isotope ratio
608 mass spectrometer (Delta V Isotope Ratio Mass Spectrometer, ThermoFisher Sci-
609 entific, Waltham, MA, USA). Leaf N content per unit leaf area (N_{area} ; gN m⁻²)
610 was calculated by multiplying N_{mass} by M_{area} .

611 We used leaf $\delta^{13}\text{C}$ values to estimate χ (unitless), which is an isotope-
612 derived estimate of the leaf $C_i:C_a$ ratio. While intercellular and atmospheric CO₂
613 concentrations were directly measured during each A_{net}/C_i curve, deriving χ from
614 $\delta^{13}\text{C}$ provides a more integrative estimate of the $C_i:C_a$ over an individual leaf's
615 lifespan. We derived χ following the approach of Farquhar et al. (1989) described
616 in Cernusak et al. (2013):

$$\chi = \frac{\Delta^{13}\text{C} - a}{b - a} \quad (3.1)$$

617 where $\Delta^{13}\text{C}$ represents the relative difference between leaf $\delta^{13}\text{C}$ (‰) and air $\delta^{13}\text{C}$
618 (‰), and is calculated from the following equation:

$$\Delta^{13}\text{C} = \frac{\delta^{13}\text{C}_{\text{air}} - \delta^{13}\text{C}_{\text{leaf}}}{1 + \delta^{13}\text{C}_{\text{leaf}}} \quad (3.2)$$

619 where $\delta^{13}\text{C}_{\text{air}}$ is assumed to be -8‰ (Keeling et al. 1979; Farquhar et al. 1989), a
620 represents the fractionation between ¹²C and ¹³C due to diffusion in air, assumed
621 to be 4.4‰, and b represents the fractionation caused by Rubisco carboxylation,
622 assumed to be 27‰ (Farquhar et al. 1989).

623 3.2.4 A_{net}/C_i curve-fitting and parameter estimation

624 We fit A_{net}/C_i curves of each individual using the ‘fitaci’ function in the
625 ‘plantecophys’ R package (Duursma 2015). This function estimates the maximum
626 rate of Rubisco carboxylation V_{cmax} ; $\mu\text{mol m}^{-2} \text{s}^{-1}$) and maximum rate of electron
627 transport for RuBP regeneration (J_{max} ; $\mu\text{mol m}^{-2} \text{s}^{-1}$) based on the Farquhar,
628 von Caemmerer, and Berry biochemical model of C₃ photosynthesis (Farquhar
629 et al. 1980). For each curve fit, we included triose phosphate utilization (TPU)
630 limitation to avoid underestimating J_{max} (Gregory et al. 2021). Curves were
631 visually examined to confirm the likely presence of TPU limitation.

632 We determined Michaelis-Menten coefficients for Rubisco affinity to CO₂
633 (K_c ; $\mu\text{mol mol}^{-1}$) and O₂ (K_o ; $\mu\text{mol mol}^{-1}$), and the CO₂ compensation point
634 (Γ^* ; $\mu\text{mol mol}^{-1}$) using leaf temperature and equations described in Medlyn et al.
635 (2002) and derived in Bernacchi et al. (2001). Specifically, K_c and K_o were
636 calculated as:

$$K_c = 404.9 * \exp^{\frac{79430(T_k - 298)}{298RT_k}} \quad (3.3)$$

637 and

$$K_o = 278.4 * \exp^{\frac{36380(T_k - 298)}{298RT_k}} \quad (3.4)$$

638 while Γ^* was calculated as:

$$\Gamma^* = 42.75 * \exp^{\frac{37830(T_k - 298)}{298RT_k}} \quad (3.5)$$

639 In all three equations, T_k is the leaf temperature (in Kelvin) during each A_{net}/C_i

640 curve and R is the universal gas constant ($8.314 \text{ J mol}^{-1} \text{ K}^{-1}$).

641 We standardized V_{cmax} and J_{max} estimates to 25°C using a modified Ar-

642 rhenius equation (Kattge and Knorr 2007):

$$k_{25} = \frac{k_{\text{obs}}}{e^{\frac{H_a(T_{\text{obs}} - T_{\text{ref}})}{T_{\text{ref}}RT_{\text{obs}}}} * \frac{1+e^{\frac{T_{\text{ref}}\Delta S - H_d}{T_{\text{obs}}}}}{1+e^{\frac{T_{\text{obs}}\Delta S - H_d}{T_{\text{obs}}}}}} \quad (3.6)$$

643 k_{25} represents the standardized V_{cmax} or J_{max} rate at 25°C , k_{obs} represents

644 the V_{cmax} or J_{max} estimate at the average leaf temperature measured inside the

645 cuvette during the A_{net}/C_i curve. H_a is the activation energy of V_{cmax} ($71,513$

646 J mol^{-1}) Kattge and Knorr (2007) or J_{max} ($49,884 \text{ J mol}^{-1}$) (Kattge and Knorr

647 2007). H_d represents the deactivation energy of both V_{cmax} and J_{max} ($200,000 \text{ J}$

648 mol^{-1}) (Medlyn et al. 2002), and R represents the universal gas constant (8.314

649 $\text{J mol}^{-1} \text{ K}^{-1}$). T_{ref} represents the standardized temperature of 298.15 K (25°C)

650 and T_{obs} represents the mean leaf temperature (in K) during each A_{net}/C_i curve.

651 ΔS is an entropy term that (Kattge and Knorr 2007) derived as a linear relation-

652 ship with average growing season temperature (T_g ; $^\circ\text{C}$), where:

$$\Delta S_{vcmax} = -1.07 T_g + 668.39 \quad (3.7)$$

653 and

$$\Delta S_{jmax} = -0.75 T_g + 659.70 \quad (3.8)$$

654 We estimated T_g in Equations 3.7 and 3.8 based on mean daily (24-hour) air
655 temperature of the 30 days leading up to the day of each sample collection using
656 the same weather station reported in the site description. We then used V_{cmax25}
657 and J_{max25} estimates to calculate the ratio of J_{max25} to V_{cmax25} ($J_{max25}:V_{cmax25}$;
658 unitless).

659 3.2.5 *Proportion of leaf nitrogen allocated to photosynthesis and structure*

660 We used equations from Niinemets and Tenhunen (1997) to estimate the
661 proportion of leaf N content allocated to Rubisco and bioenergetics. The propor-
662 tion of leaf N allocated to Rubisco (ρ_{rub} ; gN gN⁻¹) was calculated as a function
663 of V_{cmax25} and N_{area} :

$$\rho_{rubisco} = \frac{V_{cmax25} N_r}{V_{cr} N_{area}} \quad (3.9)$$

664 where N_r is the amount of nitrogen in Rubisco, set to 0.16 gN (gN in Rubisco)⁻¹
665 and V_{cr} is the maximum rate of RuBP carboxylation per unit Rubisco protein,
666 set to 20.5 μmol CO₂ (g Rubisco)⁻¹. The proportion of leaf nitrogen allocated to
667 bioenergetics (ρ_{bioe} ; gN gN⁻¹) was similarly calculated as a function of J_{max25} and
668 N_{area} :

$$\rho_{bioe} = \frac{J_{max25} N_b}{J_{mc} N_{area}} \quad (3.10)$$

669 where N_b is the amount of nitrogen in cytochrome f, set to 0.12407 gN (μmol
670 cytochrome f)⁻¹ assuming a constant 1: 1: 1.2 cytochrome f: ferredoxin NADP
671 reductase: coupling factor molar ratio (Evans and Seemann 1989; Niinemets and

672 Tenhunen 1997), and J_{mc} is the capacity of electron transport per cytochrome f,
673 set to $156 \mu\text{mol electron} (\mu\text{mol cytochrome f})^{-1}\text{s}^{-1}$.

674 We estimated the proportion of leaf N content allocated to photosynthetic
675 tissue (ρ_{photo} ; gN gN^{-1}) as the sum of ρ_{rub} and ρ_{bioe} . This calculation is an un-
676 derestimate of the proportion of leaf N allocated to photosynthetic tissue because
677 it does not include N allocated to light harvesting proteins. This leaf N pool was
678 not included because we did not perform chlorophyll extractions on focal leaves.
679 However, the proportion of leaf N content allocated to light harvesting proteins
680 tends to be small relative to ρ_{rub} and ρ_{bioe} , and may scale with changes in ρ_{rub}
681 and ρ_{bioe} (Niinemets and Tenhunen 1997).

682 Finally, we estimated the proportion of leaf N content allocated to struc-
683 tural tissue (ρ_{str} ; gN gN^{-1}) using an empirical equation from Onoda et al. (2017):

$$N_{cw} = 0.000355 * M_{area}^{1.39} \quad (3.11)$$

684 where N_{cw} is the leaf N content allocated to cell walls (gN m^{-2}). ρ_{str} was estimated
685 by dividing N_{cw} by N_{area} .

686 3.2.6 *Tradeoffs between nitrogen and water use*

687 Photosynthetic nitrogen use efficiency (PNUE; $\mu\text{mol CO}_2 \text{ mol}^{-1} \text{ N s}^{-1}$)
688 was calculated by dividing A_{net} by N_{area} , first converting N_{area} to mol N m^{-2}
689 using the molar mass of N (14 g mol^{-1}). We used χ as an indicator of water
690 use efficiency, which exploratory analyses suggest had similar responses to soil N
691 availability and pH as intrinsic water use efficiency measured from gas exchange

692 (A_{net}/g_s). Tradeoffs between nitrogen and water use were determined by cal-
693 culating the ratio of N_{area} to χ ($N_{\text{area}}:\chi$; g N m⁻²) and V_{cmax25} to χ ($V_{\text{cmax25}}:\chi$;
694 $\mu\text{mol m}^{-2} \text{s}^{-1}$). This approach is similar to tradeoff calculations in which nitrogen-
695 water use tradeoffs are measured as the ratio of N_{area} or V_{cmax25} to g_s (Paillassa
696 et al. 2020; Bialic-Murphy et al. 2021). In this study, we quantify these re-
697 lationships using χ in lieu of g_s because g_s rapidly changes with environmental
698 conditions and therefore may have been altered by recent tree branch severance
699 and/or placement in the cuvette.

700 3.2.7 *Soil nitrogen availability and pH*

701 To characterize soil N availability at the time of our leaf gas exchange
702 measurements, we used mixed bed resin bags to quantify mobile ammonium-N
703 and nitrate-N concentrations in each plot. Lycra mesh bags were filled with 5 g
704 of Dowex® Marathon MR-3 hydrogen and hydroxide form resin (MilliporeSigma,
705 Burlington, MA USA) and sealed with a zip tie. Each bag was activated by
706 soaking in 0.5 M HCl for 20 minutes, then in 2 M NaCl until pH of the saline
707 solution stabilized, as described in Allison et al. (2008). Five resin bags were
708 inserted about 10 cm below the soil surface at each plot on June 25, 2019: one
709 near each of the four plot corners and one near the plot center. All resin bags
710 were collected 24 days later on July 19, 2019 and were frozen until extracted.

711 Prior to anion and cation extraction, each resin bag was rinsed with ul-
712 trapure water (MilliQ IQ 7000; Millipore Sigma, Burlington, MA) to remove any
713 surface soil residues. Anions and cations were extracted from surface-cleaned resin
714 bags by individually soaking and shaking each bag in 100 mL of a 0.1 M HCl/2.0

715 M NaCl matrix for one hour. Using a microplate reader (Biotek Synergy H1;
716 Biotek Instruments, Winooski, VT USA), nitrate-N concentrations were quanti-
717 fied spectrophotometrically at 540 nm with the end product of a single reagent
718 vanadium (III) chloride reaction (Doane and Horwáth 2003), and ammonium-N
719 concentrations quantified at 650 nm with the end product of a modified phenol-
720 hypochlorite reaction (Weatherburn 1967; Rhine et al. 1998). Both the single
721 reagent vanadium (III) chloride and modified phenol-hypochlorite methodologies
722 have been well established for determining nitrate-N and ammonium-N concen-
723 trations in resin bag extracts (Arnone 1997; Allison et al. 2008). We used a
724 series of negative and positive controls throughout each well plate to verify the
725 accuracy and precision of our measurements, assaying each resin bag extract and
726 control in triplicate. Soil N availability was estimated as the sum of the nitrate-N
727 and ammonium-N concentration in each resin bag, normalized per g of resin and
728 duration in the field ($\mu\text{g N g}^{-1} \text{ resin d}^{-1}$), then subsequently averaged across all
729 resin bags in a plot for a plot-level mean.

730 Soil pH was measured on 0-10 cm mineral soil samples collected prior to
731 fertilization in 2019. Near each of the four plot corners, three 5.5 cm diameter soil
732 cores were collected after first removing the forest floor where present. Each set
733 of three cores was placed in a plastic bag, and later composited by hand mixing
734 and sieved to 4mm. Soil pH was determined for a 1:2 soil:water slurry (10 g field-
735 moist soil to 20 mL DI water) of each sample using an Accumet AB15 pH meter
736 with flushable junction probe (Fisher Scientific; Hampton, NH, USA), and was
737 estimated at the plot level as the mean soil pH within each plot.

738 3.2.8 *Statistical analyses*

739 We built two separate series of linear mixed-effects models to explore effects
740 of soil N availability, soil pH, species, and leaf N content on leaf physiological
741 traits. In the first series of linear mixed-effects models, we explored the effect
742 of soil N availability, soil pH, and species on leaf N content, leaf photosynthesis,
743 stomatal conductance, and nitrogen-water use tradeoffs. Models included plot-
744 level soil N availability and plot-level soil pH as continuous fixed effects, species
745 as a categorical fixed effect, and site as a categorical random intercept term.
746 Interaction terms between fixed effects were not included due to the small number
747 of experimental plots. We built a series of separate models with this independent
748 variable structure to quantify individual effects of soil N availability, soil pH,
749 and species on N_{area} , M_{area} , N_{mass} , A_{net} , V_{cmax25} , J_{max25} , $J_{\text{max25}}:V_{\text{cmax25}}$, ρ_{rubisco} ,
750 $\rho_{\text{bioenergetics}}$, ρ_{photo} , $\rho_{\text{structure}}$, χ , PNUE, $N_{\text{area}}:\chi$, and $V_{\text{cmax25}}:\chi$.

751 A second series of linear mixed-effects models were built to investigate
752 relationships between leaf N content and photosynthetic parameters. Statistical
753 models included N_{area} as a single continuous fixed effect with species and site des-
754 ignated as individual random intercept terms. We used this independent variable
755 structure to quantify individual effects of leaf N content on A_{net} , V_{cmax25} , J_{max25} ,
756 $J_{\text{max25}}:V_{\text{cmax25}}$, and χ .

757 For all linear mixed-effects models, we used Shapiro-Wilk tests of normal-
758 ity to determine whether linear mixed-effects models satisfied residual normality
759 assumptions. If residual normality assumptions were not met, then models were
760 fit using dependent variables that were natural log transformed. If residual nor-
761 mality assumptions were still not met (Shapiro-Wilk: $p < 0.05$), then models were

762 fit using dependent variables that were square root transformed. All residual nor-
763 mality assumptions for both sets of models that did not originally satisfy residual
764 normality assumptions were met with either a natural log or square root data
765 transformation (Shapiro-Wilk: $p > 0.05$ in all cases).

766 In the first series of models, models for N_{area} , M_{area} , N_{mass} , V_{cmax25} , J_{max25} ,
767 χ , $N_{\text{area}}:\chi$, and $V_{\text{cmax25}}:\chi$, ρ_{rubisco} , $\rho_{\text{bioenergetics}}$, ρ_{photo} , $\rho_{\text{structure}}$ satisfied residual
768 normality assumptions without data transformations (Shapiro-Wilk: $p > 0.05$ in
769 all cases). The model for $J_{\text{max25}}:V_{\text{cmax25}}$ satisfied residual normality assumptions
770 with a natural log data transformation, while models for A_{net} and PNUE each
771 satisfied residual normality assumptions with square root data transformations.
772 In the second series of models, models for V_{cmax25} , J_{max25} , χ , and $V_{\text{cmax25}}:\chi$ satisfied
773 residual normality assumptions without data transformations (Shapiro-Wilk: p
774 > 0.05 in all cases). The model for $J_{\text{max25}}:V_{\text{cmax25}}$ required a natural log data
775 transformation and the model for A_{net} required a square root data transformation
776 (Shapiro-Wilk: $p > 0.05$ in both cases).

777 In all models, we used the ‘lmer’ function in the ‘lme4’ R package (Bates
778 et al. 2015) to fit each model and the ‘Anova’ function in the ‘car’ R package (Fox
779 and Weisberg 2019) to calculate Type II Wald’s χ^2 and determine the significance
780 level ($\alpha = 0.05$) of each fixed effect coefficient. Finally, we used the ‘emmeans’
781 R package (Lenth, 2019) to conduct post-hoc comparisons using Tukey’s tests,
782 where degrees of freedom were approximated using the Kenward-Roger approach
783 (Kenward and Roger 1997). All analyses and plots were conducted in R version
784 4.1.1 (R Core Team 2021)). All figure regression lines and associated 95% confi-
785 dence interval error bars were plotted using predictions generated across the soil

786 nitrogen availability gradient using the ‘emmeans’ R package (Lenth 2019).

787 3.3 Results

788 3.3.1 *Leaf N content*

789 Increasing soil N availability generally increased N_{area} (Table 3.1; Fig.
790 3.1a). This pattern was driven by an increase in N_{mass} (Table 3.1; Fig. 3.1c)
791 and a marginal increase in M_{area} (Table 3.1; Fig. 3.1e) with increasing soil N
792 availability. There was no effect of soil pH on N_{area} , N_{mass} , or M_{area} (Table 3.1);
793 however, we did observe strong differences in N_{area} (Fig. 3.1b), N_{mass} (Fig. 3.1d),
794 and M_{area} (Fig. 3.1e) between species (Table 3.1).

Table 3.1. Effects of soil N availability, soil pH, and species on leaf N content per unit leaf area (N_{area}), leaf N content per unit leaf mass (N_{mass}), and leaf mass per unit leaf area (M_{area})

	df	N_{area}			N_{mass}			M_{area}		
		Coefficient	χ^2	p	Coefficient	χ^2	p	Coefficient	χ^2	p
Intercept	-	9.03E-01	-	-	1.68E+00	-	-	4.60E+01	-	-
Soil N	1	1.68E-02	11.990	0.001	1.25E-02	6.902	0.009	4.87E-01	4.143	0.042
Soil pH	1	9.28E-02	0.836	0.361	8.08E-02	0.663	0.415	4.05E+00	0.653	0.419
Species	4	-	72.128	<0.001	-	35.074	<0.001	-	29.869	<0.001

*Significance determined using Type II Wald χ^2 tests ($\alpha = 0.05$). P-values < 0.05 are in bold.

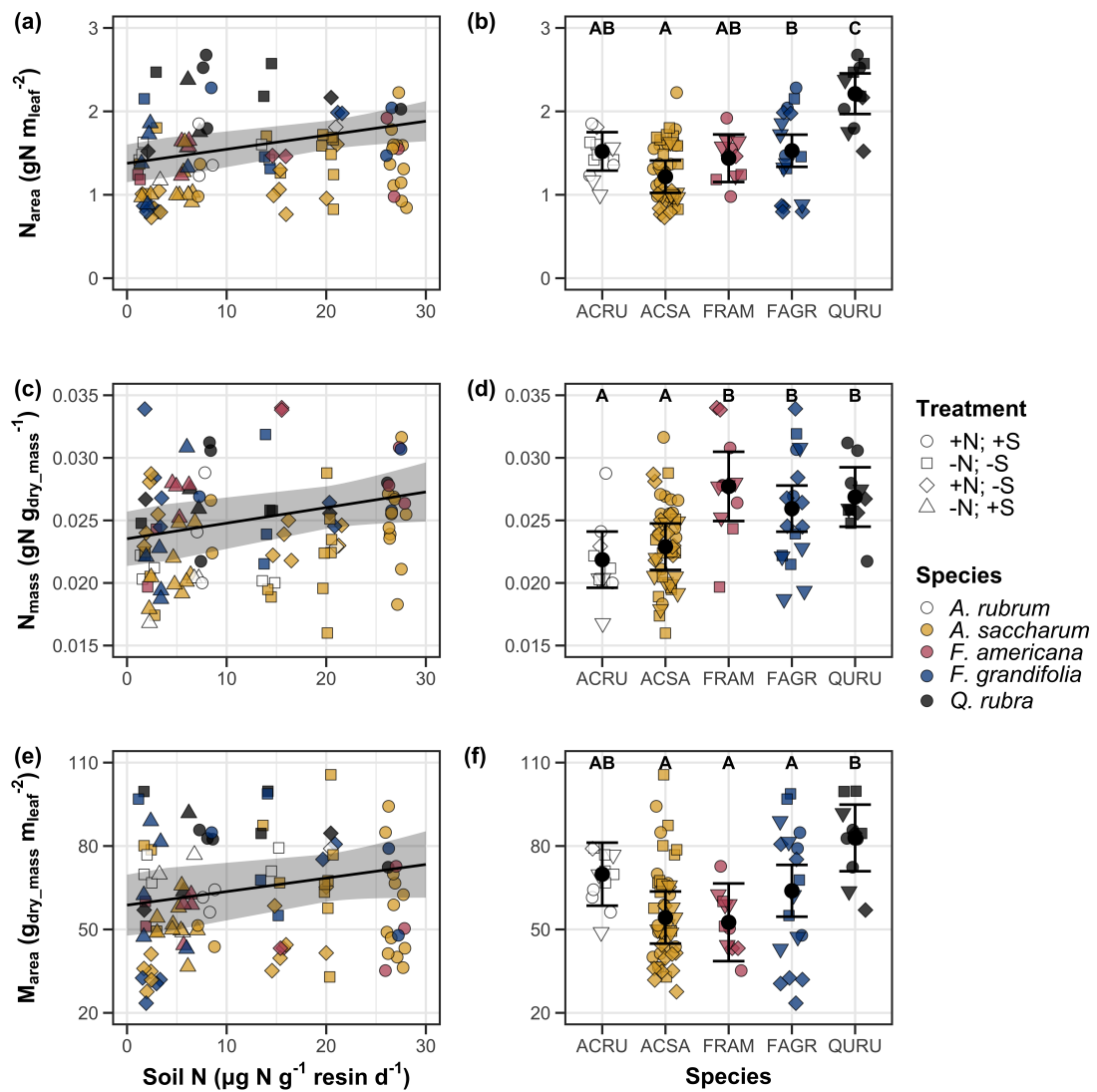


Figure 3.1. Effects of soil N availability and species on leaf N content per unit leaf area (a-b), leaf nitrogen content per unit leaf biomass (c-d), and leaf mass per unit leaf area (e-f). Soil N availability is represented on the x-axis in the left column of panels, while species is represented on the x-axis in the right column of panels. Tree species are represented as colored points and treatment plots are represented as shaped points, jittered for visibility. Species are abbreviated in the right column of panels through their assigned NRCS PLANTS Database symbol (USDA NRCS 2022), grouped along the x-axis per common mycorrhizal association, where the first three species commonly associate with arbuscular mycorrhizae (ACRU, ASCA, FAGR) and the second two species with ectomycorrhizae (FAGR, QURU). Trendlines are only included when the regression slope is statistically different from zero ($p < 0.05$).

795 3.3.2 *Net photosynthesis and leaf biochemistry*

796 Increasing soil N availability generally had no effect on A_{net} , V_{cmax25} , J_{max25} ,
797 or $J_{\text{max25}}:V_{\text{cmax25}}$ (Table 3.2, Figs. 3.2a, 3.2d, 3.2g). We also observed strong
798 species effects on all measured leaf photosynthetic traits (Table 3.2; Figs. 3.2b,
799 3.2e, 3.2h). Increasing soil pH had a marginal negative effect on A_{net} , but had no
800 effect on V_{cmax25} , J_{max25} , or $J_{\text{max25}}:V_{\text{cmax25}}$ (Table 3.2). There was a weak positive
801 effect of increasing N_{area} on A_{net} (Fig. 3.2c), but quite strong positive effects of
802 increasing N_{area} on V_{cmax25} and J_{max25} (Table 3.2; Fig. 3.2f and 3.2i).

Table 3.2. Effects of soil N availability, soil pH, species, and N_{area} on leaf biochemistry

	A_{net}			V_{cmax25}			J_{max25}			
	df	Coefficient	χ^2	p	Coefficient	χ^2	p	Coefficient	χ^2	p
(Intercept)	-	3.29E+00 ^b	-	-	6.38E+01	-	-	1.12E+02	-	-
Soil N	1	-1.23E-03 ^b	1.798	0.180	-3.84E-01	1.745	0.187	-6.70E-01	2.172	0.141
Soil pH	1	-3.09E-01 ^b	3.312	0.069	-4.91E+00	0.655	0.418	-8.18E+00	0.742	0.389
Species	4	-	11.838	0.019	-	31.748	<0.001	-	27.291	<0.001
(N_{area} int.)	-	6.59E-01 ^b	-	-	1.45E-01	-	-	2.86E+01	-	-
N_{area}	4	3.13E-01 ^b	4.790	0.029	2.43E+01	22.616	<0.001	4.04E+01	28.259	<0.001

	$J_{\text{max25}}:V_{\text{cmax25}}$			
	df	Coefficient	χ^2	p
(Intercept)	-	6.59E-01 ^a	-	-
Soil N	1	7.04E-04 ^a	0.088	0.767
Soil pH	1	-7.84E-03 ^a	0.025	0.874
Species	4	-	12.745	0.013
(N_{area} int.)	-	6.69E-01 ^a	-	-
N_{area}	4	-4.69E-02 ^a	1.142	0.285

*Significance determined using Type II Wald χ^2 tests ($\alpha = 0.05$). P -values < 0.05 are in bold, while p -values between 0.05 and 0.1 are italicized. Superscript letters indicate model coefficients fit to natural-log (^a) or square-root (^b) transformed data. Relationships between N_{area} and each response variable were fit using the second series of bivariate mixed-effects models, so model coefficients and results are independent from model coefficients and results reported for relationships between soil N, soil pH, and species for each response variable. Key: A_{net} – light saturated net photosynthesis rate; V_{cmax25} – maximum rate of Rubisco carboxylation at 25°C; J_{max25} – maximum rate of electron transport for RuBP regeneration at 25°C, $J_{\text{max25}}:V_{\text{cmax25}}$ – the ratio of J_{max25} to V_{cmax25} .

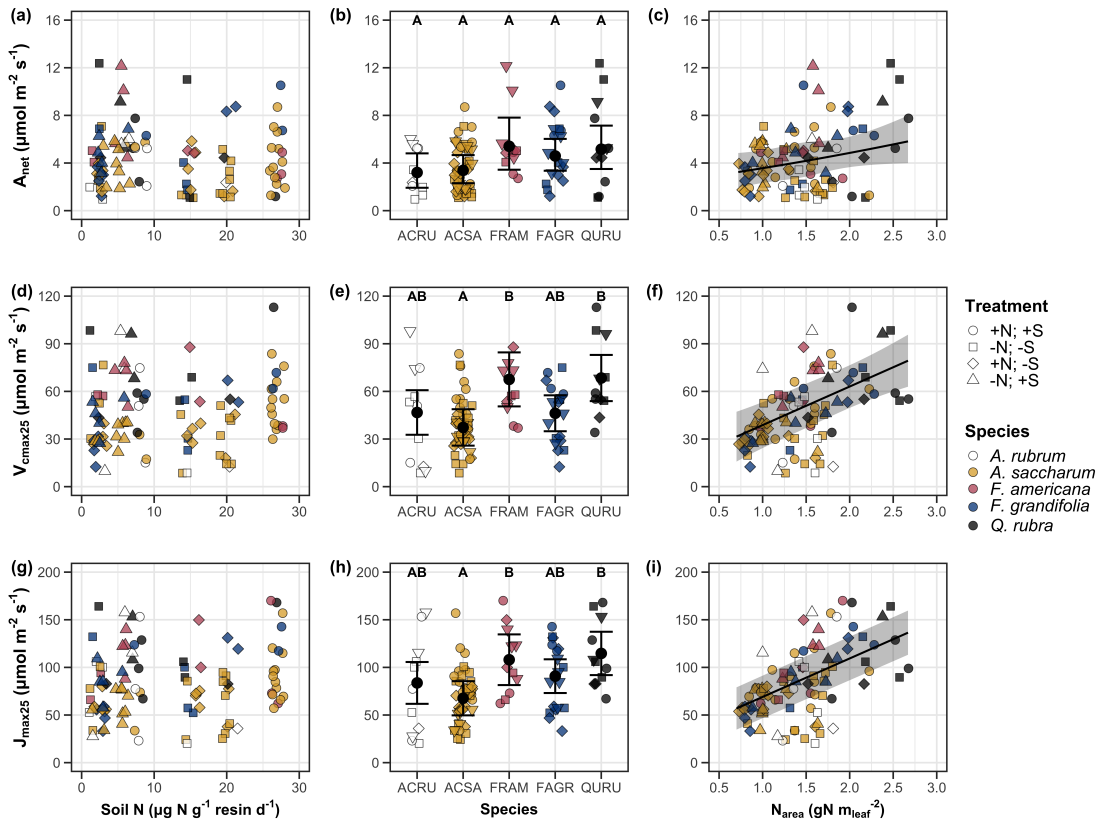


Figure 3.2. Effects of soil N availability (left column of panels), species (middle column of panels), and leaf N content per unit leaf area (right column of panels) on net photosynthesis (a-c), maximum Rubisco carboxylation rate (d-f), and maximum RuBP regeneration rate (g-i). Soil N availability is represented on the x-axis in the left column of panels, species is represented on the x-axis in the middle column of panels, and leaf N content per unit leaf area is represented continuously on the x-axis in the right column of panels. Species abbreviations and position along the x-axis in the middle column of panels, colored points, shapes, and trendlines are as explained in Figure 3.1.

803 3.3.3 *Leaf N allocation*

804 Neither soil N availability nor soil pH affected the proportion of leaf N
805 allocated to Rubisco or bioenergetics (Table 3.3; Fig. 3.3a, Fig. 3.3c), nor was
806 there any subsequent effect on the proportion of leaf N allocated to photosynthesis
807 (Table 3.3; Fig. 3.3f). We also found no effect of soil N availability or soil pH on
808 the proportion of leaf N allocated to structure (Table 3.3; Fig 3.3g). Species varied
809 in the proportion of leaf N allocated to Rubisco, photosynthesis, and structure (Fig
810 3.3b, Fig. 3.3d, Fig 3.3h), with no detectable species effect on the proportion of
811 leaf N allocated to bioenergetics (Table 3.3).

Table 3.3. Effects of soil N availability, soil pH, and species on the proportion of leaf nitrogen content allocated to photosynthesis, Rubisco, bioenergetics, and structure

	ρ_{photo}			ρ_{rub}			ρ_{bioe}			
	df	Coefficient	χ^2	p	Coefficient	χ^2	p	Coefficient	χ^2	p
Intercept	-	4.93E-01	-	-	4.17E-01	-	-	7.64E-02	-	-
Soil N	1	-1.23E-03	0.521	0.470	-1.04E-03	0.501	0.479	-1.77E-04	0.557	0.455
Soil pH	1	-4.37E-02	1.581	0.209	-3.70E-02	1.511	0.219	-6.84E-03	1.941	0.164
Species	4	-	13.106	0.011	-	14.152	0.007	-	7.300	0.121

	ρ_{str}			
	df	Coefficient	χ^2	p
Intercept	-	9.77E-02	-	-
Soil N	1	-2.29E-04	1.165	0.280
Soil pH	1	-1.87E-03	0.179	0.672
Species	4	-	16.428	0.002

*Significance determined using Type II Wald χ^2 tests ($\alpha = 0.05$). P-values < 0.05 are in bold. Key: ρ_{photo} - proportion of leaf nitrogen content allocated to photosynthesis; ρ_{rub} - proportion of leaf nitrogen content allocated to Rubisco; ρ_{bioe} - proportion of leaf nitrogen content allocated to bioenergetics; ρ_{str} - proportion of leaf nitrogen content allocated to structure.

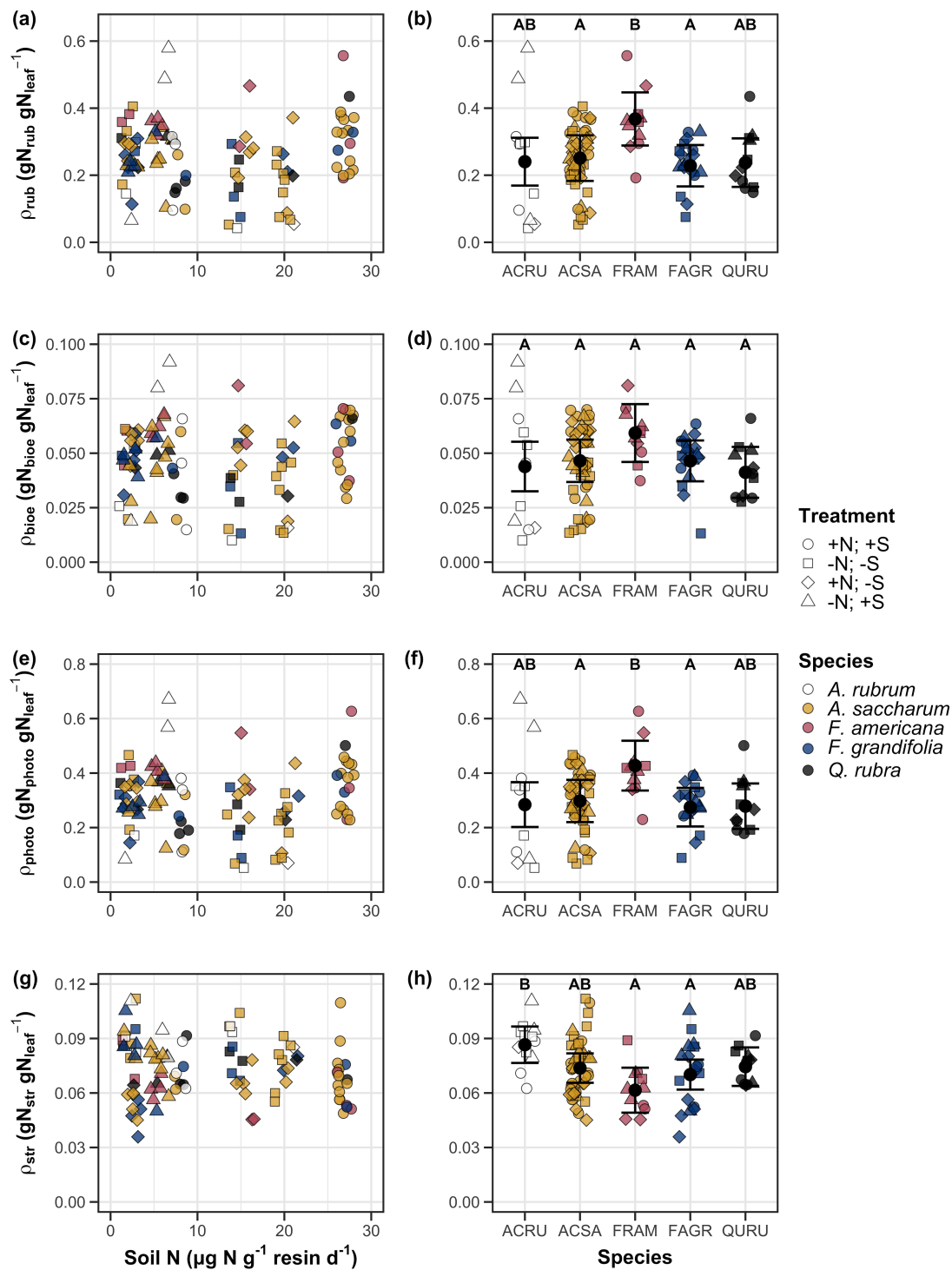


Figure 3.3. Effects of soil nitrogen availability and species on the proportion of leaf nitrogen content allocated to Rubisco (a-b), bioenergetics (c-d), photosynthesis (e-f), and structure (g-h)

812 3.3.4 *Tradeoffs between nitrogen and water use*

813 Although soil N availability did not affect χ (Table 3.4; Fig. 3.4a), increasing
814 soil N availability decreased PNUE (Table 3.4; Fig. 3.4d) and increased the
815 ratio of $N_{\text{area}}:\chi$ (Table 3.4; Fig. 3.4f). Specifically, this response yielded a 26%
816 reduction in PNUE and 37% stimulation in $N_{\text{area}}:\chi$ across the soil nitrogen avail-
817 ability gradient. There was no apparent effect of soil N availability on $V_{\text{cmax25}}:\chi$
818 (Table 3.4; Fig. 3.4h). Increasing soil pH had a weak marginal negative effect
819 on PNUE, but did not influence χ , $N_{\text{area}}:\chi$, or $V_{\text{cmax25}}:\chi$ (Table 3.4). We also
820 observed differences in χ (Fig. 3.4b), PNUE (Fig. 3.4e), $N_{\text{area}}:\chi$ (Fig. 3.4g), and
821 $V_{\text{cmax25}}:\chi$ (Fig. 3.4i) between species (Table 3.4). Finally, increasing N_{area} had a
822 strong negative effect on χ (Table 3.4; Fig. 3.4c) and a strong positive effect on
823 $V_{\text{cmax25}}:\chi$ (Table 3.4; Fig. 3.4j).

Table 3.4. Effects of soil N availability, soil pH, species, and N_{area} on tradeoffs between nitrogen and water use

	χ			PNUE			$N_{\text{area}}:\chi$			
	df	Coefficient	χ^2	p	Coefficient	χ^2	p	Coefficient	χ^2	p
(Intercept)	-	8.12E-01	-	-	9.57E+00	-	-	9.19E-01	-	-
Soil N	1	-1.14E-03	1.698	0.193	-6.63E-02	6.396	0.011	2.60E-02	9.533	0.002
Soil pH	1	-1.91E-02	1.087	0.297	-9.25E-01	2.843	<i>0.092</i>	2.03E-01	1.321	0.250
Species	4	-	18.843	0.001	-	13.454	0.009	-	52.983	<0.001
(N_{area} int.)	-	8.93E-01	-	-	-	-	-	-	-	-
N_{area}	1	-1.11E-01	80.606	<0.001	-	-	-	-	-	-

	$V_{\text{cmax25}}:\chi$			
	df	Coefficient	χ^2	p
(Intercept)	-	7.20E+01	-	-
Soil N	1	3.99E-01	0.963	0.326
Soil pH	1	-3.12E+00	0.138	0.711
Species	4	-	31.450	<0.001
(N_{area} int.)	-	1.18E+01	-	-
N_{area}	4	3.87E+01	32.797	<0.001

*Significance determined using Type II Wald χ^2 tests ($\alpha = 0.05$). P -values < 0.05 are in bold, while p -values between 0.05 and 0.1 are italicized. Superscript letters indicate model coefficients fit to natural-log ^(a) or square-root ^(b) transformed data. Relationships between N_{area} and each response variable were fit using the second series of bivariate mixed-effects models, so model coefficients and results are independent from model coefficients and results reported for relationships between soil N, soil pH, and species for each response variable. Key: χ - isotope-derived estimate of the $C_i:C_a$; PNUE - photosynthetic N use efficiency, ratio of net photosynthesis to leaf N content per unit leaf area; $N_{\text{area}}:\chi$ - ratio of N_{area} to χ ; $V_{\text{cmax25}}:\chi$ - ratio of V_{cmax25} to χ .

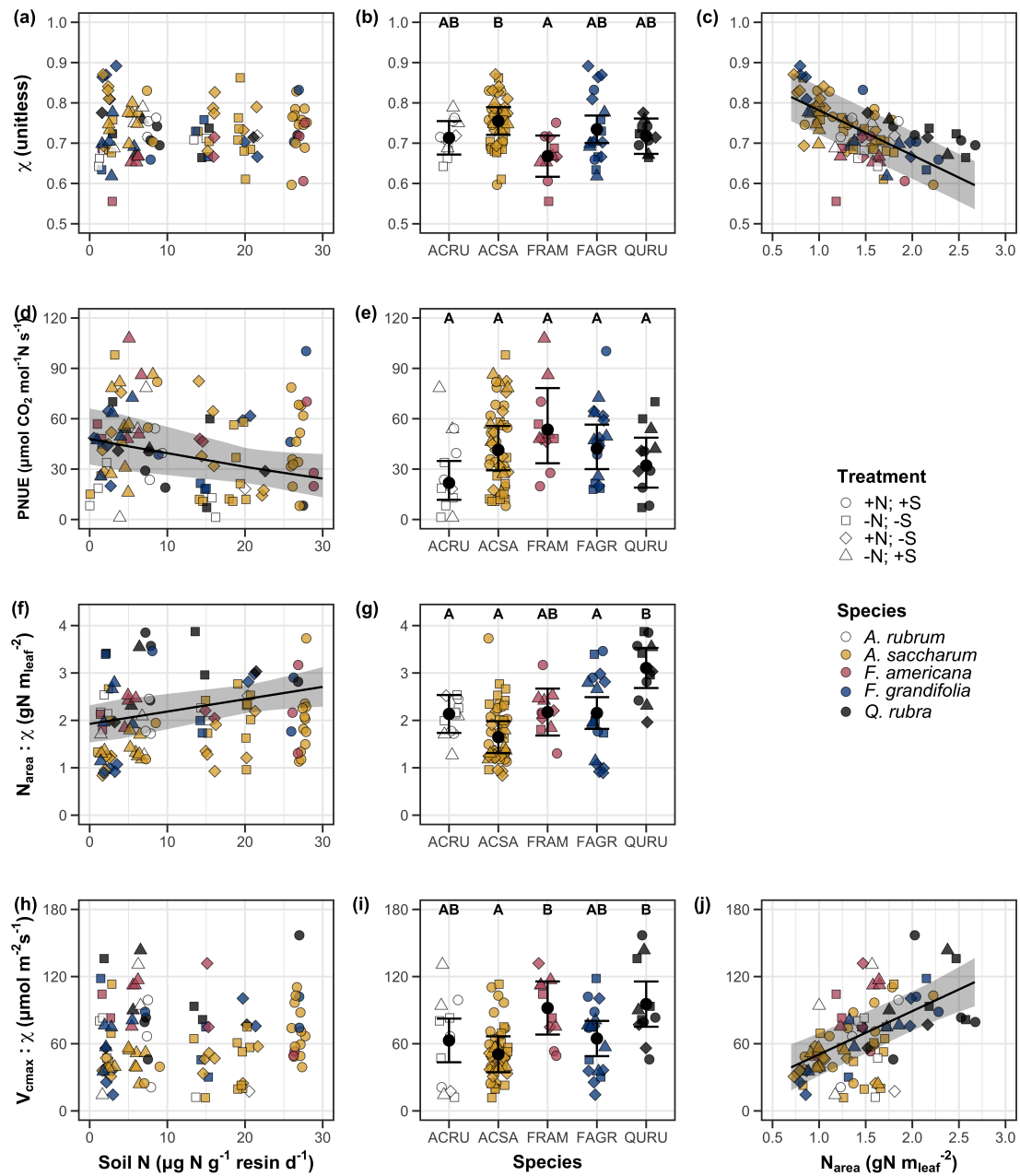


Figure 3.4. Effects of soil nitrogen availability and species on the proportion of leaf nitrogen content allocated to Rubisco (a-b), bioenergetics (c-d), photosynthesis (Rubisco + bioenergetics; e-f), and structure (g-h). Soil nitrogen availability is represented on the x-axis in the left column of panels and species are represented on the x-axis in the right column of panels. Species abbreviations and position along the x-axis in the middle column of panels, colored points, shapes, trendlines, error bars, and compact lettering are as explained in Figure 3.1.

824 3.4 Discussion

825 Photosynthetic least-cost theory provides an explanation for understand-
826 ing relationships between soil nutrient availability, leaf nutrient allocation, and
827 photosynthetic capacity. The theory suggests that plants acclimate to a given
828 environment by optimizing leaf photosynthesis rates at the lowest summed cost
829 of using nutrients and water Prentice et al. (2014), Wang et al. (2017), Smith
830 et al. (2019), Paillassa et al. (2020). The theory predicts that an increase in
831 soil nutrient availability should allow similar photosynthesis rates to be achieved
832 with increased leaf nutrient content and photosynthetic capacity (i.e., V_{cmax25} and
833 J_{max25}) at lower leaf $C_i:C_a$ (χ), resulting in an increase in water use efficiency,
834 decrease in nutrient use efficiency, and increase in both leaf nutrient content and
835 photosynthetic capacity per unit χ . The theory predicts similar leaf responses to
836 increasing soil pH under acidic conditions, presumably due to generally faster nu-
837 trient cycle dynamics and consequent reductions in the cost of acquiring nutrients
838 relative to water with increasing soil pH (Wang et al. 2017; Paillassa et al. 2020;
839 Dong et al. 2020).

840 Supporting the theory, we showed that increasing soil N availability was
841 associated with increased leaf N content (Fig 3.1a, 3.1c), a pattern that reduced
842 photosynthetic N use efficiency (Fig 3.4d) and increased leaf N content per unit
843 χ (Fig 3.4f). Increasing soil N coincided with slight, but non-significant decreases
844 in χ and increases in V_{cmax25} and J_{max25} ($p < 0.2$, Table 3.2). The positive trend
845 between soil N availability and photosynthetic capacity was supported by the con-
846 current strong increase in leaf N content with increasing soil N availability, which
847 resulted in no change in the proportion of leaf N content allocated to photosynthe-

848 sis across the soil N availability gradient. Additionally, leaf N content exhibited a
849 strong negative correlation with χ , indicative of strong nitrogen-water use trade-
850 offs at the leaf level. Responses tended to vary more due to soil N availability
851 than soil pH. Overall, these findings are consistent with the nutrient-water use
852 tradeoffs predicted from theory.

853 3.4.1 *Soil nitrogen availability modifies tradeoffs between nitrogen and water use*

854 In support of expected least-cost outcomes and past environmental gradient
855 studies (Dong et al. 2017; Paillassa et al. 2020), we found that increasing soil N
856 availability was associated with increased leaf N content. Soil N availability had
857 smaller impacts on measures of net photosynthesis and χ , which led to reductions
858 in PNUE and increases in leaf N content per unit χ , as expected from theory.
859 Photosynthetic least-cost theory suggests that reductions in PNUE should be
860 driven by an increase in the proportion of leaf N allocated to photosynthetic tissue,
861 a pattern that should allow plants to achieve optimal photosynthetic rates with
862 greater photosynthetic capacity to make better use of available light. Contrasting
863 theory predictions, we found no effect of soil N availability on photosynthetic
864 capacity. However, photosynthetic capacity did tend to increase with increasing
865 soil N availability ($p < 0.20$; Table 3.2) resulting in no effect of soil N availability on
866 the relative fraction of leaf N allocated to photosynthesis, Rubisco, or bioenergetics
867 (Fig. 3.3). These lines of evidence support the idea that trees use additional N
868 to support increased leaf N allocation toward photosynthetic tissue and enhance
869 photosynthetic capacity (Wright et al. 2003).

870 Soil N availability had a stronger effect on leaf N than photosynthetic ca-

871 pacity. This pattern suggests that additional plant N uptake due to increased
872 soil N availability was also being used to support non-photosynthetic N pools,
873 possibly to structural tissue or stress-induced amino acid and polyamine synthe-
874 sis (Minocha et al. 2000; Onoda et al. 2004; Bubier et al. 2011). While we
875 found no change in the proportion of leaf N allocated to leaf structural tissue, the
876 overall stimulation in leaf N content with increasing soil N availability suggests an
877 increase in the net amount of N invested in leaf structural tissue along the N avail-
878 ability gradient. Importantly, leaf N allocated to structure was calculated using
879 an empirical relationship between M_{area} and the amount of leaf N allocated to cell
880 walls (Onoda et al. 2017). As the generality of relationships between M_{area} and
881 the amount of leaf N allocated to cell walls has been called into question (Harrison
882 et al. 2009), future work should consider explicitly measuring N allocation to cell
883 wall tissue and stress-induced amino acid synthesis to confirm these patterns.

884 In opposition to patterns expected from least cost theory, increasing soil
885 N availability had no apparent effect on χ (Fig. 3.4a). Interestingly, despite
886 the null effect of soil N availability on χ , we observed a strong negative effect of
887 increasing N_{area} on χ (Fig. 3.4c), consistent with the nitrogen-water use tradeoffs
888 expected from theory. The null response of χ to increasing soil N availability may
889 have been due to a lack of water limitation in the system, given that the area
890 received approximately 20% more precipitation (1167 mm) during the 12-month
891 period leading up to our measurement period than normally expected (972 mm).
892 However, droughts can and do occur in temperate forests of the northeastern
893 United States (Sweet et al. 2017), so the observed increase in leaf N content
894 with increasing soil N availability could be a strategy that allows trees to hedge

895 bets against drier than normal growing seasons (Onoda et al. 2004; Onoda et al.
896 2017; Hallik et al. 2009). As was suggested in Paillassa et al. (2020), and more
897 recently by Querejeta et al. (2022), negative effects of soil N availability on χ may
898 increase with increasing aridity. This strategy would be especially advantageous if
899 it allows individuals growing in arid regions to maintain carbon assimilation rates
900 with reduced water loss. Future work should attempt to quantify interactive roles
901 of climate and soil nitrogen availability on nitrogen-water use tradeoffs, which
902 could be done by leveraging coordinated and multi-factor nutrient (Borer et al.
903 2014) and water (Knapp et al. 2017) manipulation experiments across broad
904 climatic gradients.

905 3.4.2 *Soil pH did not modify tradeoffs between nitrogen and water usage*

906 While the primary purpose of this study was to examine the role of soil N
907 availability on nitrogen-water use tradeoffs, our experimental design manipulated
908 both soil N and pH, providing an opportunity to isolate the roles of these variables.
909 Previous correlational studies along environmental gradients identified soil pH as
910 a particularly important factor that can modify tradeoffs between nutrient and
911 water use (Smith et al. 2019; Paillassa et al. 2020; Westerband et al. 2023)
912 and the proportion of leaf nitrogen allocated to photosynthesis (Luo et al. 2021).
913 Such studies implied that these patterns may be driven by reductions in the cost of
914 acquiring nutrients relative to water with increasing pH, which may be exacerbated
915 in acidic soils.

916 Consistent with theory (Wright et al. 2003; Prentice et al. 2014), our
917 results indicate that increasing soil pH was negatively associated with PNUE.

918 However, there was no effect of soil pH on leaf N content, χ , or leaf N content per
919 unit χ , most likely because the experimental N additions increased soil N sup-
920 ply while both increasing (sodium nitrate) and decreasing (ammonium sulfate)
921 soil pH. These results suggest that soil pH did not play a major role in modify-
922 ing expected photosynthetic least-cost theory patterns, contrasting findings from
923 Paillassa et al. (2020) and other gradient studies that note positive effects of in-
924 creasing soil pH on leaf N content, Rubisco carboxylation, and χ (Viet et al. 2013;
925 Cornwell et al. 2018; Luo et al. 2021). Instead, null responses to soil pH show
926 that leaf photosynthetic parameters depend more on soil N availability than pH
927 per se, and that inferences from gradient studies might be confounding covariation
928 between N availability and soil acidity.

929 3.4.3 *Species identity explains a large amount of variation in leaf and whole*
930 *plant traits*

931 Species generally explained a larger amount of variation in measured leaf
932 traits than soil N availability or soil pH. Interspecies variation is an important
933 factor to consider when deducing mechanisms that drive photosynthetic least-
934 cost theory, particularly for species that form distinct mycorrhizal associations or
935 have different photosynthetic pathways, growth forms, or leaf habit (Espelta et al.
936 2005; Adams et al. 2016; Bialic-Murphy et al. 2021; Scott and Smith 2022). The
937 need to consider species may also be important when comparing nutrient-water
938 use tradeoffs in early and late successional species, or in species with different
939 resource economic strategies (Abrams and Mostoller 1995; Ellsworth and Reich
940 1996; Wright et al. 2004; Reich 2014; Onoda et al. 2017; Ziegler et al. 2020).

941 A strength of the study design and sampling effort is that it controls for
942 many species differences that should modify nitrogen-water use tradeoffs expected
943 from theory. All tree species measured in this study shared the leaf habit of decid-
944 uous broadleaves, were growing in forests of similar successional stage, but differed
945 in mycorrhizal association and consequent resource economic strategies. As stands
946 tended to be dominated by trees that associate with arbuscular mycorrhizae (*Frax-*
947 *inus* and both *Acer* species made up 70% of total aboveground biomass across
948 stands), ecosystem biogeochemical cycle dynamics may be more closely aligned
949 to the inorganic nutrient economy proposed in Phillips et al. (2013), which may
950 promote stronger nitrogen-water use tradeoffs in tree species that associate with
951 arbuscular mycorrhizae. This result was not observed here, as photosynthetic
952 properties varied as much within as across the two mycorrhizal associations rep-
953 resented. Given the high variability in measured photosynthetic traits within
954 and across species, effects of mycorrhizal association likely require more intensive
955 sampling efforts to detect than were possible here.

956 3.4.4 *Implications for photosynthetic least-cost theory model development*

957 In the field, soil nutrient availability is heterogeneous across time and space
958 (Table S4). Unaccounted within-plot heterogeneity may have contributed to the
959 low amount of variation explained by soil N availability in our statistical mod-
960 els, as resin bags are a coarse surrogate for soil N availability. Despite this, we
961 still observed evidence for nutrient-water use tradeoffs, suggesting that observed
962 responses reported here may be an underestimate toward the net effect of soil
963 N availability on these tradeoffs. While we urge caution in the interpretation of

964 these results, they do provide a promising baseline for future studies investigating
965 patterns expected from photosynthetic least-cost theory at finer spatiotemporal
966 resolutions.

967 The general stronger relationship between leaf N content and photosynthetic parameters versus between leaf N content and soil N availability suggests
969 that leaf N content is more directly tied to photosynthesis than soil N availability.
970 While this could be due to the high spatiotemporal heterogeneity of soil N availability,
971 principles from photosynthetic least-cost theory suggest that leaf N content is the downstream product of leaf nutrient demand to build and maintain
973 photosynthetic machinery, which is set by aboveground environmental conditions
974 such as light availability, CO₂, temperature, or vapor pressure deficit (Smith
975 et al. 2019; Paillassa et al. 2020; Peng et al. 2021; Westerband et al. 2023). The
976 stronger relationship between leaf N and photosynthetic parameters paired with
977 the strong negative relationship between leaf N and χ could indicate a relatively
978 stronger effect of climate on leaf N-photosynthesis relationships than soil resource
979 availability. However, the short distance between plots and across sites limited
980 our ability to test this mechanism.

981 Variation in soil pH affected least cost responses less than variations in
982 soil N availability, in part because experimental treatments directly increased soil
983 N and affected soil pH in opposite directions. While soil pH has been shown
984 to drive nitrogen-water tradeoffs in global gradient analyses (Viet et al. 2013;
985 Paillassa et al. 2020), these responses may be due to covariations between soil pH
986 and nutrient cycling rather than a role of pH per se. The direct manipulations
987 of soil pH and soil N availability in this study allowed us to partly disentangle

988 these factors and show that variation in N availability matters more for least-cost
989 tradeoffs than pH alone.

990 3.4.5 *Conclusions*

991 Increasing soil N availability generally increased leaf N content (both area-
992 and mass-based), but did not significantly influence χ . This shift in leaf N led
993 to a reduction in PNUE, and an increase in leaf N per unit χ with increasing
994 soil N availability. Despite null effects of soil N availability on χ , we observed a
995 strong negative relationship between leaf N content and χ . These results provide
996 empirical support for the nutrient-water use tradeoffs expected from photosyn-
997 thetic least-cost theory in response to soil nutrient availability, but suggest that
998 all tenets of the theory may not hold in every environment. These results exper-
999 imentially test previous work suggesting that leaf water-nitrogen economies vary
1000 across gradients of soil nutrient availability and pH, and show that variations in
1001 nutrient availability matter more for determining variation in leaf photosynthetic
1002 traits than soil pH.

1003

Chapter 4

1004 The relative cost of resource use for photosynthesis drives variance in
1005 leaf nitrogen content across climate and soil resource availability
1006 gradients

1007 4.1 Introduction

1008 Terrestrial biosphere models, which comprise the land surface component of
1009 Earth system models, are sensitive to the formulation of photosynthetic processes
1010 (Knorr 2000; Ziehn et al. 2011; Booth et al. 2012). This is because photosynthe-
1011 sis is the largest carbon flux between the atmosphere and terrestrial biosphere,
1012 and is constrained by ecosystem carbon and nutrient cycles (Hungate et al. 2003;
1013 LeBauer and Treseder 2008; IPCC 2021; Fay et al. 2015). Many terrestrial bio-
1014 sphere models formulate photosynthesis by parameterizing photosynthetic capac-
1015 ity within plant functional groups through empirical linear relationships between
1016 area-based leaf nitrogen content (N_{area}) and the maximum carboxylation rate
1017 of Ribulose-1,5-bisphosphate carboxylase/oxygenase (Kattge et al. 2009; Rogers
1018 2014; Rogers et al. 2017). Models are also beginning to include connected carbon-
1019 nitrogen cycles (Wieder et al. 2015; Shi et al. 2016; Davies-Barnard et al. 2020;
1020 Braghieri et al. 2022), which allows leaf photosynthesis to be predicted directly
1021 through changes in N_{area} and indirectly through changes in soil nitrogen avail-
1022 ability (e.g., LPJ-GUESS, Smith et al., 2014; CLM5.0, Lawrence et al., 2019).
1023 Despite recent model developments, open questions remain regarding the gen-
1024 erality of ecological relationships between soil nitrogen availability, leaf nitrogen
1025 content, and leaf photosynthesis across edaphic and climatic gradients.
1026 Empirical support for positive relationships between soil nitrogen avail-

ability and N_{area} is abundant (Firn et al. 2019; Liang et al. 2020), and is a result often attributed to the high nitrogen cost of building and maintaining Rubisco (Evans 1989; Evans and Seemann 1989; Onoda et al. 2004; Onoda et al. 2017; Dong et al. 2020). Such patterns imply that positive relationships between soil nitrogen availability and N_{area} should cause an increase in leaf photosynthesis and photosynthetic capacity by increasing the maximum rate of Rubisco carboxylation through increased investments to Rubisco construction and maintenance. This integrated N_{area} -photosynthesis response to soil nitrogen availability has been observed both in manipulative experiments and across environmental gradients (Field and Mooney 1986; Evans 1989; Walker et al. 2014; Li et al. 2020), and is thought to be driven by ecosystem nitrogen limitation, which limits its primary productivity globally (LeBauer and Treseder 2008; Fay et al. 2015). However, this response is not consistently observed, as recent studies note variable N_{area} -photosynthesis relationships across soil nitrogen availability gradients (Liang et al. 2020; Luo et al. 2021) and that aboveground growing conditions (e.g., light availability, temperature, vapor pressure deficit) or species identity traits (e.g., photosynthetic pathway, nitrogen acquisition strategy) may be more important for explaining variance in N_{area} and photosynthetic capacity across time and space (Adams et al. 2016; Dong et al. 2017; Dong et al. 2020; Dong et al. 2022; Smith et al. 2019; Peng et al. 2021; Westerband et al. 2023).

1047 4.2 Methods

1048 4.2.1 textit{Site descriptions and sampling methodology}

1049 We collected leaf and soil samples from 24 open grassland sites across cen-
1050 tral and eastern Texas in summer 2020 and summer 2021 (Fig. 4.1). Twelve
1051 sites were visited between June and July 2020 and 14 sites (11 unique from 2020)
1052 were visited between May and June 2021 (Table 1). We explicitly chose sites
1053 that maximized variability in precipitation and edaphic variability between sites
1054 while minimizing temperature variability across the environmental gradient (Ta-
1055 ble 1). No site with personally communicated or anecdotal evidence of grazing
1056 or disturbance (e.g., mowing, feral hog activity, etc.) were used. We collected
1057 leaf material from three individuals each of the five most abundant species at ran-
1058 dom locations at each site, only selecting species that were broadly classified as
1059 graminoid, forb/herb, shrub, or subshrub growth habits per the USDA PLANTS
1060 database (USDA NRCS 2022). All collected leaves were fully expanded with no
1061 visible herbivory or other external damage and also free from shading by nearby
1062 shrubs or trees. Five soil samples were collected from 0-15cm below the soil sur-
1063 face at each site near the leaf collection sample locations. Soil samples were later
1064 mixed together by hand to create one composite soil sample per site.

1065 4.2.2 *Leaf trait measurements*

1066 Images of each leaf were taken immediately following each site visit using
1067 a flat-bed scanner. Fresh leaf area was determined from each image using the
1068 'LeafArea' R package (Katabuchi 2015), which automates leaf area calculations
1069 using ImageJ software (Schneider et al. 2012). Each leaf was dried at 65°C for at

1070 least 48 hours to a constant mass, weighed, and manually ground in a mortar and
1071 pestle until homogenized. Leaf mass per area (M_{area} ; g m⁻²) was calculated as the
1072 ratio of dry leaf biomass to fresh leaf area. Subsamples of dried and homogenized
1073 leaf tissue were used to measure leaf nitrogen content (N_{mass} ; gN g⁻¹) through el-
1074 emental combustion analysis (Costech-4010, Costech Instruments, Valencia, CA).
1075 Leaf nitrogen content per unit leaf area (N_{area} ; gN m⁻²) was then calculated as
1076 the product of N_{mass} and M_{area} .

1077 Subsamples of dried and homogenized leaf tissue were sent to the University
1078 of California-Davis Stable Isotope Facility to determine leaf $\delta^{13}\text{C}$. Leaf $\delta^{13}\text{C}$ values
1079 were determined using an elemental analyzer (PDZ Europa ANCA-GSL; Sercon
1080 Ltd., Chestshire, UK) interfaced to an isotope ratio mass spectrometer (PDZ
1081 Europa 20-20 Isotope Ratio Mass Spectrometer, Sercon Ltd., Chestshire, UK).
1082 We used leaf $\delta^{13}\text{C}$ values (‰; relative to Vienna Pee Dee Belemnite international
1083 reference standard) to estimate the ratio of intercellular (C_i) to extracellular (C_a)
1084 CO₂ ratio (leaf $C_i:C_a$, χ ; unitless) following the approach of Farquhar et al. (1989)
1085 described in Cernusak et al. (2013). We derived χ as:

$$\chi = \frac{C_i}{C_a} = \frac{\Delta^{13}\text{C} - a}{b - a} \quad (4.1)$$

1086 where $\Delta^{13}\text{C}$ represents the relative difference between leaf $\delta^{13}\text{C}$ (‰) and air $\delta^{13}\text{C}$
1087 (‰), and is calculated as:

$$\Delta^{13}\text{C} = \frac{\delta^{13}\text{C}_{\text{air}} - \delta^{13}\text{C}_{\text{leaf}}}{1 + \delta^{13}\text{C}_{\text{leaf}}} \quad (4.2)$$

1088 $\delta^{13}\text{C}_{\text{air}}$, traditionally assumed to be -8‰ (Keeling et al. 1979; Farquhar et al.

1089 1989), was calculated as a function of calendar year t using an empirical equation
1090 derived in Feng (1999):

$$\delta^{13}C_{air} = -6.429 - 0.006e^{0.0217(t-1740)} \quad (4.3)$$

1091 This calculation resulted in $\delta^{13}C_{air}$ values for 2020 and 2021 as -9.04 and -9.09,
1092 respectively. a represents the fractionation between ^{12}C and ^{13}C due to diffusion
1093 in air, assumed to be 4.4‰, and b represents the fractionation caused by Rubisco
1094 carboxylation, assumed to be 27‰ (Farquhar et al. 1989). For C_4 species, b in
1095 Eqn. 4.1 was set to 6.3‰, and was derived from:

$$b = c + (d \cdot \phi) \quad (4.4)$$

1096 Where c was set to -5.7‰ and d was set to 30‰ (Farquhar et al. 1989). ϕ , which
1097 is the bundle sheath leakiness term, was set to 0.4. All χ values less than 0.2 and
1098 greater than 1.0 were assumed to be incorrect and removed.

1099 We derived the unit cost of resource use (β) using leaf χ and site climate
1100 data with equations first described in Prentice et al. (2014) and simplified in
1101 Lavergne et al. (2020):

$$\beta = 1.6\eta^*D \frac{\chi - (\frac{\Gamma^*}{C_a})^2}{(1 - \chi)^2(K_m + \Gamma^*)} \quad (4.5)$$

1102 where η^* is the viscosity of water relative to 25°C, calculated using elevation and
1103 mean air temperature of the seven days leading up to each site visit following
1104 equations in Huber et al. (2009). D represents vapor pressure deficit (Pa), set

1105 to the mean vapor pressure deficit of the seven days leading up to each site visit,
1106 C_a represents atmospheric CO₂ concentration, arbitrarily set to 420 $\mu\text{mol mol}^{-1}$
1107 CO². K_m (Pa) is the Michaelis-Menten coefficient for Rubisco affinity to CO₂ and
1108 O₂, calculated as:

$$K_m = K_c \cdot \left(1 + \frac{O_i}{K_o}\right) \quad (4.6)$$

1109 where K_c (Pa) and K_o (Pa) are the Michaelis-Menten coefficients for Rubisco
1110 affinity to CO₂ and O₂, respectively, and O_i is the intercellular O₂ concentration.
1111 Γ^* (Pa) is the CO₂ compensation point in the absence of dark respiration. K_c , K_o ,
1112 and Γ^* were determined using equations described in Medlyn et al. (2002) and
1113 derived in Bernacchi et al. (2001), invoking an elevation correction for atmospheric
1114 pressure as explained in Stocker et al. (2020).

1115

placeholder for Table 1

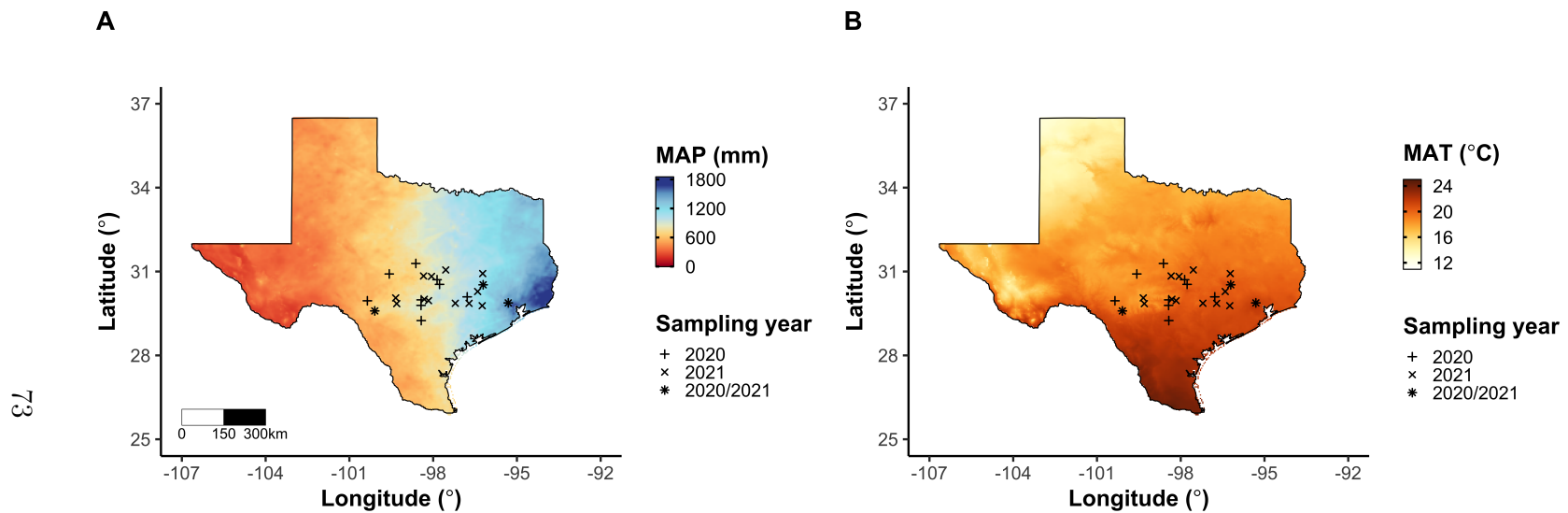


Figure 4.1. Maps that detail site locations along 2006-2020 mean annual precipitation (panel A) and mean annual temperature (panel B) gradients in Texas, USA. Precipitation and temperature data were plotted at a 4-km grid resolution and are masked to include only grid cells that occur in the Texas state boundary in the United States. In both panels, open circles refer to sites visited in 2020, open triangles to sites visited in 2021, and closed circles to sites visited in 2020 and 2021. The scale bar in panel A also applies to panel B.

1116 4.2.3 *Site climate data*

1117 We used the Parameter-elevation Regressions on Independent Slopes Model
1118 (PRISM) (Daly et al. 2008) climate product to access gridded daily temperature
1119 and precipitation data for the coterminous United States at a 4-km grid resolution
1120 between January 1, 2006 and July 31, 2021 (PRISM Climate Group, Oregon State
1121 University, <https://prism.oregonstate.edu>, data created 4 Feb 2014, accessed 24
1122 Mar 2022). Daily mean air temperature, mean VPD, and total precipitation
1123 data were extracted from the grid cell that contained the latitude and longitude
1124 of each property using the ‘extract’ function in the ‘terra’ R package (Hijmans
1125 2022). PRISM data were used in lieu of local weather station data because several
1126 rural sites did not have a local weather station present within a 20-km radius of
1127 the site. Daily site climate data were used to estimate mean annual precipitation
1128 and mean annual temperature for each site between 2006 and 2020 (Table 1). We
1129 then calculated total precipitation and mean daily VPD for the prior 1, 2, 3, 4, 5,
1130 6, 7, 8, 9, 10, 15, 20, 25, 30, 60, and 90 days leading up to each site visit.

1131 4.2.4 *Site edaphic characteristics*

1132 Subsamples of composited soil samples were sent to the Texas A & M
1133 Soil, Water and Forage Laboratory to quantify soil nitrate concentration (NO₃-N;
1134 ppm). Soil NO₃-N was determined by extracting composite soil samples in 1 M
1135 KCl, measuring absorbance values of extracts at 520 nm using the end product of
1136 a NO₃-N to NO₂-N cadmium reduction reaction (Kachurina et al. 2000). Soil tex-
1137 ture data from 0-15cm below the soil surface were accessed using the SoilGrids2.0
1138 data product (Poggio et al. 2021) through the ‘fetchSoilGrids’ function in the

1139 ‘soilDB’ R package (Beaudette et al. 2022). We used SoilGrids2.0 to access soil
1140 texture data in lieu of analyses using the collected composite soil sample due to
1141 a lack of soil material from some sites after sending samples for soil NO₃-N.

1142 Soil moisture was not measured in the field, but was estimated using
1143 the ‘Simple Process-Led Algorithms for Simulating Habitats’ model (‘SPLASH’)
1144 (Davis et al. 2017). This model, derived from the STASH model (Cramer and
1145 Prentice 1988), spins up a bucket model using Priestley-Taylor equations (Priest-
1146 ley and Taylor 1972) to calculate daily soil moisture (W_n ; mm) as a function
1147 of the previous day’s soil moisture (W_{n-1} ; mm), daily precipitation (P_n ; mm),
1148 condensation (C_n ; mm), actual evapotranspiration (E_n^a ; mm), and runoff (RO;
1149 mm):

$$W_n = W_{n-1} + P_n + C_n - E_n^a - RO \quad (4.7)$$

1150 Models were spun up by equilibrating the previous day’s soil moisture using
1151 successive model iterations with daily mean air temperature, daily precipitation
1152 total, the number of daily sunlight hours, and latitude as model inputs (Davis et al.
1153 2017). Daily sunlight hours were estimated for each day at each site using the
1154 ‘getSunlightTimes’ function in the ‘suncalc’ R package, which estimated sunrise
1155 and sunset times of each property using date and site coordinates (Thieurmel and
1156 Elmarhraoui 2019). Water holding capacity (mm), or bucket size, was estimated
1157 as a function of soil texture using pedotransfer equations explained in Saxton and
1158 Rawls (2006), as done in Stocker et al. (2020) and Bloomfield et al. (2022). A
1159 summary of these equations is included in the Supplemental Information.

1160 Daily soil moisture outputs from the SPLASH model for each site were
1161 used to calculate mean daily soil moisture for the prior 1, 2, 3, 4, 5, 6, 7, 8, 9,
1162 10, 15, 20, 25, 30, 60, and 90 days leading up to each site visit. Mean daily
1163 soil moisture values were then expressed as a fraction of water holding capacity
1164 to normalize across sites with different bucket depths, as done in Stocker et al.
1165 (2018).

1166 4.2.5 *Plant functional group assignments*

1167 Plant functional group was assigned to each species and used as the pri-
1168 mary descriptor of species identity. Specifically, we assigned plant functional
1169 groups based on photosynthetic pathway (C_3 , C_4) and ability to form associations
1170 with symbiotic nitrogen-fixing bacteria. The ability to form associations with
1171 symbiotic nitrogen-fixing bacteria was assigned based on whether species were in
1172 the *Fabaceae* family, and photosynthetic pathway of each species was determined
1173 from past literature and confirmed through leaf $\delta^{13}\text{C}$ values. We chose these plant
1174 functional groups based on *a priori* hypotheses regarding the functional role of
1175 nitrogen fixation and photosynthetic pathway on the sensitivity of plant nitrogen
1176 uptake and leaf nitrogen allocation to soil nutrient availability and aboveground
1177 growing conditions. These plant functional group classifications resulted in three
1178 distinct plant functional groups within our dataset: C_3 legumes ($n = 53$), C_3
1179 non-legumes ($n = 350$), and C_4 non-legumes ($n = 117$).

1180 4.2.6 *Data analysis*

1181 All analyses and plotting were conducted in R version 4.1.1 (R Core Team
1182 2021). We constructed a series of separate linear mixed-effects models to inves-
1183 tigate environmental drivers of β , χ , N_{area} , N_{mass} , and M_{area} , followed by a path
1184 analysis using a piecewise structural equation model to investigate direct and
1185 indirect effects of climate and soil resource availability on N_{area} .

1186 To explore environmental drivers of β , we built a linear mixed-effects model
1187 that included soil moisture, soil nitrogen availability, and plant functional group
1188 as fixed effect coefficients. Species were designated as a random intercept term.
1189 Interaction coefficients between all possible combinations of the three fixed effect
1190 coefficients were also included. β was natural log transformed to linearize data.
1191 We used an information-theoretic model selection approach to determine whether
1192 90-, 60-, 30-, 20-, 15-, 10-, 9-, 8-, 7-, 6-, 5-, 4-, 3-, 2-, or 1-day mean daily
1193 soil moisture conferred the best model fit for β . To do this, we constructed 16
1194 separate linear mixed-effects models where log-transformed β was included as the
1195 response variable and each soil moisture timestep was separately included as a
1196 single continuous fixed effect. Species were included as a random intercept term
1197 for all models. We used corrected Akaike Information Criterion (AICc) to select
1198 the soil moisture timescale that conferred the best model fit, indicated by the
1199 model with the lowest AICc score (Table S2; Fig. S2).

1200 To explore environmental drivers of χ , we constructed a second linear mixed
1201 effects model that included VPD, soil moisture, soil nitrogen availability, and plant
1202 functional group as fixed effect coefficients. Two-way interactions between plant
1203 functional group and VPD, soil nitrogen availability, or soil moisture were also

1204 included as fixed effect coefficients, in addition to a three-way interaction between
1205 soil moisture, soil nitrogen availability, and plant functional group. Species were
1206 included as a random intercept term. We used an information-theoretic model
1207 selection approach to determine whether 90-, 60-, 30-, 20-, 15-, 10-, 9-, 8-, 7-, 6-,
1208 5-, 4-, 3-, 2-, or 1-day mean daily VPD conferred the best model fit for χ using
1209 the same approach explained above for the soil moisture effect on β . The soil
1210 moisture timescale was set to the same timescale that conferred the best fit for β .

1211 To explore environmental drivers of N_{area} , N_{mass} , and M_{area} , we constructed
1212 three separate linear mixed effects model that each included χ , soil nitrogen avail-
1213 ability, soil moisture, and plant functional group as fixed effect coefficients. Two-
1214 way interactions between plant functional group and β , χ , soil nitrogen availability,
1215 or soil moisture were included as additional fixed effect coefficients, in addition to
1216 a three-way interaction between soil nitrogen availability, soil moisture, and plant
1217 functional group. Species were included as a random intercept term, with the soil
1218 moisture timescale set to the same timescale that conferred the best fit for β .

1219 In all linear mixed-effects models explained above, including those to select
1220 relevant timescales, we used the 'lmer' function in the 'lme4' R package (Bates
1221 et al. 2015) to fit each model and the 'Anova' function in the 'car' R package (Fox
1222 and Weisberg 2019) to calculate Type II Wald's χ^2 and determine the significance
1223 level ($\alpha = 0.05$) of each fixed effect coefficient. We also used the 'emmeans'
1224 R package (Lenth 2019) to conduct post-hoc comparisons using Tukey's tests,
1225 where degrees of freedom were approximated using the Kenward-Roger approach
1226 (Kenward and Roger 1997). Trendlines and error ribbons for all plots were drawn
1227 using a series of 'emmeans' outputs across the range in plotted x-axis values.

Finally, we conducted a path analysis using a piecewise structural equation model to examine direct and indirect pathways that determined variance in N_{area} . Seven separate linear mixed effects models were loaded into the piecewise structural equation model. Models were constructed per our *a priori* hypotheses following patterns expected from photosynthetic least-cost theory. The first model regressed N_{area} against χ , N_{mass} , and M_{area} . The second model regressed M_{area} against χ . The third model regressed N_{mass} against χ and M_{area} (Dong et al. 2017; Dong et al. 2020). The fourth model regressed χ against β and VPD. The fifth model regressed β against soil nitrogen availability, soil moisture, ability to associate with symbiotic nitrogen-fixing bacteria, and photosynthetic pathway. The sixth model regressed soil nitrogen availability against soil moisture, while the seventh model regressed VPD against soil moisture (Novick et al. 2016; Sulman et al. 2016). All models included the relevant timescale selected in the individual linear mixed effect models explained above (2-day soil moisture, 4-day vapor pressure deficit). Models also included species as a random intercept term, were built using the ‘lme’ function in the ‘nlme’ R package (Pinheiro and Bates 2022), and subsequently loaded into the piecewise structural equation model using the ‘psem’ function in the ‘piecewiseSEM’ R package (Lefcheck 2016).

1246 4.3 Results

1247 4.3.1 Cost to acquire nitrogen relative to water (β)

Model selection indicated that 2-day soil moisture was the timescale that conferred the best model fit for β ($AIC_c = 1227.83$; Table S2; Fig. S1). Increasing soil nitrogen availability generally decreased β ($p < 0.001$; Table 2), a

1251 pattern driven by a negative effect of increasing soil nitrogen availability on β in
1252 C₃ nonlegumes (Tukey: $p < 0.001$) and C₃ legumes (Tukey: $p = 0.004$; Fig. 2a).
1253 C₄ nonlegumes also demonstrated a negative trend in the effect of increasing soil
1254 nitrogen availability on β , but this pattern was not significantly different from
1255 zero (Tukey: $p = 0.307$; Fig. 2a). There was no apparent effect of soil moisture
1256 on β ($p = 0.264$; Table 1; Fig. 2b). A functional group effect ($p < 0.001$; Ta-
1257 ble 1) indicated that C₄ nonlegumes generally had lower β values than both C₃
1258 legumes and C₃ non-legumes when averaged across soil moisture and soil nitrogen
1259 availability values (Tukey: $p < 0.001$ in both cases), while average β values in C₃
1260 legumes did not differ from C₃ nonlegumes (Tukey: $p = 0.691$).

1261

placeholder Table 2

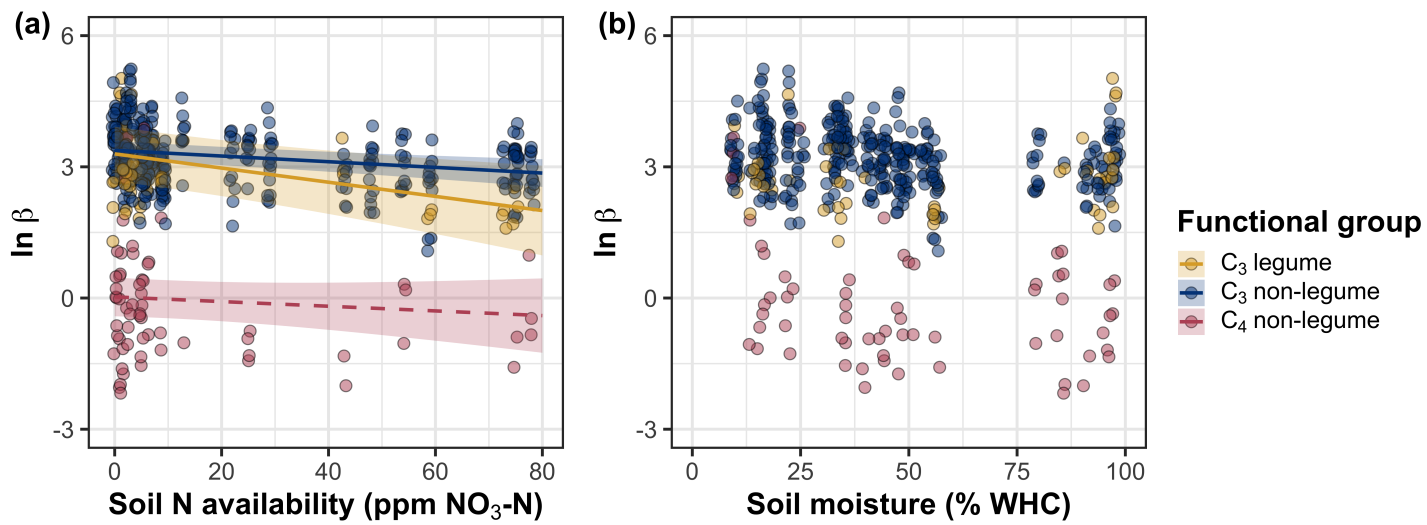


Figure 4.2. Effects of soil nitrogen availability (a) and soil moisture (b) on the unit cost ratio β . In (b), soil moisture is represented as a percent of site water holding capacity. Yellow shading and trendlines indicate C₃ legumes, blue shading and trendlines indicate C₃ non-legumes, and red shading and trendlines indicate C₄ non-legumes. Points are jittered for visibility. Variably colored trendlines are only included if there is an interaction between the x-axis and plant functional group, where solid trendlines indicate slopes that are different from zero ($p < 0.05$) and dashed trendlines indicate slopes that are not different from zero ($p > 0.05$). Error ribbons represent the upper and lower 95% confidence intervals of each fitted trendline.

1262 4.3.2 *Leaf C_i:C_a*

1263 Model selection indicated that 4-day daily VPD was the timescale that
1264 conferred the best model fit for χ (AICc = -883.97; Table S1; Fig. S2).

1265 Variance in χ was driven by a series of two-way interactions between func-
1266 tional group and VPD ($p = 0.006$; Table 3), soil moisture ($p = 0.033$, Table 3),
1267 and soil nitrogen availability ($p = 0.022$; Table 3). The interaction between 4-day
1268 VPD and functional group revealed that the general negative effect of increasing
1269 VPD ($p < 0.001$; Table 3) was driven by a negative effect of increasing VPD
1270 on χ in C₃ nonlegumes (Tukey: $p < 0.001$) and marginal negative effect in C₃
1271 legumes (Tukey: $p = 0.074$) paired with a positive trending, but insignificant
1272 effect of increasing VPD in C₄ nonlegumes (Tukey: $p = 0.130$; Fig. 3a). The
1273 interaction between 2-day soil moisture and functional group indicated that the
1274 general negative effect of increasing soil moisture on χ was driven by a positive
1275 effect of increasing soil moisture on χ in C₄ nonlegumes (Tukey: $p = 0.009$) de-
1276 spite a positive trending but insignificant effect of increasing soil moisture on χ
1277 in C₃ legumes (Tukey: $p = 0.116$) and a null effect of soil moisture on χ in C₃
1278 nonlegumes (Tukey: $p = 0.693$; Fig. 3c). The interaction between soil nitrogen
1279 availability and plant functional group revealed a weak negative effect of increas-
1280 ing soil nitrogen availability on χ in C₃ legumes (Tukey: $p = 0.045$), with no
1281 apparent effect in C₃ nonlegumes (Tukey: $p = 0.706$) or C₄ nonlegumes (Tukey:
1282 $p = 0.757$). Finally, an individual effect of functional group ($p < 0.001$; Table 3)
1283 revealed that C₄ nonlegumes generally had lower χ than C₃ legumes and C₃ non-
1284 legumes (Tukey: $p < 0.001$ in both cases), with no apparent difference between
1285 C₃ legumes and C₃ nonlegumes (Tukey: $p = 0.831$).

1286

placeholder Table 3

1287 4.3.3 *Leaf nitrogen content*

1288 An interaction between χ and plant functional group ($p < 0.001$; Table
1289 4) revealed that the general negative effect of increasing χ on N_{area} ($p < 0.001$;
1290 Table 4) was driven by a negative effect of increasing χ on N_{area} in C₃ nonlegumes
1291 (Tukey: $p < 0.001$) and C₃ legumes (Tukey: $p = 0.002$) despite a null effect of χ
1292 on N_{area} in C₄ nonlegumes (Tukey: $p = 0.795$; Fig. 4a). An interaction between
1293 soil nitrogen availability and soil moisture ($p = 0.028$; Table 4) indicated that the
1294 marginal positive effect of increasing soil nitrogen availability on N_{area} ($p = 0.091$;
1295 Table 4) decreased with increasing soil moisture, despite no apparent individual
1296 effect of soil moisture on N_{area} ($p = 0.692$; Table 4). Finally, a plant functional
1297 group effect ($p < 0.001$; Table 4) indicated that C₄ nonlegumes had lower N_{area}
1298 values on average compared to C₃ legumes (Tukey: $p < 0.001$) and C₃ nonlegumes
1299 (Tukey: $p = 0.001$), while C₃ legumes had lower average N_{area} values compared
1300 to C₃ nonlegumes (Tukey: $p = 0.012$).

1301 A marginal interaction between χ and plant functional group ($p = 0.088$;
1302 Table 4) revealed that, despite no apparent general effect of χ on N_{mass} ($p = 0.273$;
1303 Table 4), increasing χ decreased N_{mass} in C₃ nonlegumes (Tukey: $p = 0.021$), but
1304 this effect was not apparent in C₄ nonlegumes (Tukey: $p = 0.693$) or C₃ legumes
1305 (Tukey: $p = 0.477$). An interaction between soil nitrogen availability and soil
1306 moisture ($p < 0.001$; Table 4) indicated that the general positive effect of increas-
1307 ing soil nitrogen availability on N_{mass} ($p < 0.001$; Table 4) generally decreased
1308 with increasing soil moisture, despite an apparent general positive effect of in-
1309 creasing soil moisture on N_{mass} ($p < 0.001$; Table 4). This interaction indicated
1310 that the positive effect of increasing soil nitrogen availability on N_{mass} was only

1311 apparent when soil moisture was less than 70% the maximum water holding ca-
1312 pacity (Tukey: $p < 0.05$ in all cases) despite a positive effect of increasing soil
1313 moisture on N_{mass} ($p < 0.001$; Table 4). Finally, a plant functional group effect
1314 ($p < 0.001$; Table 4) indicated that C₄ nonlegumes had lower N_{mass} values on
1315 average compared to C₃ legumes (Tukey: $p = 0.002$) and C₃ nonlegumes (Tukey:
1316 $p = 0.019$), while N_{mass} did not differ between C₃ legumes and C₃ nonlegumes
1317 (Tukey: $p = 0.149$).

1318 An interaction between χ and functional group ($p = 0.005$; Table 4) indi-
1319 cated that the general negative effect of increasing χ on M_{area} ($p < 0.001$; Table
1320 4; Fig. 4c) was driven by a negative effect of increasing χ on M_{area} in C₃ legumes
1321 and C₃ nonlegumes (Tukey: $p < 0.001$ in both cases) despite a nonsignificant
1322 effect of increasing χ on M_{area} in C₄ nonlegumes (Tukey: $p = 0.724$). An in-
1323 teraction between soil nitrogen and soil moisture ($p < 0.001$; Table 4) indicated
1324 that the general negative effect of increasing soil nitrogen availability on M_{area} (p
1325 < 0.001 ; Table 4) decreased with increasing soil moisture, despite an apparent
1326 general negative effect of increasing soil moisture on M_{area} ($p = 0.002$; Table 4).
1327 Specifically, the negative effect of increasing soil nitrogen availability on M_{area} was
1328 only apparent when soil moisture was less than 65% the maximum water holding
1329 capacity (Tukey: $p < 0.05$ in all cases). An additional interaction between soil
1330 nitrogen availability and functional group ($p = 0.034$; Table 4) indicated that the
1331 general negative effect of increasing soil nitrogen availability on M_{area} was driven
1332 by decreases in C₃ nonlegumes (Tukey: $p < 0.001$) and C₄ nonlegumes (Tukey:
1333 $p = 0.003$), with no apparent effect of soil nitrogen availability on M_{area} in C₃
1334 legumes (Tukey: $p = 0.997$).

1335

placeholder Table 4

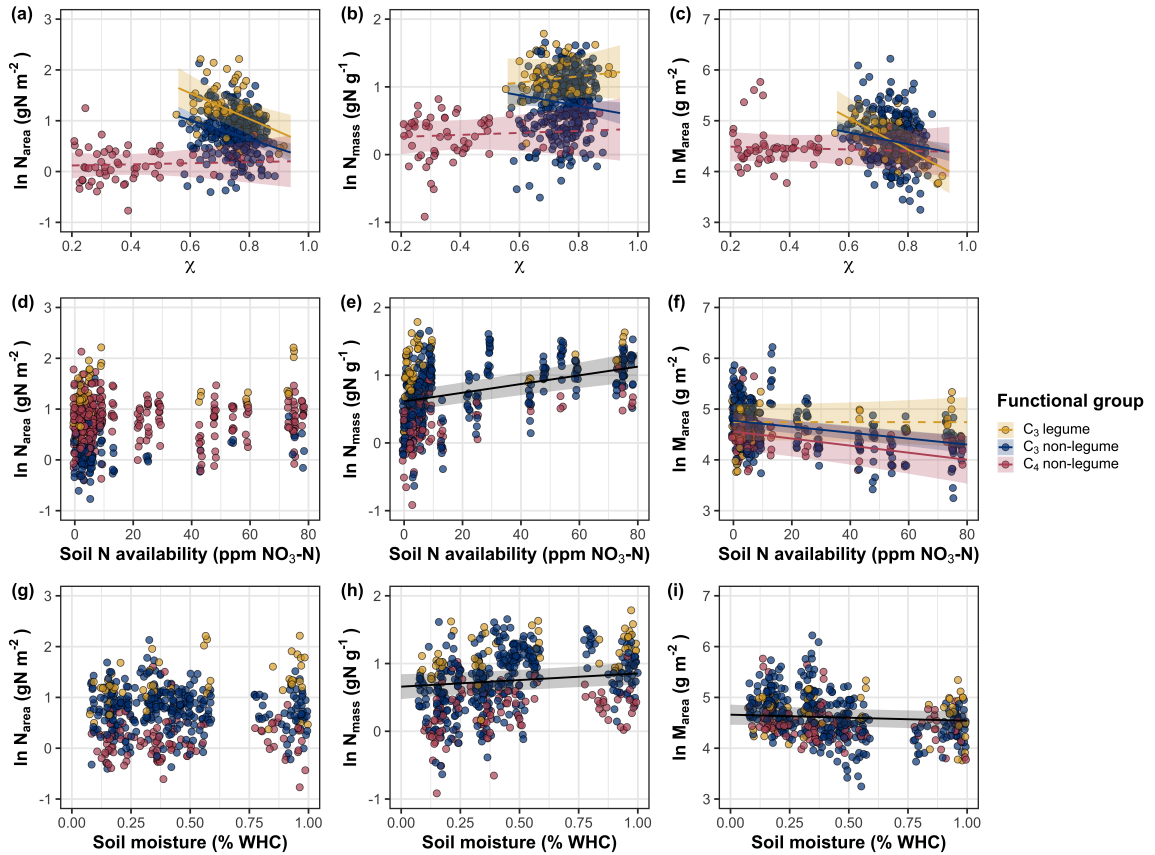


Figure 4.4. Effects of χ (a-c), soil nitrogen availability (d-f), and soil moisture (g-i) on leaf nitrogen content per unit leaf area (a, d, g), leaf nitrogen content per unit leaf biomass (b, e, h), and leaf mass per area (c, f, i). A solid black trendline indicates the bivariate relationship between the fixed effect the x-axis and response variable on the y-axis and is only included when there is no interaction between the x-axis and plant functional group.

1336 4.3.4 *Structural equation model*

1337 The piecewise structural equation model explained 90%, 54%, 80%, 92%,
1338 and 41% of variance in N_{area} , N_{mass} , M_{area} , χ , and β , respectively (Table 5; Fig.
1339 5). Variance in N_{area} was driven by a negative effect of increasing χ ($p < 0.001$;
1340 Table 5) paired with positive effects of increasing N_{mass} and M_{area} ($p < 0.001$ in
1341 both cases; Table 5; Fig. 5). Model results indicated that the negative effect
1342 of χ on N_{area} was driven by a strong reduction in M_{area} with increasing χ ($p <$
1343 0.001; Table 5) paired with no change in χ due to Nmass ($p = 0.150$; Table 5).
1344 However, there was a strong negative effect of increasing M_{area} on N_{mass} ($p <$
1345 0.001; Table 5; Fig. 5). χ generally increased with increasing β ($p < 0.001$; Table
1346 5) and decreased with increasing VPD ($p < 0.001$; Table 5; Fig. 5). Variance in β
1347 was driven by a negative effect of increasing soil nitrogen availability ($p < 0.001$;
1348 Table 5) and was generally higher in C₃ species ($p < 0.001$; Table 5; Fig. 5).
1349 However, β did not change with soil moisture ($p = 0.332$; Table 5) or with ability
1350 to acquire nitrogen via symbiotic nitrogen fixation ($p = 0.546$; Table 5). Finally,
1351 soil nitrogen availability was positively associated with increasing soil moisture (p
1352 < 0.001 ; Table 5; Fig. 5), while VPD was negatively associated with increasing
1353 soil moisture ($p < 0.001$; Table 5; Fig. 5).

1354

placeholder Table 5

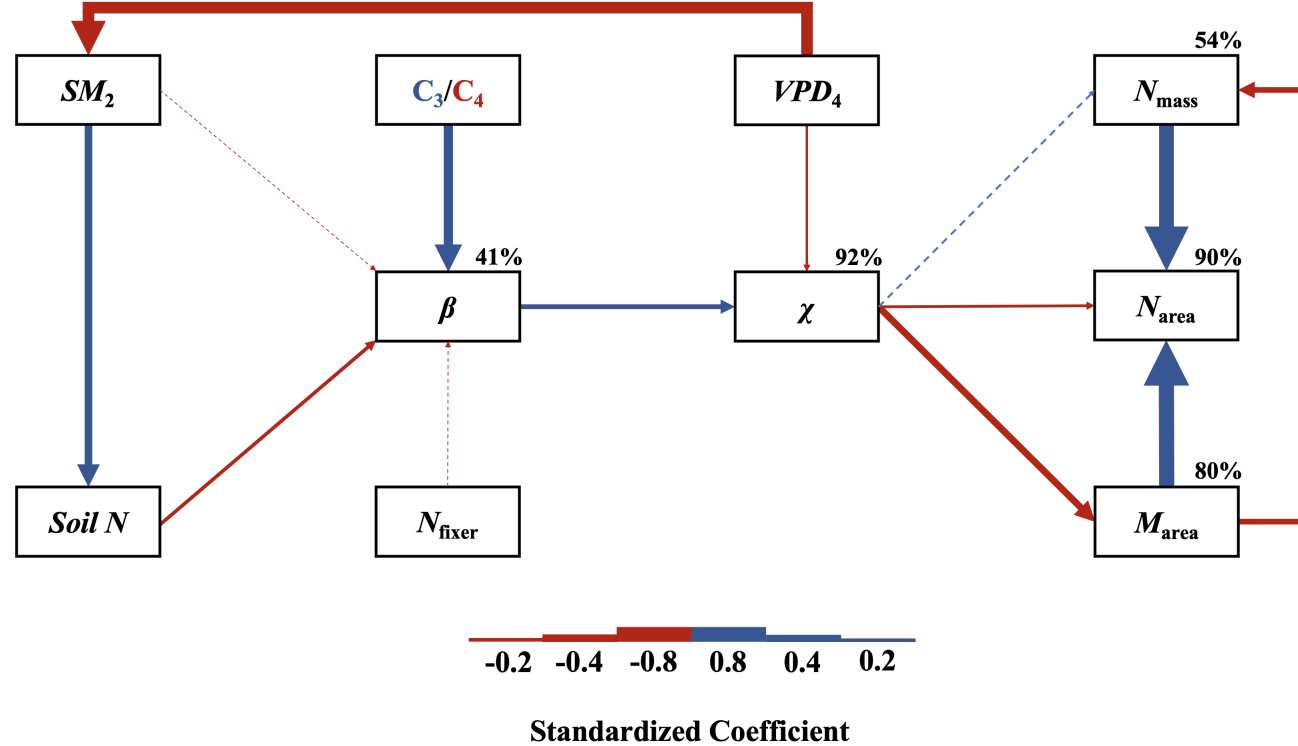


Figure 4.5. Structural equation model results exploring direct and indirect drivers of N_{area} . Boxes indicate measured edaphic factors, climatic factors, and leaf traits. Percentages above boxes indicate conditional R^2 values of each respective leaf trait. Solid arrows indicate bivariate relationships where $p < 0.05$, while dashed arrows indicate bivariate relationships where $p > 0.05$. Positive model coefficients are indicated through blue arrows, while negative model coefficients are indicated through red arrows. Arrow thickness scales with the standardized model coefficient of each bivariate relationship. A positive coefficient for photosynthetic pathway indicates generally larger values in C_3 species, while a positive coefficient for N_{fixer} indicates generally larger values in N-fixing species. Standardized model coefficients and associated p -values are reported in Table 5.

1355 4.4 Discussion

1356

Chapter 5

1357
1358

Optimal resource investment to photosynthetic capacity maximizes
nutrient allocation to whole plant growth under elevated CO₂

1359 5.1 Introduction

1360 Terrestrial ecosystems are regulated by complex carbon and nitrogen cy-
1361 cles. As a result, terrestrial biosphere models, which are beginning to include
1362 coupled carbon and nitrogen cycles (Shi et al. 2016; Davies-Barnard et al. 2020;
1363 Braghieri et al. 2022), must accurately represent these cycles under different
1364 environmental scenarios to reliably simulate carbon and nitrogen atmosphere-
1365 biosphere fluxes (Hungate et al. 2003; Prentice et al. 2015). While the inclusion
1366 of coupled carbon and nitrogen cycles tends to reduce model uncertainty (Arora
1367 et al. 2020), large uncertainty in role of soil nitrogen availability and nitrogen ac-
1368 quisition strategy on leaf and whole plant acclimation responses to CO₂ remains
1369 (Smith and Dukes 2013; Terrer et al. 2018; Smith and Keenan 2020). This source
1370 of uncertainty likely contributes to the widespread divergence in future carbon
1371 and nitrogen flux simulations across terrestrial biosphere models (Friedlingstein
1372 et al. 2014; Zaehle et al. 2014; Meyerholt et al. 2020).

1373 Plants grown under elevated CO₂ generally have less leaf nitrogen content
1374 than those grown under ambient CO₂, a response that often corresponds with
1375 reductions in photosynthetic capacity and stomatal conductance at the leaf-level
1376 and biomass stimulation over time at the whole plant level (Curtis 1996; Drake
1377 et al. 1997; Ainsworth et al. 2002; Makino 2003; Morgan et al. 2004; Ainsworth
1378 and Long 2005; Ainsworth and Rogers 2007; Smith and Dukes 2013; Poorter et al.
1379 2022). As net primary productivity is generally limited by nitrogen availability

1380 (Vitousek and Howarth 1991; LeBauer and Treseder 2008; Fay et al. 2015), and
1381 soil nitrogen availability is often positively correlated with leaf nitrogen content
1382 and photosynthetic capacity (Field and Mooney 1986; Evans and Seemann 1989;
1383 Evans 1989; Walker et al. 2014; Firn et al. 2019; Liang et al. 2020), some
1384 have hypothesized that leaf and whole plant acclimation responses to CO₂ are
1385 constrained by soil nitrogen availability. The progressive nitrogen limitation hy-
1386 pothesis predicts that elevated CO₂ will increase plant nitrogen demand, which
1387 will increase plant nitrogen uptake and progressively deplete soil nitrogen if soil
1388 nitrogen supply does not exceed plant nitrogen demand (Luo et al. 2004). The
1389 hypothesis predicts that this response should result in strong acute stimulations in
1390 whole plant growth and primary productivity that diminish over time as nitrogen
1391 becomes more limiting. Assuming a positive relationship between soil nitrogen
1392 availability, leaf nitrogen content, and photosynthetic capacity, this hypothesis
1393 also implies that progressive reductions in soil nitrogen availability should be the
1394 mechanism that drives the downregulation in leaf nitrogen content and photosyn-
1395 thetic capacity under elevated CO₂. This hypothesis has received some support
1396 from free air CO₂ enrichment experiments (Reich et al. 2006; Norby et al. 2010),
1397 although is not consistently observed across experiments (Finzi et al. 2006; Moore
1398 et al. 2006; Liang et al. 2016).

1399 While possible that progressive nitrogen limitation may determine leaf and
1400 whole plant acclimation responses to CO₂, growing evidence indicates that leaf ni-
1401 trogen and photosynthetic capacity are more strongly determined through above-
1402 ground growing conditions than by soil resource availability (Dong et al. 2017;
1403 Dong et al. 2020; Dong et al. 2022; Smith et al. 2019; Smith and Keenan 2020;

1404 Paillassa et al. 2020; Peng et al. 2021; Querejeta et al. 2022; Westerband et al.
1405 2023), and satellite-derived chlorophyll fluorescence data indicate that increasing
1406 atmospheric CO₂ may decrease leaf and canopy demand for nitrogen (Dong et al.
1407 2022). Together, results from these studies suggest that the downregulation in
1408 leaf nitrogen content and photosynthetic capacity due to increasing CO₂ may not
1409 be as tightly linked to progressive nitrogen limitation as previously hypothesized.

1410 A unification of optimal coordination and photosynthetic least-cost the-
1411 ories predicts that leaves acclimate to elevated CO₂ by downregulating nitrogen
1412 allocation to Ribulose-1,5-bisphosphate (RuBP) carboxylase/oxygenase (Rubisco)
1413 to optimize resource use efficiencies at the leaf level, which allows for greater re-
1414 source allocation to whole plant growth (Drake et al. 1997; Wright et al. 2003;
1415 Prentice et al. 2014; Smith et al. 2019). The theory predicts that the downregu-
1416 lation in nitrogen allocation to Rubisco results in a stronger downregulation in the
1417 maximum rate of Rubisco carboxylation (V_{cmax}) than the maximum rate of RuBP
1418 regeneration (J_{max}), which maximizes photosynthetic efficiency by allowing net
1419 photosynthesis rates to be equally co-limited by Rubisco carboxylation and RuBP
1420 regeneration (Chen et al. 1993; Maire et al. 2012). This acclimation response
1421 allows plants to make more efficient use of available light while avoiding overin-
1422 vestment in Rubisco, which has high nitrogen and energetic costs of building and
1423 maintaining (Evans 1989; Evans and Clarke 2019). Instead, additional acquired
1424 resources not needed to optimize leaf photosynthesis are allocated to the mainte-
1425 nance of structures that support whole plant growth (e.g., total leaf area, whole
1426 plant biomass, etc.) or to allocation processes not related to leaf photosynthesis
1427 or growth, such as plant defense mechanisms or leaf structural tissue. Regardless,

1428 optimized resource allocation at the leaf level should allow for greater resource
1429 allocation to whole plant growth. The theory indicates that leaf acclimation re-
1430 sponses to CO₂ should be independent of changes in soil nitrogen availability.
1431 While this leaf acclimation response maximizes nitrogen allocation to structures
1432 that support whole plant growth, the theory suggests that the positive effect of
1433 elevated CO₂ on whole plant growth may be further stimulated by soil nitrogen
1434 availability through a reduction in the cost of acquiring nitrogen (Bae et al. 2015;
1435 Perkowski et al. 2021; Lu et al. 2022).

1436 Plants acquire nitrogen by allocating photosynthetically derived carbon be-
1437 lowground in exchange for nitrogen through different nitrogen acquisition strate-
1438 gies. These nitrogen acquisition strategies can include direct uptake pathways
1439 such as mass flow or diffusion (Barber 1962), symbioses with mycorrhizal fungi or
1440 symbiotic nitrogen-fixing bacteria (Vance and Heichel 1991; Marschner and Dell
1441 1994; Smith and Read 2008; Udvardi and Poole 2013), or through the release
1442 of root exudates that prime free-living soil microbial communities (Phillips et al.
1443 2011; Wen et al. 2022). Plants cannot acquire nitrogen without first allocating
1444 carbon belowground, which implies an inherent carbon cost to the plant for acquir-
1445 ing nitrogen regardless of nitrogen acquisition strategy. Carbon costs to acquire
1446 nitrogen often vary in species with different nitrogen acquisition strategies and
1447 are dependent on external environmental factors such as atmospheric CO₂, light
1448 availability, and soil nitrogen availability (Brzostek et al. 2014; Terrer et al. 2016;
1449 Terrer et al. 2018; Allen et al. 2020; Perkowski et al. 2021; Lu et al. 2022), which
1450 suggests that acquisition strategy may be an important factor in determining ef-
1451 fects of soil nitrogen availability on leaf and whole plant acclimation responses to

1452 elevated CO₂.

1453 A recent meta-analysis using data across 20 grassland and forest CO₂ en-
1454 richment experiments suggested that species which acquire nitrogen from sym-
1455 biotic nitrogen-fixing bacteria had reduced costs of nitrogen acquisition under
1456 elevated CO₂ (Terrer et al. 2018). Findings from this meta-analysis indicated
1457 that reductions in costs of nitrogen acquisition in species that form associations
1458 with symbiotic nitrogen-fixing bacteria under elevated CO₂ may drive stronger
1459 stimulations in whole plant growth and downregulations in V_{cmax} than species that
1460 associate with arbuscular mycorrhizal fungi (Smith and Keenan 2020), which gen-
1461 erally have higher costs of nitrogen acquisition under elevated CO₂ (Terrer et al.
1462 2018). However, plant investments in symbiotic nitrogen fixation generally de-
1463 cline with increasing nitrogen availability (Dovrat et al. 2018; Perkowski et al.
1464 2021), a response that has been previously inferred to be the result of a shift in
1465 the dominant mode of nitrogen acquisition to direct uptake pathways as costs of
1466 direct uptake decrease with increasing soil nitrogen availability (Rastetter et al.
1467 2001; Perkowski et al. 2021). Thus, effects of symbiotic nitrogen fixation on plant
1468 acclimation responses to CO₂ should decline with increasing soil nitrogen avail-
1469 ability, although manipulative experiments that directly test these patterns are
1470 rare.

1471 Here, we conducted a 7-week growth chamber experiment using *Glycine*
1472 *max* L. (Merr.) to examine the effects of soil nitrogen fertilization and inocula-
1473 tion with symbiotic nitrogen-fixing bacteria on leaf and whole plant acclimation
1474 responses to elevated CO₂. Following patterns expected from theory, we hypoth-
1475 esized that individual leaves should acclimate to elevated CO₂ by more strongly

1476 downregulating V_{cmax} relative to J_{max} , allowing leaf photosynthesis to approach
1477 optimal coordination. We expected this response to correspond with a stronger
1478 downregulation in leaf nitrogen content than V_{cmax} and J_{max} , which would in-
1479 crease the fraction of leaf nitrogen content allocated to photosynthesis and photo-
1480 synthetic nitrogen use efficiency. At the whole-plant level, we hypothesized that
1481 plants would acclimate to elevated CO₂ by stimulating whole plant growth and
1482 productivity, a response that would be driven by a strong positive response of
1483 total leaf area and aboveground biomass to elevated CO₂. We predicted that
1484 leaf acclimation responses to elevated CO₂ would be independent of soil nitro-
1485 gen fertilization and inoculation with symbiotic nitrogen-fixing bacteria; however,
1486 we expected that increasing soil nitrogen fertilization would increase the posi-
1487 tive effect of elevated CO₂ on measures of whole plant growth due to a stronger
1488 reduction in the cost of acquiring nitrogen under elevated CO₂ with increasing
1489 fertilization. We also expected stronger stimulations in whole plant growth due
1490 to inoculation, but that this effect would only be apparent under low fertilization
1491 due to a reduction in root nodulation with increasing fertilization.

1492 5.2 Methods

1493 5.2.1 *Seed treatments and experimental design*

1494 *Glycine max* L. (Merr) seeds were planted in 144 6-liter surface sterilized
1495 pots (NS-600, Nursery Supplies, Orange, CA, USA) containing a steam-sterilized
1496 70:30 v:v mix of Sphagnum peat moss (Premier Horticulture, Quakertown, PA,
1497 USA) to sand (Pavestone, subsidiary of Quikrete Companies, Atlanta, GA, USA).
1498 Before planting, all *G. max* seeds were surface sterilized in 2% sodium hypochlorite

1499 for 3 minutes, followed by three separate 3-minute washes with ultrapure water
1500 (MilliQ 7000; MilliporeSigma, Burlington, MA USA). A subset of surface steril-
1501 ized seeds were inoculated with *Bradyrhizobium japonicum* (Verdesian N-Dure™
1502 Soybean, Cary, NC, USA) in a slurry following manufacturer recommendations
1503 (3.12 g inoculant and 241 g deionized water per 1 kg seed).

1504 Seventy-two pots were randomly planted with surface-sterilized seeds inoc-
1505 ulated with *B. japonicum*, while the remaining 72 pots were planted with surface-
1506 sterilized uninoculated seeds. Thirty-six pots within each inoculation treatment
1507 were randomly placed in one of two atmospheric CO₂ treatments (ambient and
1508 1000 μmol mol⁻¹ CO₂). Pots within each unique inoculation-by-CO₂ treatment
1509 combination randomly received one of nine soil nitrogen fertilization treatments
1510 equivalent to 0, 35, 70, 105, 140, 210, 280, 350, or 630 ppm N. Nitrogen fertil-
1511 ization treatments were created using a modified Hoagland solution (Hoagland
1512 and Arnon 1950) designed to keep concentrations of other macronutrients and
1513 micronutrients equivalent across treatments (Table S1). Pots received the same
1514 fertilization treatment throughout the entire duration experiment, which were ap-
1515 plied twice per week in 150 mL doses as topical agents to the soil surface through-
1516 out the duration of the experiment. This experimental design yielded a fully
1517 factorial experiment with four replicates per unique fertilization-by-inoculation-
1518 by-CO₂ combination.

1519 5.2.2 *Growth chamber conditions*

1520 Upon experiment initiation, pots were randomly placed in one of six Per-
1521 cival LED-41L2 growth chambers (Percival Scientific Inc., Perry, IA, USA) over

1522 two experimental iterations due to chamber space limitation. two iterations were
1523 conducted such that one iteration included all elevated CO₂ pots and the second
1524 iteration included all ambient CO₂ pots. Average (\pm SD) CO₂ concentrations
1525 across chambers throughout the experiment were $439 \pm 5 \mu\text{mol mol}^{-1}$ for the
1526 ambient CO₂ treatment and $989 \pm 4 \mu\text{mol mol}^{-1}$ for the elevated CO₂ treatment.

1527 Daytime growing conditions were simulated using a 16-hour photoperiod,
1528 with incoming light radiation set to chamber maximum (mean \pm SD: 1240 ± 32
1529 $\mu\text{mol m}^{-2} \text{s}^{-1}$ across chambers), air temperature set to 25°C, and relative humid-
1530 ity set to 50%. The remaining 8 hours simulated nighttime growing conditions,
1531 with incoming light radiation set to 0 $\mu\text{mol m}^{-2} \text{s}^{-1}$, chamber temperature set
1532 to 17°C, and relative humidity set to 50%. Transitions between daytime and
1533 nighttime growing conditions were simulated by ramping incoming light radiation
1534 in 45-minute increments and temperature in 90-minute increments over a 3-hour
1535 period (Table S2).

1536 Including the two, 3-hour ramping periods, pots grew under average (\pm
1537 SD) daytime light intensity of $1049 \pm 27 \mu\text{mol m}^{-2} \text{s}^{-1}$. In the elevated CO₂
1538 iteration, pots grew under $24.0 \pm 0.2^\circ\text{C}$ during the day, $16.4 \pm 0.8^\circ\text{C}$ during the
1539 night, and $51.6 \pm 0.4\%$ relative humidity. In the ambient CO₂ iteration, pots grew
1540 under $23.9 \pm 0.2^\circ\text{C}$ during the day, $16.0 \pm 1.4^\circ\text{C}$ during the night, and $50.3 \pm 0.2\%$
1541 relative humidity. We accounted for climatic differences across the six chambers
1542 by shuffling the same group of pots daily throughout the growth chambers. This
1543 process was done by iteratively moving the group of pots on the top rack of a
1544 chamber to the bottom rack of the same chamber, while simultaneously moving
1545 the group of pots on the bottom rack of a chamber to the top rack of the adjacent

1546 chamber. We moved pots within and across chambers every day throughout the
1547 course of each experiment iteration.

1548 5.2.3 *Leaf gas exchange measurements*

1549 Gas exchange measurements were collected for all individuals on the sev-
1550 enth week of development. All gas exchange measurements were collected on
1551 the center leaf of the most recent fully expanded trifoliate leaf set. Specifi-
1552 cally, we measured net photosynthesis (A_{net} ; $\mu\text{mol m}^{-2} \text{s}^{-1}$), stomatal conduc-
1553 tance (g_{sw} ; $\text{mol m}^{-2} \text{s}^{-1}$), and intercellular CO_2 (C_i ; $\mu\text{mol mol}^{-1}$) concentrations
1554 across a range of atmospheric CO_2 concentrations (i.e., an A_{net}/C_i curve) using the
1555 Dynamic Assimilation Technique™. The Dynamic Assimilation Technique™ has
1556 been shown to correspond well with traditional steady-state CO_2 response curves
1557 in *G. max* (Saathoff and Welles 2021). A_{net}/C_i curves were generated along a
1558 reference CO_2 ramp down from $420 \mu\text{mol mol}^{-1} \text{CO}_2$ to $20 \mu\text{mol mol}^{-1} \text{CO}_2$, fol-
1559 lowed by a ramp up from $420 \mu\text{mol mol}^{-1} \text{CO}_2$ to $1620 \mu\text{mol mol}^{-1} \text{CO}_2$ after
1560 a 90-second wait period at $420 \mu\text{mol mol}^{-1} \text{CO}_2$. The ramp rate for each curve
1561 was set to $200 \mu\text{mol mol}^{-1} \text{min}^{-1}$, logging every five seconds, which generated 96
1562 data points per response curve. All A_{net}/C_i curves were generated after A_{net} and
1563 g_{sw} stabilized in a LI-6800 cuvette set to a 500 mol s^{-1} , 10,000 rpm mixing fan
1564 speed, 1.5 kPa vapor pressure deficit, 25°C leaf temperature, $2000 \mu\text{mol m}^{-2} \text{s}^{-1}$
1565 incoming light radiation, and initial reference CO_2 set to $420 \mu\text{mol mol}^{-1}$.

1566 With the same focal leaf used to generate A_{net}/C_i curves, we measured
1567 dark respiration (R_{d25} ; $\mu\text{mol m}^{-2} \text{s}^{-1}$) following at least a 30-minute period of
1568 darkness. Measurements were collected on a 5-second log interval for 60 seconds

1569 after stabilizing in a LI-6800 cuvette set to a 500 mol s^{-1} , 10,000 rpm mixing fan
1570 speed, 1.5 kPa vapor pressure deficit, 25°C leaf temperature, and $420 \mu\text{mol mol}^{-1}$
1571 reference CO₂ concentration (for both CO₂ concentrations), with incoming light
1572 radiation set to $0 \mu\text{mol m}^{-2} \text{ s}^{-1}$. A single dark respiration value was determined
1573 for each focal leaf by calculating the mean dark respiration value (i.e. the absolute
1574 value of A_{net} during the logging period) across the logging interval.

1575 5.2.4 *Leaf trait measurements*

1576 The focal leaf used to generate A_{net}/C_i curves and dark respiration was
1577 harvested immediately following gas exchange measurements. Images of each focal
1578 leaf were curated using a flat-bed scanner to determine wet leaf area using the
1579 'LeafArea' R package (Katabuchi 2015), which automates leaf area calculations
1580 using ImageJ software (Schneider et al. 2012). Each leaf was dried at 65°C for
1581 at least 48 hours, and subsequently weighed and ground until homogenized. Leaf
1582 mass per area (M_{area} ; g m⁻²) was calculated as the ratio of dry leaf biomass
1583 to fresh leaf area. Using subsamples of ground and homogenized leaf tissue, we
1584 measured leaf nitrogen content (N_{mass} ; gN g⁻¹) through elemental combustion
1585 analysis (Costech-4010, Costech, Inc., Valencia, CA, USA). Leaf nitrogen content
1586 per unit leaf area (N_{area} ; gN m⁻²) was calculated by multiplying N_{mass} and M_{area} .

1587 We extracted chlorophyll content from a second leaf in the same trifoliolate
1588 leaf set as the focal leaf used to generate A_{net}/C_i curves. Prior to chlorophyll
1589 extraction, we used a cork borer to punch between 3 and 5 0.6 cm² disks from
1590 the leaf. Separate images of each punched leaf and set of leaf disks were curated
1591 using a flat-bed scanner to determine wet leaf area, again quantified using the

1592 'LeafArea' R package (Katabuchi 2015). The punched leaf was dried and weighed
1593 after at least 65°C in the drying oven to determine Marea of the chlorophyll leaf.

1594 Leaf disks were shuttled into a test tube containing 10mL dimethyl sul-
1595 foxide, vortexed, and incubated at 65degreeC for 120 minutes (Barnes et al.
1596 1992). Incubated test tubes were vortexed again before loaded in 150 μ L trip-
1597 licate aliquots to a 96-well plate. Dimethyl sulfoxide was also loaded in a 150
1598 μ L triplicate aliquot as a blank. Absorbance measurements at 649.1 nm ($A_{649.1}$)
1599 and 665.1 nm ($A_{665.1}$) were read in each well using a plate reader (Biotek Synergy
1600 H1; Biotek Instruments, Winooski, VT USA) (Wellburn 1994), with triplicates
1601 subsequently averaged and corrected by the mean of the blank absorbance value.
1602 Blank-corrected absorbance values were used to estimate Chl_a (μ g mL $^{-1}$) and
1603 Chl_b (μ g mL $^{-1}$) following equations from Wellburn (1994):

$$Chl_a = 12.47A_{665.1} - 3.62A_{649.1} \quad (5.1)$$

1604 and

$$Chl_b = 25.06A_{665.1} - 6.50A_{649.1} \quad (5.2)$$

1605 Chl_a and Chl_b were converted to mmol mL $^{-1}$ using the molar mass of chlorophyll a
1606 (893.51 g mol $^{-1}$) and the molar mass of chlorophyll b (907.47 g mol $^{-1}$), then added
1607 together to calculate total chlorophyll content in the dimethyl sulfoxide extractant
1608 (mmol mL $^{-1}$). Total chlorophyll content was multiplied by the volume of the
1609 dimethyl sulfoxide extractant (10 mL) and converted to area-based chlorophyll
1610 content by dividing by the total area of the leaf disks (Chl_{area} ; mmol m $^{-2}$). Mass-
1611 based chlorophyll content (Chl_{mass} ; mmol g $^{-1}$) was calculated by dividing Chl_{area}

1612 by the leaf mass per area of the punched leaf.

1613 5.2.5 *A/C_i curve fitting and parameter estimation*

1614 We fit A_{net}/C_i curves of each individual using the ‘fitaci’ function in the
1615 ‘plantecophys’ R package (Duursma 2015). This function estimates the maximum
1616 rate of Rubisco carboxylation V_{cmax} ; $\mu\text{mol m}^{-2} \text{s}^{-1}$) and maximum rate of electron
1617 transport for RuBP regeneration (J_{max} ; $\mu\text{mol m}^{-2} \text{s}^{-1}$) based on the Farquhar bio-
1618 chemical model of C₃ photosynthesis (Farquhar et al. 1980). Triose phosphate
1619 utilization (TPU) limitation was included in all curve fits, and all curve fits in-
1620 cluded measured dark respiration values. As A_{net}/C_i curves were generated using
1621 a common leaf temperature, curves were fit using Michaelis-Menton coefficients
1622 for Rubisco affinity to CO₂ (K_c ; $\mu\text{mol mol}^{-1}$) and O₂ (K_o ; $\mu\text{mol mol}^{-1}$), and the
1623 CO₂ compensation point (Γ^* ; $\mu\text{mol mol}^{-1}$) reported in Bernacchi et al. (2001).
1624 Specifically, K_c was set to 404.9 $\mu\text{mol mol}^{-1}$, K_o was set to 278.4 $\mu\text{mol mol}^{-1}$, and
1625 Γ^* was set to 42.75 $\mu\text{mol mol}^{-1}$. The use of a common leaf temperature across
1626 curves and dark respiration measurements also eliminated the need to manually
1627 temperature standardize rate estimates. For clarity, we reference V_{cmax} , J_{max} , and
1628 R_d estimates throughout the rest of the paper as V_{cmax25} , J_{max25} , and R_{d25} .

1629 5.2.6 Stomatal limitation

1630 We quantified the extent by which stomatal conductance limited photo-
1631 synthesis (l; unitless) following equations originally described in Farquhar and
1632 Sharkey (1982). Stomatal limitation was calculated as:

$$l = 1 - \frac{A_{net}}{A_{mod}} \quad (5.3)$$

1633 where A_{mod} represents the photosynthetic rate where $C_i = C_a$. A_{mod} was calcu-

1634 lated as:

$$A_{mod} = V_{cmax25} - \frac{420 - \Gamma^*}{420 + K_m} - R_{d25} \quad (5.4)$$

1635 K_m is the Michaelis-Menten coefficient for Rubisco-limited photosynthesis, calcu-

1636 lated as:

$$K_m = K_c \cdot \left(1 + \frac{O_i}{K_o}\right) \quad (5.5)$$

1637 where O_i refers to leaf intercellular O_2 concentrations, set to $210 \mu\text{mol mol}^{-1}$.

1638 5.2.7 *Proportion of leaf nitrogen allocated to photosynthesis and structure*

1639 We used equations from Niinemets and Tenhunen (1997) to estimate the

1640 proportion of leaf N content allocated to Rubisco bioenergetics, and light harvest-

1641 ing proteins. The proportion of leaf N allocated to Rubisco (ρ_{rub} ; gN gN^{-1}) was

1642 calculated as a function of V_{cmax25} and N_{area} :

$$\rho_{rubisco} = \frac{V_{cmax25} N_r}{V_{cr} N_{area}} \quad (5.6)$$

1643 where N_r is the amount of nitrogen in Rubisco, set to $0.16 \text{ gN (gN in Rubisco)}^{-1}$

1644 and V_{cr} is the maximum rate of RuBP carboxylation per unit Rubisco protein,

1645 set to $20.5 \mu\text{mol CO}_2 (\text{g Rubisco})^{-1}$. The proportion of leaf nitrogen allocated to

1646 bioenergetics (ρ_{bioe} ; gN gN^{-1}) was similarly calculated as a function of J_{max25} and

1647 N_{area} :

$$\rho_{\text{bioe}} = \frac{J_{\text{max}25} N_b}{J_{\text{mc}} N_{\text{area}}} \quad (5.7)$$

1648 where N_b is the amount of nitrogen in cytochrome f, set to 0.12407 gN (μmol cytochrome f) $^{-1}$ assuming a constant 1: 1: 1.2 cytochrome f: ferredoxin NADP reductase: coupling factor molar ratio (Evans and Seemann 1989; Niinemets and Tenhunen 1997), and J_{mc} is the capacity of electron transport per cytochrome f, set to 156 μmol electron (μmol cytochrome f) $^{-1}\text{s}^{-1}$.

1653 The proportion of leaf nitrogen allocated to light harvesting proteins was calculated as a function of Chl_{mass} and N_{mass} :

$$\rho_{\text{light}} = \frac{Chl_{\text{mass}}}{N_{\text{mass}} c_b} \quad (5.8)$$

1655 where c_b is the stoichiometry of the light-harvesting chlorophyll complexes of photosystem II, set to 2.75 mmol chlorophyll (gN in chlorophyll) $^{-1}$. We used the N_{mass} value of the focal leaf used to generate A_{net}/C_i curves instead of the leaf used to extract chlorophyll content, as the two leaves are from the same trifoliolate leaf set and are highly correlated with each other (Figure SX).

1660 The proportion of leaf nitrogen content allocated to photosynthetic tissue (ρ_{photo} ; gN gN $^{-1}$) was estimated as the sum of ρ_{rubisco} , ρ_{bioe} , and ρ_{light} .

1662 Finally, the proportion of leaf N content allocated to structural tissue (ρ_{str} ; gN gN $^{-1}$) was estimated as:

$$\rho_{\text{structure}} = \frac{N_{\text{cw}}}{N_{\text{area}}} \quad (5.9)$$

1664 where N_{cw} is the leaf N content allocated to cell walls (gN m^{-2}), calculated as a
1665 function of M_{area} using an empirical equation from Onoda et al. (2017):

$$N_{cw} = 0.000355 * M_{area}^{1.39} \quad (5.10)$$

1666 5.2.8 *Whole plant traits*

1667 Seven weeks after experiment initiation and immediately following gas ex-
1668 change measurements, we harvested all experimental individuals and separated
1669 biomass of each experimental individual into major organ types (leaves, stems,
1670 roots, and nodules when present). Fresh leaf area of all harvested leaves was mea-
1671 sured using an LI-3100C (Li-COR Biosciences, Lincoln, Nebraska, USA). Total
1672 fresh leaf area (cm^2) was calculated as the sum of all leaf areas, including the focal
1673 leaf used to collect gas exchange data and the focal leaf used to extract chlorophyll
1674 content. All harvested material was dried in an oven set to 65°C for at least 48
1675 hours, weighed, and ground to homogeneity. Leaves and nodules were manually
1676 ground either with a mortar and pestle, while stems and roots were ground using
1677 a Wiley mill (E3300 Mini Mill; Eberbach Corp., MI, USA). Total dry biomass (g)
1678 was calculated as the sum of dry leaf (including focal leaf for both the A_{net}/C_i
1679 curve and leaf used to extract chlorophyll content), stem, root, and root nodule
1680 biomass. We also quantified carbon and nitrogen content of each respective organ
1681 type through elemental combustion (Costech-4010, Costech, Inc., Valencia, CA,
1682 USA) using subsamples of ground and homogenized organ tissue.

1683 Following the approach explained in Perkowski et al. (2021), we calcu-
1684 lated structural carbon costs to acquire nitrogen as the ratio of total belowground

1685 carbon biomass to whole plant nitrogen biomass (N_{cost} ; gC gN⁻¹). Belowground
1686 carbon biomass (C_{bg} ; gC) was calculated as the sum of root carbon biomass
1687 and root nodule carbon biomass. Root carbon biomass and root nodule carbon
1688 biomass was calculated as the product of the organ biomass and the respective
1689 organ carbon content. Whole plant nitrogen biomass (N_{wp} ; gN) was similarly
1690 calculated as the sum of total leaf, stem, root, and root nodule nitrogen biomass,
1691 including the focal leaf used for A_{net}/C_i curve and chlorophyll extractions. Leaf,
1692 stem, root, and root nodule nitrogen biomass was calculated as the product of
1693 the organ biomass and the respective organ nitrogen content. This calculation
1694 only quantifies plant structural carbon costs to acquire nitrogen and does not
1695 include any additional costs of nitrogen acquisition associated with respiration,
1696 root exudation, or root turnover. An explicit explanation of the limitations for
1697 interpreting this calculation can be found in Perkowski et al. (2021) and Terrer
1698 et al. (2018).

1699 Finally, plant investments in nitrogen fixation were calculated as the ratio
1700 of root nodule biomass to root biomass, where increasing values indicate an in-
1701 crease in plant investments to nitrogen fixation (Dovrat et al. 2018; Dovrat et al.
1702 2020; Perkowski et al. 2021). We also calculated the percent of leaf nitrogen
1703 acquired from the atmosphere (% N_{dfa}) using leaf $\delta^{15}\text{N}$ and the following equation
1704 from Andrews et al. (2011):

$$\%N_{\text{dfa}} = \frac{\delta^{15}N_{\text{reference}} - \delta^{15}N_{\text{sample}}}{\delta^{15}N_{\text{reference}} - B} \quad (5.11)$$

1705 where $\delta^{15}\text{N}_{\text{reference}}$ refers to a reference plant that exclusively acquires nitrogen via

1706 direct uptake, $\delta^{15}\text{N}_{\text{sample}}$ refers to an individual's leaf $\delta^{15}\text{N}$, and B refers to individuals
1707 that are entirely reliant on nitrogen fixation. Within each unique nitrogen
1708 fertilization treatment-by-CO₂ treatment combination, we calculated the mean
1709 leaf $\delta^{15}\text{N}$ for individuals growing in the non-inoculated treatment for $\delta^{15}\text{N}_{\text{reference}}$.
1710 Any individuals with visual confirmation of root nodule formation or nodule initia-
1711 tion were omitted from the calculation of $\delta^{15}\text{N}_{\text{reference}}$. Following recommendations
1712 from Andrews et al. (2011) we calculated B within each CO₂ treatment using the
1713 mean leaf $\delta^{15}\text{N}$ of inoculated individuals that received 0 ppm N. We did not calcu-
1714 late B within each unique soil nitrogen x CO₂ treatment combination, as previous
1715 studies suggest decreased reliance on nitrogen fixation with increasing soil nitro-
1716 gen availability (Perkowski et al. 2021). This approach for estimating nitrogen
1717 fixation standardizes values such that approaching 1 indicates increasing reliance
1718 on nitrogen fixation.

1719 5.2.9 *Statistical analyses*

1720 Any uninoculated pots that had substantial root nodule formation (nodule
1721 biomass: root biomass values greater than 0.05 g g⁻¹) were removed from our
1722 analyses. This was because they were assumed to have been colonized by symbiotic
1723 nitrogen-fixing bacteria from outside sources. This decision resulted in the removal
1724 of sixteen pots from our analysis: two pots in the elevated CO₂ treatment that
1725 received 35 ppm N, three pots in the elevated CO₂ treatment that received 70
1726 ppm N, one pot in the elevated CO₂ treatment that received 210 ppm N, two pots
1727 in the elevated CO₂ treatment that received 280 ppm N, two pots in the ambient
1728 CO₂ treatment that received 0 ppm N, three pots in the ambient CO₂ treatment

1729 that received 70 ppm N, two pots in the ambient CO₂ treatment that received
1730 105 ppm N, and one pot in the ambient CO₂ treatment that received 280 ppm N.

1731 We built a series of linear mixed effects models to investigate the impacts of
1732 CO₂ concentration, soil nitrogen fertilization, and inoculation with *B. japonicum*
1733 on *G. max* gas exchange, tradeoffs between nitrogen and water use, whole plant
1734 growth, and investment in nitrogen fixation. All models included CO₂ treatment
1735 as a categorical fixed effect, inoculation treatment as a categorical fixed effect,
1736 soil nitrogen fertilization as a continuous fixed effect, with interaction terms be-
1737 tween all three fixed effects. All models also accounted for climatic difference
1738 between chambers across experiment iterations by including a random intercept
1739 term that nested starting chamber rack by CO₂ treatment. Models with this
1740 independent variable structure were created for each of the following dependent
1741 variables: N_{area} , M_{area} , N_{mass} , Chl_{area} , V_{cmax25} , J_{max25} , $J_{\text{max25}}:V_{\text{cmax25}}$, R_{d25} , g_{sw} ,
1742 stomatal limitation, ρ_{rubisco} , ρ_{bioe} , ρ_{light} , ρ_{photo} , $\rho_{\text{structure}}$, N_{cost} , C_{bg} , N_{wp} , total
1743 biomass, total leaf area, nodule biomass, and the ratio of nodule biomass to root
1744 biomass.

1745 We used Shapiro-Wilk tests of normality to determine whether linear mixed
1746 effects models satisfied residual normality assumptions. If residual normality as-
1747 sumptions were not met (Shapiro-Wilk: $p < 0.05$), then models were fit using
1748 dependent variables that were natural log transformed. All residual normality
1749 assumptions that did not originally satisfy residual normality assumptions were
1750 met with either a natural log or square root data transformation (Shapiro-Wilk:
1751 $p > 0.05$ in all cases). Specifically, models for N_{area} , N_{mass} , Chl_{area} , V_{cmax25} ,
1752 J_{max25} , $J_{\text{max25}}:V_{\text{cmax25}}$, g_{sw} , stomatal limitation, ρ_{rubisco} , ρ_{bioe} , ρ_{light} , ρ_{photo} , and to-

1753 total leaf area satisfied residual normality assumptions without data transformation.

1754 Models for M_{area} , $\rho_{\text{structure}}$, N_{cost} , C_{bg} , N_{wp} , and total biomass satisfied residual

1755 normality assumptions with a natural log data transformation, while models for

1756 nodule biomass and nodule biomass: root biomass satisfied residual normality

1757 assumptions with a square root data transformation.

1758 In all statistical models, we used the 'lmer' function in the 'lme4' R package

1759 (Bates et al. 2015) to fit each model and the 'Anova' function in the 'car' R

1760 package (Fox and Weisberg 2019) to calculate Type II Wald's χ^2 and determine the

1761 significance ($\alpha = 0.05$) of each fixed effect coefficient. We then used the 'emmeans'

1762 R package (Lenth 2019) to conduct post-hoc comparisons using Tukey's tests,

1763 where degrees of freedom were approximated using the Kenward-Roger approach

1764 (Kenward and Roger 1997). All analyses and plots were conducted in R version

1765 4.2.0 (R Core Team 2021).

1766 5.3 Results

1767 5.3.1 Leaf nitrogen content, chlorophyll content, and mass per area

1768 Elevated CO₂ reduced N_{area} , N_{mass} , and Chl_{area} by 29%, 50%, and 31%,

1769 respectively, and stimulated M_{area} by 44% ($p < 0.001$ in all cases; Table 1). An in-

1770 teraction between fertilization and CO₂ (CO₂-by-fertilization interaction: $p_{N_{\text{area}}} =$

1771 0.017, $p_{N_{\text{mass}}} < 0.001$, $p_{M_{\text{area}}} = 0.006$, $p_{Chl_{\text{area}}} = 0.083$; Table 1) indicated that the

1772 general positive effect of increasing fertilization on N_{area} , N_{mass} , and Chl_{area} ($p <$

1773 0.001 in all cases; Table 1) was generally stronger under ambient CO₂ (Tukey _{N_{area}} :

1774 $p = 0.026$; Tukey _{N_{mass}} : $p < 0.001$; Tukey _{M_{area}} : $p = 0.009$; Tukey _{Chl_{area}} : $p = 0.065$;

1775 Table 1; Figs. 1a-d). This pattern resulted in a stronger reduction in N_{area} , N_{mass} ,

1776 and Chl_{area} as well as a stronger stimulation in M_{area} under elevated CO₂ with
1777 increasing fertilization. An additional interaction between inoculation and CO₂
1778 on N_{area} (CO₂-by-inoculation interaction: $p = 0.030$; Table 1) indicated that the
1779 general positive effect of inoculation on N_{area} ($p < 0.001$; Table 1) was stronger
1780 under elevated CO₂ (45% increase; Tukey: $p < 0.001$) than under ambient CO₂
1781 (18% increase; Tukey: $p < 0.001$), a result that increased the reduction in N_{area}
1782 in inoculated pots under elevated CO₂. Inoculation treatment did not modify the
1783 downregulation in N_{mass} (CO₂-by-inoculation interaction: $p = 0.148$; Table 1) and
1784 Chl_{area} ($p = 0.147$; Table 1) or the stimulation in M_{area} ($p = 0.866$; Table 1) un-
1785 der elevated CO₂. However, interactions between fertilization and inoculation on
1786 N_{area} (fertilization-by-inoculation interaction: $p < 0.001$; Table 1; Fig. 1a), N_{mass}
1787 ($p = 0.001$; Table 1; Fig. 1b), M_{area} ($p = 0.025$; Table 1; Fig. 1c), and Chl_{area} (p
1788 < 0.001 ; Table 1; Fig. 1d) indicated that the general positive effect of increasing
1789 fertilization on each trait was stronger in uninoculated pots (Tukey _{N_{area}} : $p <$
1790 0.001; Tukey _{N_{mass}} : $p = 0.001$; Tukey _{M_{area}} : $p = 0.031$; Tukey _{Chl_{area}} : $p < 0.001$).

Table 5.1. Effects of soil nitrogen fertilization, inoculation, and CO₂ treatments on N_{area} , N_{mass} , M_{area} , and Chl_{area}

		N_{area}			N_{mass}			M_{area}^a		
	df	Coefficient	χ^2	p	Coefficient	χ^2	p	Coefficient	χ^2	p
(Intercept)	-	1.10E+00	-	-	3.05E-02	-	-	3.64E+00	-	-
CO ₂	1	-5.67E-01	155.908	<0.001	-1.80E-02	272.362	<0.001	3.04E-01	151.319	<0.001
Inoculation (I)	1	6.21E-01	86.029	<0.001	7.54E-03	15.576	<0.001	1.81E-01	19.158	<0.001
Fertilization (N)	1	3.06E-03	316.408	<0.001	5.78E-05	106.659	<0.001	3.10E-04	21.440	<0.001
CO ₂ *I	1	2.63E-01	4.729	0.030	3.96E-03	2.025	0.155	-3.37E-02	0.029	0.866
CO ₂ *N	1	-3.68E-04	5.723	0.017	-2.85E-05	22.542	<0.001	2.80E-04	7.619	0.006
I*N	1	-1.36E-03	43.381	<0.001	-2.00E-05	11.137	0.001	-3.36E-04	5.022	0.025
CO ₂ *I*N	1	-3.23E-04	0.489	0.484	-2.59E-06	0.041	0.839	1.15E-04	0.208	0.649
Chl_{area}										
	df	Coefficient	χ^2	p						
(Intercept)	-	2.13E-02	-	-						
CO ₂	1	-1.33E-02	69.233	<0.001						
Inoculation (I)	1	1.24E-01	136.341	<0.001						
Fertilization (N)	1	3.35E-04	163.111	<0.001						
CO ₂ *I	1	-3.18E-02	2.102	0.147						
CO ₂ *N	1	-8.79E-05	2.999	0.083						
I*N	1	-2.65E-04	75.769	<0.001						
CO ₂ *I*N	1	7.68E-05	2.144	0.147						

*Significance determined using Type II Wald χ^2 tests ($\alpha = 0.05$). P-values < 0.05 are in bold, while p-values between 0.05 and 0.1 are italicized. A superscript “a” is included after trait labels to indicate if models were fit with natural log transformed response variables. Key: df = degrees of freedom, N_{area} = leaf nitrogen content per unit leaf area, N_{mass} = leaf nitrogen content, M_{area} = leaf mass per unit leaf area.

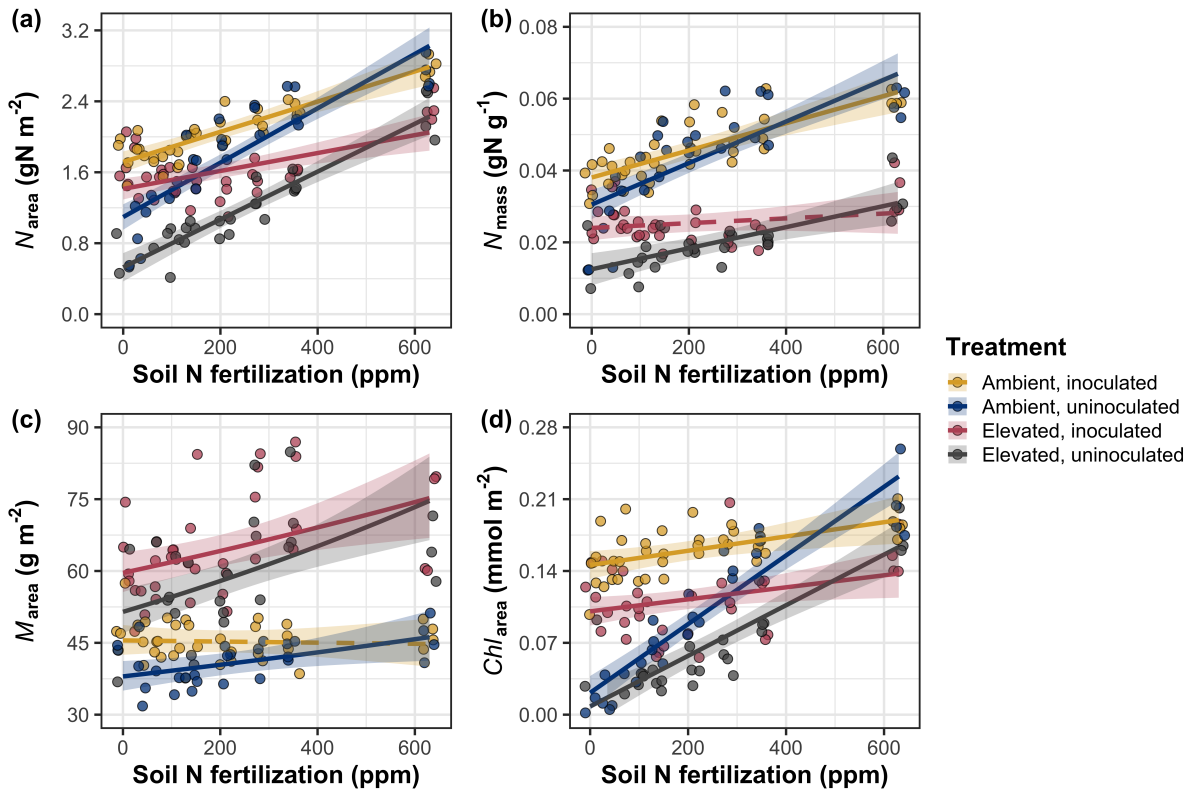


Figure 5.1. Effects of CO_2 , fertilization, and inoculation on leaf nitrogen per unit leaf area (a), leaf nitrogen content (b), leaf mass per unit leaf area (c), and chlorophyll content per unit leaf area (d). Soil nitrogen fertilization is represented on the x-axis in all panels. Yellow points and trendlines indicate inoculated individuals grown under ambient CO_2 , blue points and trendlines indicate uninoculated individuals grown under ambient CO_2 , red points and trendlines indicate inoculated individuals grown under elevated CO_2 , and grey points indicate uninoculated individuals grown under elevated CO_2 . Solid trendlines indicate regression slopes that are different from zero ($p < 0.05$), while dashed trendlines indicate slopes that are not distinguishable from zero ($p > 0.05$).

1791 5.3.2 *Leaf biochemistry and stomatal conductance*

1792 Elevated CO₂ resulted in plants with 16% lower V_{cmax25} ($p < 0.001$; Table
1793 2) and 10% lower J_{max25} ($p = 0.014$; Table 2) as compared to those grown un-
1794 der ambient CO₂, but did not influence R_{d25} ($p = 0.613$; Table 2). A relatively
1795 stronger downregulation in V_{cmax25} than J_{max25} resulted in an 8% stimulation in
1796 $J_{max25}:V_{cmax25}$ under elevated CO₂ ($p < 0.001$; Table 2; Fig. 2E). The downregu-
1797 latory effect of CO₂ on V_{cmax25} and J_{max25} was not modified across the fertilization
1798 gradient (CO₂-by-fertilization interaction: $p = 0.185$, $p = 0.389$ for V_{cmax25} and
1799 J_{max25} , respectively; Table 2; Fig. 2A, 2C) or between inoculation treatments
1800 (CO₂-by-inoculation interaction: $p = 0.799$ and $p = 0.714$ for V_{cmax25} and J_{max25} ,
1801 respectively; Table 2). However, a strong interaction between fertilization and
1802 inoculation (fertilization-by-inoculation interaction: $p \leq 0.001$ in all cases; Table
1803 2) indicated that the general positive effect of increasing fertilization on V_{cmax25} (p
1804 < 0.001 ; Table 2), J_{max25} ($p < 0.001$; Table 2), and R_{d25} ($p = 0.015$; Table 2) was
1805 only observed in uninoculated pots (Tukey: $p \leq 0.001$ in all cases), as there was
1806 no apparent effect of fertilization on V_{cmax25} (Tukey: $p = 0.456$), J_{max25} (Tukey: p
1807 = 0.180), or R_{d25} (Tukey: $p = 0.443$) in inoculated pots (Figs. 2B, 2D, 2F, 2H). A
1808 relatively stronger positive effect of increasing fertilization on V_{cmax25} than J_{max25}
1809 resulted in a general reduction in $J_{max25}:V_{cmax25}$ with increasing fertilization ($p <$
1810 0.001), though this pattern was only seen in uninoculated pots (Tukey: $p = 0.003$)
1811 and not inoculated plants (Tukey: $p > 0.05$).

1812 Elevated CO₂ reduced stomatal conductance by 20% ($p < 0.001$; Table 2)
1813 compared to ambient CO₂, but this downregulation did not influence stomatal
1814 limitation of photosynthesis ($p = 0.355$; Table 2). As with V_{cmax25} and J_{max25} , the

1815 downregulation of stomatal conductance due to elevated CO₂ was not modified
1816 across the fertilization gradient (CO₂-by-fertilization interaction: $p = 0.141$; Table
1817 2) or between inoculation treatments (CO₂-by-inoculation interaction: $p = 0.179$;
1818 Table 2). Fertilization also did not modify the general null effect of CO₂ on stom-
1819 atal limitation (CO₂-by-fertilization interaction: $p = 0.554$; Table 2), although
1820 an interaction between CO₂ and inoculation (CO₂-by-inoculation interaction: p
1821 = 0.043; Table 2) indicated that inoculation increased stomatal limitation un-
1822 der ambient CO₂ (Tukey: $p = 0.021$), but not under elevated CO₂ (Tukey: p
1823 > 0.999). An interaction between inoculation and fertilization on stomatal con-
1824 ductance (fertilization-by-inoculation interaction: $p < 0.001$; Table 2) indicated
1825 that increasing fertilization increased stomatal conductance in uninoculated pots
1826 (Tukey: $p = 0.003$) but decreased stomatal conductance in inoculated pots (Tukey:
1827 $p = 0.021$). The similar in magnitude, but opposite direction, trend in the effect of
1828 increasing fertilization on stomatal conductance between inoculation treatments
1829 likely drove a null general response of stomatal conductance to increasing fertil-
1830 ization ($p = 0.642$; Table 2).

Table 5.2. Effects of soil nitrogen fertilization, inoculation, and CO₂ on leaf biochemistry

		<i>V</i> _{cmax25}			<i>J</i> _{max25}			<i>R</i> _{d25}		
	df	Coefficient	χ^2	<i>p</i>	Coefficient	χ^2	<i>p</i>	Coefficient	χ^2	<i>p</i>
(Intercept)	-	4.36E+01	-	-	8.30E+01	-	-	1.69E+00	-	-
CO ₂	1	-7.05E+00	18.039	<0.001	-9.11E+00	6.042	0.014	4.53E-01	0.256	0.613
Inoculation (I)	1	5.87E+01	98.579	<0.001	9.62E+01	85.064	<0.001	1.04E+00	3.094	0.079
Fertilization (N)	1	1.32E-01	37.053	<0.001	2.09E-01	25.356	<0.001	2.86E-03	5.965	0.015
CO ₂ *I	1	-4.65E+00	0.065	0.799	7.84E-01	0.667	0.414	-5.71E-01	2.563	0.109
CO ₂ *N	1	-3.58E-02	1.758	0.185	-4.33E-02	0.742	0.389	-1.55E-03	2.675	0.102
I*N	1	-1.35E-01	60.394	<0.001	-2.30E-01	57.410	<0.001	-2.84E-03	12.083	0.001
CO ₂ *I*N	1	2.73E-02	0.748	0.387	3.46E-02	0.377	0.539	7.21E-04	0.244	0.622

		<i>J</i> _{max25} : <i>V</i> _{cmax25}			<i>g</i> _{sw}			Stomatal limitation		
	df	Coefficient	χ^2	<i>p</i>	Coefficient	χ^2	<i>p</i>	Coefficient	χ^2	<i>p</i>
(Intercept)	-	1.92E+00	-	-	1.95E-01	-	-	2.12E-01	-	-
CO ₂	1	5.71E-02	92.010	<0.001	-6.23E-02	9.718	0.002	3.91E-02	0.856	0.355
Inoculation (I)	1	-1.79E-01	27.768	<0.001	1.30E-01	22.351	<0.001	7.87E-02	4.582	0.032
Fertilization (N)	1	-4.61E-04	28.147	<0.001	2.50E-04	0.066	0.797	2.60E-04	32.218	<0.001
CO ₂ *I	1	8.94E-02	2.916	0.088	6.69E-02	1.810	0.179	-7.84E-02	4.093	0.043
CO ₂ *N	1	2.35E-04	3.210	0.073	-8.50E-05	2.165	0.141	-1.24E-04	0.350	0.554
I*N	1	3.27E-04	9.607	0.002	-3.09E-04	14.696	<0.001	-1.67E-04	2.547	0.110
CO ₂ *I*N	1	-1.66E-04	1.102	0.294	-8.89E-05	0.234	0.629	1.67E-04	2.231	0.135

*Significance determined using Type II Wald χ^2 tests ($\alpha = 0.05$). *P*-values < 0.05 are in bold, while *p*-values between 0.05 and 0.1 are italicized. Key: *V*_{cmax25} – maximum rate of Rubisco carboxylation at 25°C; *J*_{max25} – maximum rate of electron transport for RuBP regeneration at 25°C, *R*_{d25} - dark respiration at 25°C; *J*_{max25}:*V*_{cmax25} – the ratio of *J*_{max25} to *V*_{cmax25}; *g*_{sw} - stomatal conductance.

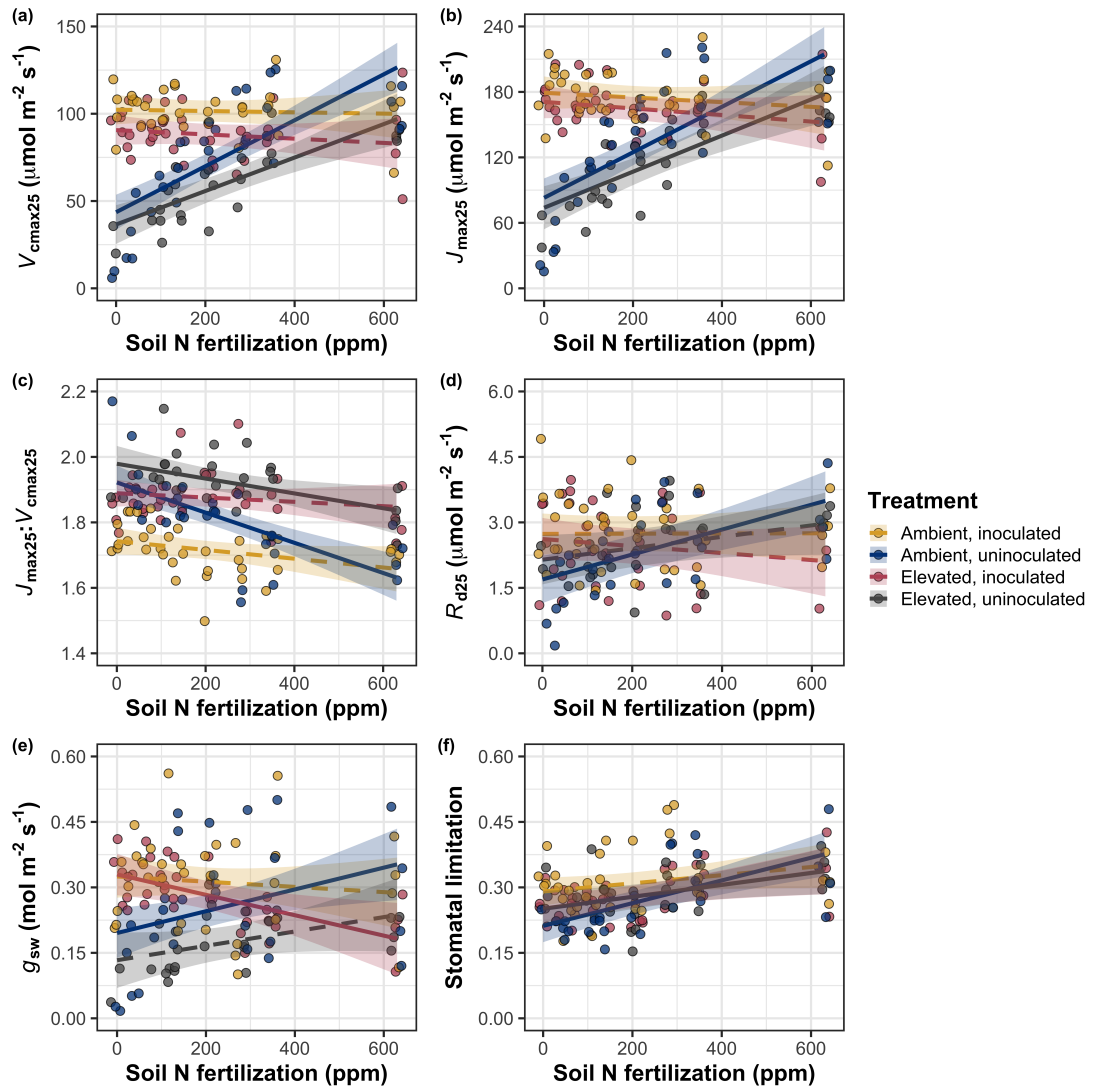


Figure 5.2. Effects of CO₂, fertilization, and inoculation on maximum rate of Rubisco carboxylation (a), the maximum rate of RuBP regeneration (b), and the ratio of the maximum rate of RuBP regeneration to the maximum rate of Rubisco carboxylation leaf mass per unit leaf area (c), dark respiration (d), stomatal conductance (e), and stomatal limitation (f). Soil nitrogen fertilization is represented on the x-axis in all panels. Colored points and trendlines are as explained in Figure 1.

1831 5.3.3 *Leaf nitrogen allocation*

1832 A relatively stronger downregulation in N_{area} than V_{cmax25} or J_{max25} resulted
1833 in an 20% and 29% respective stimulation in ρ_{rubisco} and ρ_{bioe} under elevated CO₂
1834 ($p < 0.001$ in both cases; Table 3). There was no apparent CO₂ effect on ρ_{light}
1835 ($p = 0.700$; Table 3), but the strong stimulation in ρ_{rubisco} and ρ_{bioe} resulted
1836 in a 21% stimulation of ρ_{photo} under elevated CO₂ ($p < 0.001$; Table 3; Fig.
1837 3A). The stimulation of ρ_{rubisco} , ρ_{bioe} , and ρ_{photo} due to elevated CO₂ was not
1838 modified across the fertilization gradient (CO₂-by-fertilization interaction: p_{rubisco}
1839 = 0.269, $p_{\text{bioe}} = 0.298$, $p_{\text{photo}} = 0.281$; Table 3). A marginal interaction between
1840 inoculation and CO₂ on ρ_{rubisco} and ρ_{photo} (CO₂-by-inoculation interaction: p_{rubisco}
1841 = 0.057, $p_{\text{photo}} = 0.057$; Table 3) indicated that the general positive effect of
1842 inoculation on ρ_{rubisco} and ρ_{photo} ($p < 0.001$ in both cases; Table 3) was only
1843 apparent under ambient CO₂ (Tukey: $p < 0.001$ in both cases), with no apparent
1844 effect of inoculation under elevated CO₂ (Tukey_{rubisco}: $p = 0.200$; Tukey_{photo}: p
1845 = 0.147). Inoculation did not modify the stimulation of ρ_{bioe} under elevated CO₂
1846 (CO₂-by-inoculation interaction: $p = 0.122$; Table 3) or the null effect of CO₂ on
1847 ρ_{bioe} (CO₂-by-inoculation interaction: $p = 0.298$; Table 3). Strong interactions
1848 between fertilization and inoculation on ρ_{rubisco} , ρ_{bioe} , and ρ_{photo} (fertilization-
1849 by-inoculation interaction: $p < 0.001$ in all cases; Table 3) indicated that the
1850 general negative effect of increasing fertilization ($p < 0.001$ in all cases; Table
1851 3) was only observed in inoculated pots (Tukey: $p < 0.001$ in all cases), with
1852 no apparent effect of fertilization on ρ_{rubisco} (Tukey: $p = 0.612$), ρ_{bioe} (Tukey:
1853 $p = 0.544$), or ρ_{photo} (Tukey: $p = 0.521$; Fig 3B) in uninoculated pots. An
1854 additional interaction between fertilization and inoculation on ρ_{light} (fertilization-

1855 by-inoculation interaction: $p < 0.001$; Table 3) indicated a negative effect of
1856 increasing fertilization on ρ_{light} in inoculated pots (Tukey: $p = 0.041$), but a
1857 positive effect of increasing fertilization in uninoculated pots (Tukey: $p < 0.001$).

1858 The stimulation in M_{area} resulted in an 133% stimulation of $\rho_{\text{structure}}$ under
1859 elevated CO₂ ($p < 0.001$; Table 3; Fig 3C). An interaction between fertilization
1860 and CO₂ (CO₂-by-fertilization interaction: $p = 0.039$; Table 3) indicated that the
1861 general negative effect of increasing fertilization ($p < 0.001$; Table 3) on $\rho_{\text{structure}}$
1862 was marginally stronger under ambient CO₂ (Tukey: $p = 0.055$), resulting in a
1863 stronger stimulation in $\rho_{\text{structure}}$ under elevated CO₂ with increasing fertilization.
1864 A marginal interaction between inoculation and CO₂ (CO₂-by-inoculation inter-
1865 action: $p = 0.057$; Table 3) indicated that the general positive effect of inoculation
1866 on $\rho_{\text{structure}}$ ($p < 0.001$; Table 3) was only observed under elevated CO₂ (Tukey:
1867 $p < 0.001$), with no apparent inoculation effect observed under ambient CO₂
1868 (Tukey: $p = 0.513$). Finally, an interaction between fertilization and inoculation
1869 (fertilization-by-inoculation interaction: $p < 0.001$; Table 3; Fig. 3D) indicated
1870 that, while increasing fertilization generally increased $\rho_{\text{structure}}$ ($p < 0.001$; Table
1871 3), this response was generally stronger in uninoculated pots (Tukey: $p = 0.001$).

Table 5.3. Effects of soil N availability, soil pH, species, and N_{area} on leaf nitrogen allocation

	ρ_{rubisco}			ρ_{bioe}			ρ_{light}			
	df	Coefficient	χ^2	p	Coefficient	χ^2	p	Coefficient	χ^2	p
(Intercept)	-	2.70E-01	-	-	5.26E-02	-	-	8.48E-03	-	-
CO ₂	1	1.42E-01	23.510	<0.001	3.00E-02	53.899	<0.001	2.03E-03	0.149	0.700
Inoculation (I)	1	1.83E-01	23.475	<0.001	2.80E-02	13.860	<0.001	2.04E-02	147.234	<0.001
Fertilization (N)	1	1.35E-04	16.609	<0.001	1.22E-05	26.827	<0.001	3.22E-05	19.378	<0.001
CO ₂ *I	1	-1.07E-01	3.629	<i>0.057</i>	-1.67E-02	2.390	0.122	-5.33E-03	0.684	0.408
CO ₂ *N	1	-2.16E-04	1.223	<i>0.269</i>	-3.59E-05	1.085	0.298	-7.01E-06	0.351	0.553
I*N	1	-4.26E-04	20.045	<0.001	-6.87E-05	15.458	<0.001	-4.37E-05	64.042	<0.001
CO ₂ *I*N	1	2.50E-04	3.327	<i>0.068</i>	4.08E-05	2.651	0.103	1.74E-05	3.735	<i>0.053</i>

	ρ_{photo}			$\rho_{\text{structure}}^a$			
	df	Coefficient	χ^2	p	Coefficient	χ^2	p
(Intercept)	-	3.32E-01	-	-	-2.93E+00	-	-
CO ₂	1	1.81E-01	27.651	<0.001	8.77E-01	229.571	<0.001
Inoculation (I)	1	2.31E-01	26.238	<0.001	-2.55E-01	13.872	<0.001
Fertilization (N)	1	1.76E-04	15.899	<0.001	-1.51E-03	38.128	<0.001
CO ₂ *I	1	-1.36E-01	3.671	<i>0.055</i>	-2.99E-01	3.622	<i>0.057</i>
CO ₂ *N	1	-2.72E-04	1.163	<i>0.281</i>	3.14E-04	4.266	0.039
I*N	1	-5.37E-04	21.355	<0.001	7.00E-04	11.025	0.001
CO ₂ *I*N	1	3.29E-04	4.009	0.045	4.52E-04	0.669	0.413

*Significance determined using Type II Wald χ^2 tests ($\alpha = 0.05$). P-values < 0.05 are in bold, while p-values between 0.05 and 0.1 are italicized. A superscript “a” is included after trait labels to indicate if models were fit with natural log transformed response variables. Key: df=degrees of freedom, ρ_{rubisco} = proportion of leaf N allocated to photosynthesis, ρ_{bioe} = proportion of leaf N allocated to bioenergetics, ρ_{light} =proportion of leaf N allocated to light harvesting proteins, ρ_{photo} =proportion of leaf N allocated to photosynthesis, $\rho_{\text{structure}}$ =proportion of leaf N allocated to cell wall structural tissue

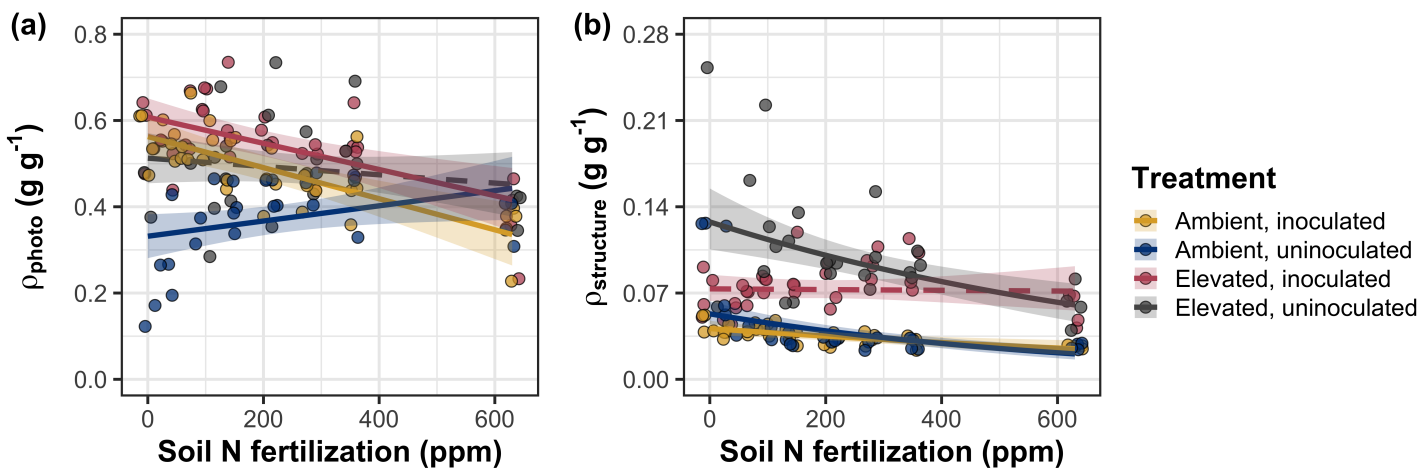


Figure 5.3. Effects of CO_2 , fertilization, and inoculation on the relative fraction of leaf nitrogen allocated to photosynthesis (a) and the fraction of leaf nitrogen allocated to structure (b). Soil nitrogen fertilization is represented on the x-axis in both panels. Colored points and trendlines are as explained in Figure 1.

1872 5.3.4 *Whole plant growth and total leaf area*

1873 Total leaf area was 51% greater and total biomass was 102% greater un-
1874 der elevated CO₂ ($p < 0.001$ in both cases; Table 4), a pattern that was en-
1875 hanced by fertilization (CO₂-by-fertilization interaction: $p < 0.001$ in both cases;
1876 Table 4; Fig. 4a-b) but was not modified across inoculation treatments (CO₂-
1877 by-inoculation interaction: $p_{total_leaf_area} = 0.151$, $p_{total_biomass} = 0.472$; Table 4).
1878 Specifically, the general positive effect of increasing fertilization on total leaf area
1879 and whole plant biomass ($p < 0.001$ in both cases; Table 4) was stronger under
1880 elevated CO₂ (Tukey: $p < 0.001$ in both cases). The general positive effect of
1881 increasing fertilization on total leaf area was modified by inoculation treatment
1882 (fertilization-by-inoculation interaction: $p < 0.001$ in both cases; Table 4), in-
1883 dicating a stronger positive effect of increasing fertilization in uninoculated pots
1884 (Tukey: $p_{total_leaf_area} = 0.002$, $p_{total_biomass} = 0.001$).

1885 5.3.5 *Carbon costs to acquire nitrogen*

1886 A general 62% stimulation in N_{cost} under elevated CO₂ was modified thr-
1887 ough a strong three-way interaction between CO₂, fertilization, and inoculation
1888 (CO₂-by-inoculation-by-fertilization interaction: $p < 0.001$; Table 4). This in-
1889 teraction revealed a general negative effect of increasing fertilization on N_{cost} (p
1890 < 0.001 ; Table 4) that was observed in all treatment combinations (Tukey: $p <$
1891 0.001 in all cases) except for inoculated pots grown under elevated CO₂ (Tukey:
1892 $p = 0.779$; Fig. 5c). This response also resulted in generally stronger negative ef-
1893 ffects of increasing fertilization on N_{cost} in uninoculated pots grown under elevated
1894 CO₂ than uninoculated pots grown under ambient CO₂ (Tukey: $p = 0.001$) and

1895 inoculated pots grown under either ambient CO₂ (Tukey: $p < 0.001$) or elevated
1896 CO₂ (Tukey: $p < 0.001$), while uninoculated pots grown under ambient CO₂ had
1897 generally stronger negative effects of increasing fertilization on N_{cost} than inocu-
1898 lated pots grown under elevated CO₂ (Tukey: $p = 0.002$), but not inoculated pots
1899 grown under ambient CO₂ (Tukey: $p = 0.216$). The general reduction in N_{cost}
1900 with increasing fertilization and in uninoculated pots were driven by a stronger
1901 positive effect of increasing fertilization on N_{wp} (denominator of N_{cost}) than C_{bg}
1902 (numerator of N_{cost}), while the general stimulation in N_{cost} under elevated CO₂
1903 was driven by a stronger positive effect of elevated CO₂ on C_{bg} than N_{wp} (Table
1904 4).

Table 5.4. Effects of soil N availability, soil pH, species, and N_{area} on total leaf area, whole plant biomass, and costs of nitrogen acquisition

	Total leaf area			Total biomass			N_{cost}			
	df	Coefficient	χ^2	p	Coefficient	χ^2	p	Coefficient	χ^2	p
(Intercept)	-	8.78E+01	-	-	9.96E-01	-	-	8.67E+00	-	-
CO_2	1	3.36E+01	69.291	<0.001	5.07E-01	131.477	<0.001	8.75E+00	88.189	<0.001
Inoculation (I)	1	1.88E+02	35.715	<0.001	7.96E-01	34.264	<0.001	-1.68E+00	136.343	<0.001
Fertilization (N)	1	9.35E-01	274.199	<0.001	3.14E-03	269.046	<0.001	-8.50E-03	80.501	<0.001
$\text{CO}_2 * \text{I}$	1	6.44E+01	2.064	0.151	-7.69E-02	0.518	0.472	-8.38E+00	85.237	<0.001
$\text{CO}_2 * \text{N}$	1	5.05E-01	18.655	<0.001	1.61E-03	16.877	<0.001	-9.17E-03	1.050	0.306
$\text{I} * \text{N}$	1	-3.84E-01	10.804	0.001	-1.45E-03	15.779	<0.001	4.20E-03	46.489	<0.001
$\text{CO}_2 * \text{I} * \text{N}$	1	-2.97E-03	<0.001	0.990	-1.14E-04	0.023	0.880	1.32E-02	18.125	<0.001

126

	C_{bg}			N_{wp}			
	df	Coefficient	χ^2	p	Coefficient	χ^2	p
(Intercept)	-	-1.70E+00	-	-	1.24E-01	-	-
CO_2	1	9.21E-01	84.134	<0.001	-3.41E-03	23.890	<0.001
Inoculation (I)	1	1.18E+00	41.030	<0.001	1.68E-01	134.460	<0.001
N fertilization (N)	1	3.38E-03	152.248	<0.001	6.69E-04	529.021	<0.001
$\text{CO}_2 * \text{I}$	1	-6.18E-01	8.965	0.003	3.68E-02	1.190	0.275
$\text{CO}_2 * \text{N}$	1	-3.66E-05	1.188	0.276	1.58E-04	5.915	0.015
$\text{I} * \text{N}$	1	-2.22E-03	22.648	<0.001	-3.20E-04	55.562	<0.001
$\text{CO}_2 * \text{I} * \text{N}$	1	8.09E-04	1.109	0.292	-7.54E-05	0.620	0.431

*Significance determined using Type II Wald χ^2 tests ($\alpha = 0.05$). P-values < 0.05 are in bold, while p-values between 0.05 and 0.1 are italicized. A superscript “a” after trait labels indicates if models were fit using natural log transformed response variables, while a superscript “b” indicates if models were fit using square root transformed variables. Key: df=degrees of freedom

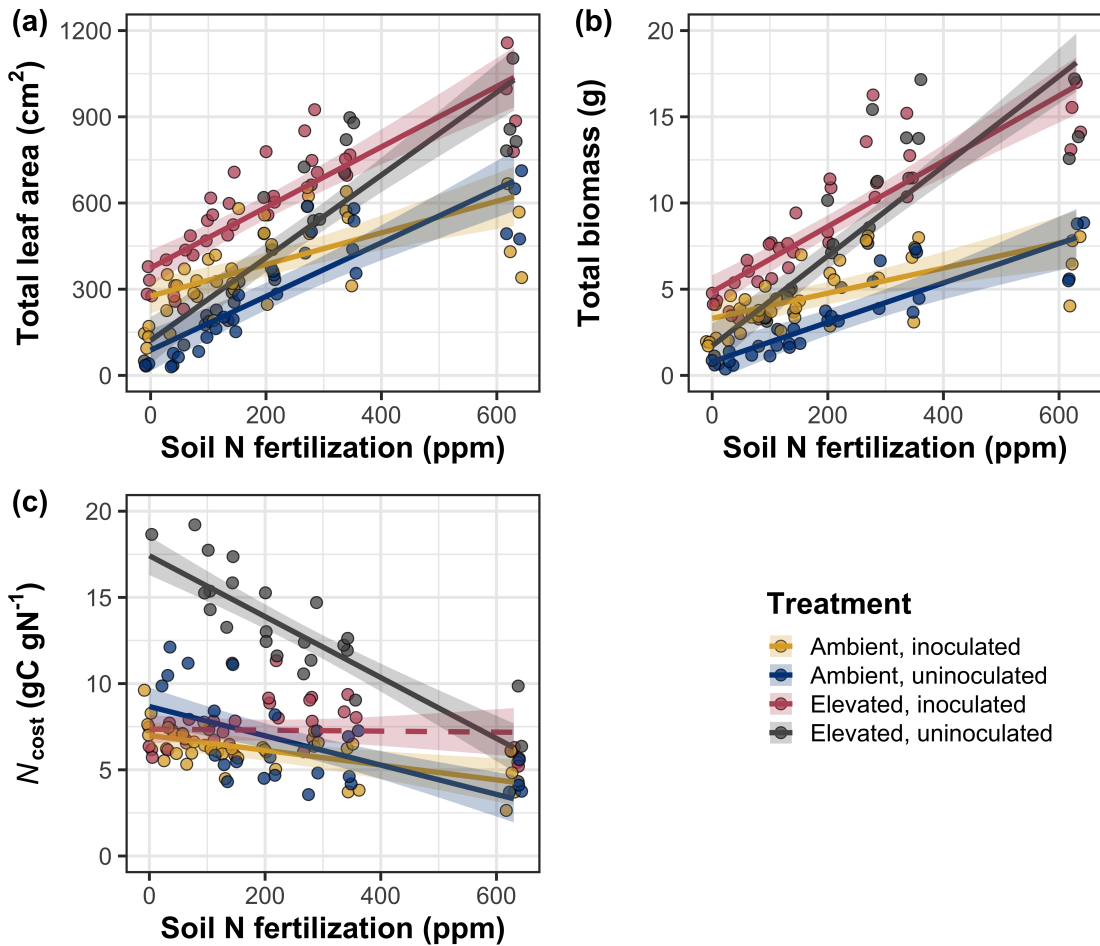


Figure 5.4. Effects of CO_2 , fertilization, and inoculation on total leaf area (a), total biomass (b), and structural carbon costs to acquire nitrogen (c). Soil nitrogen fertilization is represented continuously on the x-axis in all panels. Colored points and trendlines are as explained in Figure 1.

1905 5.3.6 *Nitrogen fixation*

1906 Nodule biomass was stimulated by 30% under elevated CO₂ ($p < 0.001$;
1907 Table 5), a pattern that was modified across the fertilization gradient (CO₂-by-
1908 fertilization interaction: $p = 0.479$; Table 5), but not between inoculation treat-
1909 ments (CO₂-by-inoculation interaction: $p = 0.404$; Table 5). Specifically, the
1910 general negative effect of increasing fertilization on nodule biomass ($p < 0.001$;
1911 Table 5) was stronger under elevated CO₂ than ambient CO₂ (Tukey: $p < 0.001$;
1912 Fig. 5a), which reduced the stimulation in nodule biomass under elevated CO₂
1913 with increasing fertilization. A strong interaction between fertilization and inocu-
1914 lation (fertilization-by-inoculation interaction: $p < 0.001$; Table 5) was driven by
1915 a stronger negative effect of increasing fertilization in inoculated pots (Tukey: p
1916 < 0.001 ; Fig. 5a).

1917 There was no effect of CO₂ on nodule: root biomass ($p = 0.767$; Table 5),
1918 although an interaction between CO₂ and inoculation (CO₂-by-inoculation inter-
1919 action: $p < 0.001$; Table 5) indicated that the general positive effect of inoculation
1920 on nodule: root biomass ($p < 0.001$; Table 5) was stronger under ambient CO₂
1921 (3129% increase; Tukey: $p < 0.001$) than elevated CO₂ (379% increase; Tukey:
1922 $p < 0.001$; Fig. 5b). The null effect of CO₂ on nodule: root biomass was con-
1923 sistently observed across the fertilization gradient ($p = 0.183$; Table 5; Fig. 5b).
1924 An interaction between fertilization and inoculation (fertilization-by-inoculation
1925 interaction: $p < 0.001$; Table 5) indicated that the general negative effect of in-
1926 creasing fertilization on nodule: root biomass ($p < 0.001$; Table 5) was stronger
1927 in inoculated pots (Tukey: $p < 0.001$; Fig. 5b).

1928 There was no effect of CO₂ on %N_{dfa} ($p = 0.472$; Table 5), a pattern

1929 that was not modified by inoculation (CO_2 -by-inoculation interaction: $p = 0.156$;
1930 Table 5) or fertilization (CO_2 -by-fertilization interaction: $p = 0.099$; Table 5).
1931 An interaction between fertilization and inoculation (fertilization-by-inoculation
1932 interaction: $p < 0.001$; Table 5) indicated that the general negative effect of
1933 increasing fertilization on $\%N_{dfa}$ ($p < 0.001$; Table 5) was only observed in inoc-
1934 ulated pots (Tukey: $p < 0.001$), with no apparent effect of fertilization on $\%N_{dfa}$
1935 in uninoculated pots (Tukey: $p = 0.651$; Table 5; Fig. 5c).

Table 5.5. Effects of soil N availability, soil pH, species, and N_{area} on leaf biochemistry

	N_{area}			V_{cmax25}			J_{max25}			
	df	Coefficient	χ^2	p	Coefficient	χ^2	p	Coefficient	χ^2	p
(Intercept)	-		-	-		-	-		-	-
CO_2	1									
Inoculation	1									
(I)										
N fertilization	1									
(N)										
$\text{CO}_2 * \text{I}$	1									
$\text{CO}_2 * \text{N}$	1									
$\text{I} * \text{N}$	1									
$\text{CO}_2 * \text{I} * \text{N}$	1									

	$J_{\text{max25}}:V_{\text{cmax25}}$			
	df	Coefficient	χ^2	p
(Intercept)	-			
CO_2	1			
Inoculation	1			
(I)				
N fertilization	1			
(N)				
$\text{CO}_2 * \text{I}$	1			
$\text{CO}_2 * \text{N}$	1			
$\text{I} * \text{N}$	1			
$\text{CO}_2 * \text{I} * \text{N}$	1			

*Significance determined using Type II Wald χ^2 tests ($\alpha = 0.05$). P-values < 0.05 are in bold, while p-values between 0.05 and 0.1 are italicized. Superscript letters indicate model coefficients fit to natural-log ^(a) or square-root ^(b) transformed data. Key: A_{net} – light saturated net photosynthesis rate; V_{cmax25} – maximum rate of Rubisco carboxylation at 25°C; J_{max25} – maximum rate of electron transport for RuBP regeneration at 25°C, $J_{\text{max25}}:V_{\text{cmax25}}$ – the ratio of J_{max25} to V_{cmax25} .

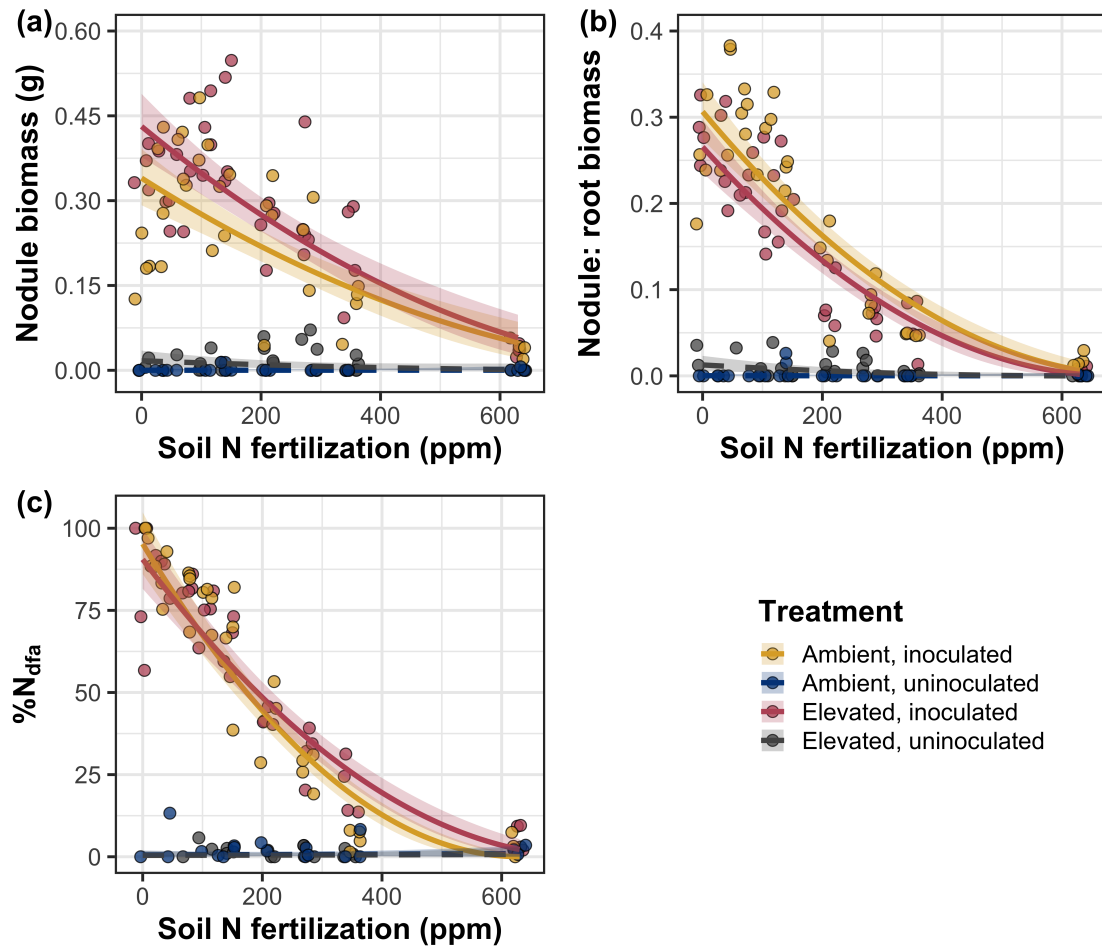


Figure 5.5. Effects of CO_2 , fertilization, and inoculation on nodule biomass (a), nodule: root biomass (b), and percent nitrogen fixed from the atmosphere (c). Soil nitrogen fertilization is represented on the x-axis. Yellow points and trendlines indicate inoculated individuals grown under ambient CO_2 , blue points and trendlines indicate uninoculated individuals grown under ambient CO_2 , red points and trendlines indicate inoculated individuals grown under elevated CO_2 , and grey points indicate uninoculated individuals grown under elevated CO_2 . Solid trendlines indicate slopes that are different from zero ($p < 0.05$), while dashed trendlines indicate slopes that are not different from zero ($p > 0.05$). Curvilinear trendlines occur as a result of back-transforming models where response variables received either a natural log or square root transformation prior to fitting.

1936 5.4 Discussion

1937 In this study, we determined leaf and whole plant acclimation responses of
1938 7-week *G. max* seedlings grown under two CO₂ concentrations, two inoculation
1939 treatments, and nine soil nitrogen fertilization treatments in a full-factorial growth
1940 chamber experiment. In support of our hypotheses and patterns expected from
1941 theory, elevated CO₂ reduced N_{area} , V_{cmax25} , and J_{max25} . The relatively stronger
1942 downregulation in V_{cmax25} than J_{max25} under elevated CO₂ resulted in a stimu-
1943 lation in $J_{\text{max25}}:V_{\text{cmax25}}$ under elevated CO₂. The downregulation of V_{cmax25} and
1944 J_{max25} under elevated CO₂ was similar across fertilization and inoculation treat-
1945 ments, indicating that the CO₂ responses were not due to nitrogen limitation.
1946 Interestingly, our results indicate that elevated CO₂ increased the fraction of leaf
1947 nitrogen allocated to photosynthesis and structure, leading to a stimulation in
1948 nitrogen use efficiency under elevated CO₂ despite the apparent downregulation
1949 in N_{area} , V_{cmax25} , and J_{max25} . The downregulation in leaf photosynthetic processes
1950 under elevated CO₂ also corresponded with a strong stimulation in total leaf area
1951 and total biomass. Strong stimulations in whole plant growth due to elevated CO₂
1952 were generally enhanced with increasing fertilization and were negatively related
1953 to structural carbon costs to acquire nitrogen. Inoculation generally did not mod-
1954 ify whole plant responses to elevated CO₂ across the fertilization gradient, likely
1955 due to a strong reduction in root nodulation with increasing fertilization. However,
1956 strong positive effects of inoculation on whole plant growth were observed under
1957 low fertilization, consistent with our hypothesis. Overall, observed leaf and whole
1958 plant acclimation responses to CO₂ support our hypotheses and patterns expected
1959 from photosynthetic least-cost theory, showing that leaf acclimation responses to

1960 CO₂ were decoupled from soil nitrogen availability and ability to acquire nitrogen
1961 via symbiotic nitrogen fixation. Instead, leaf acclimation responses were driven
1962 by optimal resource investment to photosynthetic capacity, which maximized ni-
1963 trogen allocation to structures that support whole plant growth.

1964

Chapter 6

1965

Conclusions

1966

References

- 1967** Abrams, M. D. and S. A. Mostoller (1995). Gas exchange, leaf structure and nitrogen in contrasting successional tree species growing in open and under-story sites during a drought. *Tree Physiology* 15(6), 361–370.
- 1968**
- 1969**
- 1970** Adams, M. A., T. L. Turnbull, J. I. Sprent, and N. Buchmann (2016). Legumes are different: Leaf nitrogen, photosynthesis, and water use efficiency. *Proceedings of the National Academy of Sciences of the United States of America* 113(15), 4098–4103.
- 1971**
- 1972**
- 1973**
- 1974** Ainsworth, E. A., P. A. Davey, C. J. Bernacchi, O. C. Dermody, E. A. Heaton, D. J. Moore, P. B. Morgan, S. L. Naidu, H. S. Y. Ra, X. G. Zhu, P. S. Curtis, and S. P. Long (2002). A meta-analysis of elevated [CO₂] effects on soybean (*Glycine max*) physiology, growth and yield. *Global Change Biology* 8(8), 695–709.
- 1975**
- 1976**
- 1977**
- 1978**
- 1979** Ainsworth, E. A. and S. P. Long (2005). What have we learned from 15 years of free-air CO₂ enrichment (FACE)? A meta-analytic review of the responses of photosynthesis, canopy properties and plant production to rising CO₂. *New Phytologist* 165(2), 351–372.
- 1980**
- 1981**
- 1982**
- 1983** Ainsworth, E. A. and A. Rogers (2007). The response of photosynthesis and stomatal conductance to rising [CO₂]: mechanisms and environmental interactions. *Plant, Cell and Environment* 30(3), 258–270.
- 1984**
- 1985**
- 1986** Allen, K., J. B. Fisher, R. P. Phillips, J. S. Powers, and E. R. Brzostek (2020).
- 1987** Modeling the carbon cost of plant nitrogen and phosphorus uptake across temperate and tropical forests. *Frontiers in Forests and Global Change* 3,
- 1988**

- 1989** 1–12.
- 1990** Allison, S. D., C. I. Czimczik, and K. K. Treseder (2008). Microbial activity
- 1991** and soil respiration under nitrogen addition in Alaskan boreal forest. *Global*
- 1992** *Change Biology* 14(5), 1156–1168.
- 1993** Andersen, M. K., H. Hauggaard-Nielsen, P. Ambus, and E. S. Jensen (2005).
- 1994** Biomass production, symbiotic nitrogen fixation and inorganic N use in dual
- 1995** and tri-component annual intercrops. *Plant and Soil* 266(1-2), 273–287.
- 1996** Andrews, M., E. K. James, J. I. Sprent, R. M. Boddey, E. Gross, and F. B. dos
- 1997** Reis (2011). Nitrogen fixation in legumes and actinorhizal plants in natural
- 1998** ecosystems: Values obtained using ^{15}N natural abundance. *Plant Ecology*
- 1999** and *Diversity* 4(2-3), 117–130.
- 2000** Arndal, M. F., A. Tolver, K. S. Larsen, C. Beier, and I. K. Schmidt (2018). Fine
- 2001** root growth and vertical distribution in response to elevated CO₂, warming
- 2002** and drought in a mixed heathland–grassland. *Ecosystems* 21(1), 15–30.
- 2003** Arnone, J. A. (1997). Indices of plant N availability in an alpine grassland under
- 2004** elevated atmospheric CO₂. *Plant and Soil* 190(1), 61–66.
- 2005** Arora, V. K., A. Katavouta, R. G. Williams, C. D. Jones, V. Brovkin,
- 2006** P. Friedlingstein, J. Schwinger, L. Bopp, O. Boucher, P. Cadule, M. A.
- 2007** Chamberlain, J. R. Christian, C. Delire, R. A. Fisher, T. Hajima, T. Ilyina,
- 2008** E. Joetzjer, M. Kawamiya, C. D. Koven, J. P. Krasting, R. M. Law, D. M.
- 2009** Lawrence, A. Lenton, K. Lindsay, J. Pongratz, T. Raddatz, R. Séférian,
- 2010** K. Tachiiri, J. F. Tjiputra, A. Wiltshire, T. Wu, and T. Ziehn (2020).
- 2011** Carbon-concentration and carbon-climate feedbacks in CMIP6 models and
- 2012** their comparison to CMIP5 models. *Biogeosciences* 17(16), 4173–4222.

- 2013** Bae, K., T. J. Fahey, R. D. Yanai, and M. Fisk (2015). Soil nitrogen availability affects belowground carbon allocation and soil respiration in northern hardwood forests of New Hampshire. *Ecosystems* 18(7), 1179–1191.
- 2014**
- 2015**
- 2016** Barber, S. A. (1962). A diffusion and mass-flow concept of soil nutrient availability. *Soil Science* 93(1), 39–49.
- 2017**
- 2018** Barnes, J. D., L. Balaguer, E. Manrique, S. Elvira, and A. W. Davison (1992).
- 2019** A reappraisal of the use of DMSO for the extraction and determination of chlorophylls a and b in lichens and higher plants. *Environmental and Experimental Botany* 32(2), 85–100.
- 2020**
- 2021**
- 2022** Bates, D., M. Mächler, B. Bolker, and S. Walker (2015). Fitting linear mixed-effects models using lme4. *Journal of Statistical Software* 67(1), 1–48.
- 2023**
- 2024** Beaudette, D., J. Skovlin, S. Roeker, and A. Brown (2022). soilDB: Soil Database Interface.
- 2025**
- 2026** Bengtson, P., J. Barker, and S. J. Grayston (2012). Evidence of a strong coupling between root exudation, C and N availability, and stimulated SOM decomposition caused by rhizosphere priming effects. *Ecology and Evolution* 2(8), 1843–1852.
- 2027**
- 2028**
- 2029**
- 2030** Bernacchi, C. J., E. L. Singsaas, C. Pimentel, A. R. Portis, and S. P. Long (2001). Improved temperature response functions for models of Rubisco-limited photosynthesis. *Plant, Cell and Environment* 24(2), 253–259.
- 2031**
- 2032**
- 2033** Bialic-Murphy, L., N. G. Smith, P. Voothuluru, R. M. McElderry, M. D. Roche, S. T. Cassidy, S. N. Kivlin, and S. Kalisz (2021). Invasion-induced root–fungal disruptions alter plant water and nitrogen economies. *Ecology*
- 2034**
- 2035**

- 2036** *Letters* 24(6), 1145–1156.
- 2037** Bloom, A. J., F. S. Chapin, and H. A. Mooney (1985). Resource limitation
2038 in plants - an economic analogy. *Annual Review of Ecology and Systemat-*
2039 *ics* 16(1), 363–392.
- 2040** Bloomfield, K. J., B. D. Stocker, T. F. Keenan, and I. C. Prentice (2022).
2041 Environmental controls on the light use efficiency of terrestrial gross primary
2042 production. *Global Change Biology*, 0–2.
- 2043** Bonan, G. B., M. D. Hartman, W. J. Parton, and W. R. Wieder (2013). Evaluat-
2044 ing litter decomposition in earth system models with long-term litterbag ex-
2045 periments: an example using the Community Land Model version 4 (CLM4).
2046 *Global Change Biology* 19(3), 957–974.
- 2047** Bonan, G. B., P. J. Lawrence, K. W. Oleson, S. Levis, M. Jung, M. Reich-
2048 stein, D. M. Lawrence, and S. C. Swenson (2011). Improving canopy pro-
2049 cesses in the Community Land Model version 4 (CLM4) using global flux
2050 fields empirically inferred from FLUXNET data. *Journal of Geophysical Re-*
2051 *search* 116(G2), G02014.
- 2052** Booth, B. B. B., C. D. Jones, M. Collins, I. J. Totterdell, P. M. Cox, S. Sitch,
2053 C. Huntingford, R. A. Betts, G. R. Harris, and J. Lloyd (2012). High sen-
2054 sitivity of future global warming to land carbon cycle processes. *Environ-*
2055 *mental Research Letters* 7(2), 024002.
- 2056** Borer, E. T., W. S. Harpole, P. B. Adler, E. M. Lind, J. L. Orrock, E. W.
2057 Seabloom, and M. D. Smith (2014). Finding generality in ecology: A model
2058 for globally distributed experiments. *Methods in Ecology and Evolution* 5(1),
2059 65–73.

- 2060** Braghieri, R. K., J. B. Fisher, K. Allen, E. Brzostek, M. Shi, X. Yang, D. M.
2061 Ricciuto, R. A. Fisher, Q. Zhu, and R. P. Phillips (2022). Modeling global
2062 carbon costs of plant nitrogen and phosphorus acquisition. *Journal of Ad-*
2063 *vances in Modeling Earth Systems* 14(8), 1–23.
- 2064** Brix, H. (1971). Effects of nitrogen fertilization on photosynthesis and respira-
2065 tion in Douglas-fir. *Forest Science* 17(4), 407–414.
- 2066** Brzostek, E. R., J. B. Fisher, and R. P. Phillips (2014). Modeling the carbon
2067 cost of plant nitrogen acquisition: Mycorrhizal trade-offs and multipath
2068 resistance uptake improve predictions of retranslocation. *Journal of Geo-*
2069 *physical Research: Biogeosciences* 119, 1684–1697.
- 2070** Bubier, J. L., R. Smith, S. Juutinen, T. R. Moore, R. Minocha, S. Long, and
2071 S. Minocha (2011). Effects of nutrient addition on leaf chemistry, morphol-
2072 ogy, and photosynthetic capacity of three bog shrubs. *Oecologia* 167(2),
2073 355–368.
- 2074** Cernusak, L. A., N. Ubierna, K. Winter, J. A. M. Holtum, J. D. Marshall, and
2075 G. D. Farquhar (2013). Environmental and physiological determinants of
2076 carbon isotope discrimination in terrestrial plants. *New Phytologist* 200(4),
2077 950–965.
- 2078** Chen, J.-L., J. F. Reynolds, P. C. Harley, and J. D. Tenhunen (1993). Coor-
2079 dination theory of leaf nitrogen distribution in a canopy. *Oecologia* 93(1),
2080 63–69.
- 2081** Clark, D. B., L. M. Mercado, S. Sitch, C. D. Jones, N. Gedney, M. J. Best,
2082 M. Pryor, G. G. Rooney, R. L. H. Essery, E. Blyth, O. Boucher, R. J.
2083 Harding, C. Huntingford, and P. M. Cox (2011). The Joint UK Land Envi-

- 2084 ronment Simulator (JULES), model description. Part 2: Carbon fluxes and
2085 vegetation dynamics. *Geoscientific Model Development* 4(3), 701–722.
- 2086 Cornwell, W. K., J. H. C. Cornelissen, K. Amatangelo, E. Dorrepaal, V. T.
2087 Eviner, O. Godoy, S. E. Hobbie, B. Hoorens, H. Kurokawa, N. Pérez-
2088 Harguindeguy, H. M. Quested, L. S. Santiago, D. A. Wardle, I. J. Wright,
2089 R. Aerts, S. D. Allison, P. van Bodegom, V. Brovkin, A. Chatain, T. V.
2090 Callaghan, S. Díaz, E. Garnier, D. E. Gurvich, E. Kazakou, J. A. Klein,
2091 J. Read, P. B. Reich, N. A. Soudzilovskaia, M. V. Vaieretti, and M. Westoby
2092 (2008). Plant species traits are the predominant control on litter decompo-
2093 sition rates within biomes worldwide. *Ecology Letters* 11(10), 1065–1071.
- 2094 Cornwell, W. K., I. J. Wright, J. Turner, V. Maire, M. M. Barbour, L. A.
2095 Cernusak, T. E. Dawson, D. S. Ellsworth, G. D. Farquhar, H. Griffiths,
2096 C. Keitel, A. Knohl, P. B. Reich, D. G. Williams, R. Bhaskar, J. H. C. Cor-
2097 nelissen, A. Richards, S. Schmidt, F. Valladares, C. Körner, E.-D. Schulze,
2098 N. Buchmann, and L. S. Santiago (2018). Climate and soils together regulate
2099 photosynthetic carbon isotope discrimination within C₃ plants worldwide.
2100 *Global Ecology and Biogeography* 27(9), 1056–1067.
- 2101 Cramer, W. and I. C. Prentice (1988). Simulation of regional soil moisture
2102 deficits on a European scale. *Norsk Geografisk Tidsskrift - Norwegian Jour-*
2103 *nal of Geography* 42(2-3), 149–151.
- 2104 Curtis, P. S. (1996). A meta-analysis of leaf gas exchange and nitrogen in trees
2105 grown under elevated carbon dioxide. *Plant, Cell and Environment* 19(2),
2106 127–137.
- 2107 Daly, C., M. Halbleib, J. I. Smith, W. P. Gibson, M. K. Doggett, G. H. Taylor,

- 2108** J. Curtis, and P. P. Pasteris (2008). Physiographically sensitive mapping
2109 of climatological temperature and precipitation across the conterminous
2110 United States. *International Journal of Climatology* 28(15), 2031–2064.
- 2111** Davies-Barnard, T., J. Meyerholt, S. Zaehle, P. Friedlingstein, V. Brovkin,
2112 Y. Fan, R. A. Fisher, C. D. Jones, H. Lee, D. Peano, B. Smith, D. Wårlind,
2113 and A. J. Wiltshire (2020). Nitrogen cycling in CMIP6 land surface models:
2114 progress and limitations. *Biogeosciences* 17(20), 5129–5148.
- 2115** Davis, T. W., I. C. Prentice, B. D. Stocker, R. T. Thomas, R. J. Whitley,
2116 H. Wang, B. J. Evans, A. V. Gallego-Sala, M. T. Sykes, and W. Cramer
2117 (2017). Simple process-led algorithms for simulating habitats (SPLASH
2118 v.1.0): robust indices of radiation, evapotranspiration and plant-available
2119 moisture. *Geoscientific Model Development* 10, 689–708.
- 2120** Delaire, M., E. Frak, M. Sigogne, B. Adam, F. Beaujard, and X. Le Roux
2121 (2005). Sudden increase in atmospheric CO₂ concentration reveals strong
2122 coupling between shoot carbon uptake and root nutrient uptake in young
2123 walnut trees. *Tree Physiology* 25(2), 229–235.
- 2124** Doane, T. A. and W. R. Horwáth (2003). Spectrophotometric determination of
2125 nitrate with a single reagent. *Analytical Letters* 36(12), 2713–2722.
- 2126** Dong, N., I. C. Prentice, B. J. Evans, S. Caddy-Retalic, A. J. Lowe, and I. J.
2127 Wright (2017). Leaf nitrogen from first principles: field evidence for adaptive
2128 variation with climate. *Biogeosciences* 14(2), 481–495.
- 2129** Dong, N., I. C. Prentice, I. J. Wright, B. J. Evans, H. F. Togashi, S. Caddy-
2130 Retalic, F. A. McInerney, B. Sparrow, E. Leitch, and A. J. Lowe (2020).
2131 Components of leaf-trait variation along environmental gradients. *New Phy-*

- 2132** *tologist* 228(1), 82–94.
- 2133** Dong, N., I. C. Prentice, I. J. Wright, H. Wang, O. K. Atkin, K. J. Bloomfield,
- 2134** T. F. Domingues, S. M. Gleason, V. Maire, Y. Onoda, H. Poorter, and N. G.
- 2135** Smith (2022). Leaf nitrogen from the perspective of optimal plant function.
- 2136** *Journal of Ecology* 110(11), 2585–2602.
- 2137** Dong, N., I. J. Wright, J. M. Chen, X. Luo, H. Wang, T. F. Keenan, N. G.
- 2138** Smith, and I. C. Prentice (2022). Rising CO₂ and warming reduce global
- 2139** canopy demand for nitrogen. *New Phytologist* 235(5), 1692–1700.
- 2140** Dovrat, G., H. Bakhshian, T. Masci, and E. Sheffer (2020). The nitrogen eco-
- 2141** nomic spectrum of legume stoichiometry and fixation strategy. *New Phytol-*
- 2142** *ogist* 227(2), 365–375.
- 2143** Dovrat, G., T. Masci, H. Bakhshian, E. Mayzlish Gati, S. Golan, and E. Shef-
- 2144** fer (2018). Drought-adapted plants dramatically downregulate dinitrogen
- 2145** fixation: Evidences from Mediterranean legume shrubs. *Journal of Ecol-*
- 2146** *ogy* 106(4), 1534–1544.
- 2147** Drake, B. G., M. A. Gonzàlez-Meler, and S. P. Long (1997). More efficient
- 2148** plants: a consequence of rising atmospheric CO₂? *Annual Review of Plant*
- 2149** *Biology* 48, 609–639.
- 2150** Duursma, R. A. (2015). Plantecophys - An R Package for Analysing and Mod-
- 2151** elling Leaf Gas Exchange Data. *PLOS ONE* 10(11), e0143346.
- 2152** Eastman, B. A., M. B. Adams, E. R. Brzostek, M. B. Burnham, J. E. Carrara,
- 2153** C. Kelly, B. E. McNeil, C. A. Walter, and W. T. Peterjohn (2021). Altered
- 2154** plant carbon partitioning enhanced forest ecosystem carbon storage after 25

- 2155 years of nitrogen additions. *New Phytologist* 230(4), 1435–1448.
- 2156 Ellsworth, D. S. and P. B. Reich (1996). Photosynthesis and leaf nitrogen in five
2157 Amazonian tree species during early secondary succession. *Ecology* 77(2),
2158 581–594.
- 2159 Espelta, J. M., P. Cortés, M. Mangirón, and J. Retana (2005). Differences in
2160 biomass partitioning, leaf nitrogen content, and water use efficiency d13C
2161 result in similar performance of seedlings of two Mediterranean oaks with
2162 contrasting leaf habit. *Ecoscience* 12(4), 447–454.
- 2163 Evans, J. R. (1989). Photosynthesis and nitrogen relationships in leaves of C₃
2164 plants. *Oecologia* 78(1), 9–19.
- 2165 Evans, J. R. and V. C. Clarke (2019). The nitrogen cost of photosynthesis.
2166 *Journal of Experimental Botany* 70(1), 7–15.
- 2167 Evans, J. R. and H. Poorter (2001). Photosynthetic acclimation of plants to
2168 growth irradiance: the relative importance of specific leaf area and nitrogen
2169 partitioning in maximizing carbon gain. *Plant, Cell and Environment* 24(8),
2170 755–767.
- 2171 Evans, J. R. and J. R. Seemann (1989). The allocation of protein nitrogen in
2172 the photosynthetic apparatus: costs, consequences, and control. *Photosyn-*
2173 *thesis* 8, 183–205.
- 2174 Exbrayat, J.-F., A. A. Bloom, P. Falloon, A. Ito, T. L. Smallman, and
2175 M. Williams (2018). Reliability ensemble averaging of 21st century projec-
2176 tions of terrestrial net primary productivity reduces global and regional
2177 uncertainties. *Earth System Dynamics* 9(1), 153–165.

- 2178 Farquhar, G. D., J. R. Ehleringer, and K. T. Hubick (1989). Carbon Isotope
2179 Discrimination and Photosynthesis. *Annual Review of Plant Physiology and*
2180 *Plant Molecular Biology* 40(1), 503–537.
- 2181 Farquhar, G. D. and T. D. Sharkey (1982). Stomatal conductance and photo-
2182 synthesis. *Annual Review of Plant Physiology* 33(1), 317–345.
- 2183 Farquhar, G. D., S. von Caemmerer, and J. A. Berry (1980). A biochemical
2184 model of photosynthetic CO₂ assimilation in leaves of C₃ species.
2185 *Planta* 149(1), 78–90.
- 2186 Fay, P. A., S. M. Prober, W. S. Harpole, J. M. H. Knops, J. D. Bakker, E. T.
2187 Borer, E. M. Lind, A. S. MacDougall, E. W. Seabloom, P. D. Wragg, P. B.
2188 Adler, D. M. Blumenthal, Y. M. Buckley, C. Chu, E. E. Cleland, S. L.
2189 Collins, K. F. Davies, G. Du, X. Feng, J. Firn, D. S. Gruner, N. Hagenah,
2190 Y. Hautier, R. W. Heckman, V. L. Jin, K. P. Kirkman, J. A. Klein, L. M.
2191 Ladwig, Q. Li, R. L. McCulley, B. A. Melbourne, C. E. Mitchell, J. L. Moore,
2192 J. W. Morgan, A. C. Risch, M. Schütz, C. J. Stevens, D. A. Wedin, and
2193 L. H. Yang (2015). Grassland productivity limited by multiple nutrients.
2194 *Nature Plants* 1(7), 15080.
- 2195 Feng, X. (1999). Trends in intrinsic water-use efficiency of natural trees for the
2196 past 100-200 years: A response to atmospheric CO₂ concentration. *Geochim-
2197 ica et Cosmochimica Acta* 63(13-14), 1891–1903.
- 2198 Field, C. B. and H. A. Mooney (1986). The photosynthesis-nitrogen relationship
2199 in wild plants. In T. J. Givnish (Ed.), *On the Economy of Plant Form and*
2200 *Function*, pp. 25–55. Cambridge: Cambridge University Press.
- 2201 Finzi, A. C., D. J. P. Moore, E. H. DeLucia, J. Lichter, K. S. Hofmockel, R. B.

- 2202** Jackson, H. S. Kim, R. Matamala, H. R. McCarthy, R. Oren, J. S. Pippen,
2203 and W. H. Schlesinger (2006). Progressive nitrogen limitation of ecosystem
2204 processes under elevated CO₂ in a warm-temperate forest. *Ecology* 87(1),
2205 15–25.
- 2206** Firn, J., J. M. McGree, E. Harvey, H. Flores Moreno, M. Schutz, Y. M. Buckley,
2207 E. T. Borer, E. W. Seabloom, K. J. La Pierre, A. M. MacDougall, S. M.
2208 Prober, C. J. Stevens, L. L. Sullivan, E. Porter, E. Ladouceur, C. Allen,
2209 K. H. Moromizato, J. W. Morgan, W. S. Harpole, Y. Hautier, N. Eisen-
2210 hauer, J. P. Wright, P. B. Adler, C. A. Arnillas, J. D. Bakker, L. Biederman,
2211 A. A. D. Broadbent, C. S. Brown, M. N. Bugalho, M. C. Caldeira, E. E. Cle-
2212 land, A. Ebeling, P. A. Fay, N. Hagenah, A. R. Kleinhesselink, R. Mitchell,
2213 J. L. Moore, C. Nogueira, P. L. Peri, C. Roscher, M. D. Smith, P. D. Wragg,
2214 and A. C. Risch (2019). Leaf nutrients, not specific leaf area, are consistent
2215 indicators of elevated nutrient inputs. *Nature Ecology and Evolution* 3(3),
2216 400–406.
- 2217** Fisher, J. B., S. Sitch, Y. Malhi, R. A. Fisher, C. Huntingford, and S.-Y. Tan
2218 (2010). Carbon cost of plant nitrogen acquisition: A mechanistic, globally
2219 applicable model of plant nitrogen uptake, retranslocation, and fixation.
2220 *Global Biogeochemical Cycles* 24(1), 1–17.
- 2221** Fox, J. and S. Weisberg (2019). *An R companion to applied regression* (Third
2222 edit ed.). Thousand Oaks, California: Sage.
- 2223** Franklin, O., R. E. McMurtrie, C. M. Iversen, K. Y. Crous, A. C. Finzi, D. Tis-
2224 sue, D. S. Ellsworth, R. Oren, and R. J. Norby (2009). Forest fine-root
2225 production and nitrogen use under elevated CO₂: contrasting responses

- 2226** in evergreen and deciduous trees explained by a common principle. *Global*
2227 *Change Biology* 15(1), 132–144.
- 2228** Friedlingstein, P., M. Meinshausen, V. K. Arora, C. D. Jones, A. Anav, S. K.
2229 Liddicoat, and R. Knutti (2014). Uncertainties in CMIP5 climate projections
2230 due to carbon cycle feedbacks. *Journal of Climate* 27(2), 511–526.
- 2231** Friel, C. A. and M. L. Friesen (2019). Legumes modulate allocation to rhizobial
2232 nitrogen fixation in response to factorial light and nitrogen manipulation.
2233 *Frontiers in Plant Science* 10, 1316.
- 2234** Fujikake, H., A. Yamazaki, N. Ohtake, K. Sueoshi, S. Matsuhashi, T. Ito,
2235 C. Mizuniwa, T. Kume, S. Hoshimoto, N.-S. Ishioka, S. Watanabe, A. Osa,
2236 T. Sekine, H. Uchida, A. Tsuji, and T. Ohyama (2003). Quick and reversible
2237 inhibition of soybean root nodule growth by nitrate involves a decrease in
2238 sucrose supply to nodules. *Journal of Experimental Botany* 54(386), 1379–
2239 1388.
- 2240** Ghimire, B., W. J. Riley, C. D. Koven, J. Kattge, A. Rogers, P. B. Reich, and
2241 I. J. Wright (2017). A global trait-based approach to estimate leaf nitro-
2242 gen functional allocation from observations:. *Ecological Applications* 27(5),
2243 1421–1434.
- 2244** Giardina, C. P., M. D. Coleman, J. E. Hancock, J. S. King, E. A. Lilleskov,
2245 W. M. Loya, K. S. Pregitzer, M. G. Ryan, and C. C. Trettin (2005). The
2246 response of belowground carbon allocation in forests to global change. In
2247 D. Binkley and O. Manyailo (Eds.), *Tree Species Effects on Soils: Implica-*
2248 *tions for Global Change* (Volume 55 ed.), Chapter Chapter 7, pp. 119–154.
2249 Berlin/Heidelberg: Springer-Verlag.

- 2250** Gibson, A. H. and J. E. Harper (1985). Nitrate effect on nodulation of soybean
2251 by *Bradyrhizobium japonicum*. *Crop Science* 25(3), 497–501.
- 2252** Gill, A. L. and A. C. Finzi (2016). Belowground carbon flux links biogeochemical
2253 cycles and resource-use efficiency at the global scale. *Ecology Letters* 19(12),
2254 1419–1428.
- 2255** Goll, D. S., V. Brovkin, B. R. Parida, C. H. Reick, J. Kattge, P. B. Reich, P. M.
2256 van Bodegom, and Ü. Niinemets (2012). Nutrient limitation reduces land
2257 carbon uptake in simulations with a model of combined carbon, nitrogen
2258 and phosphorus cycling. *Biogeosciences Discussions* 9(3), 3173–3232.
- 2259** Gregory, L. M., A. M. McClain, D. M. Kramer, J. D. Pardo, K. E. Smith, O. L.
2260 Tessmer, B. J. Walker, L. G. Ziccardi, and T. D. Sharkey (2021, oct). The
2261 triose phosphate utilization limitation of photosynthetic rate: Out of global
2262 models but important for leaf models. *Plant, Cell and Environment* 44(10),
2263 3223–3226.
- 2264** Guerrieri, R., M. Mencuccini, L. J. Sheppard, M. Saurer, M. P. Perks, P. Levy,
2265 M. A. Sutton, M. Borghetti, and J. Grace (2011). The legacy of enhanced
2266 N and S deposition as revealed by the combined analysis of $\delta^{13}\text{C}$, $\delta^{18}\text{O}$ and
2267 $\delta^{15}\text{N}$ in tree rings. *Global Change Biology* 17(5), 1946–1962.
- 2268** Gulmon, S. L. and C. C. Chu (1981). The effects of light and nitrogen on pho-
2269 tosynthesis, leaf characteristics, and dry matter allocation in the chaparral
2270 shrub, <i>Diplacus aurantiacus</i>. *Oecologia* 49(2), 207–212.
- 2271** Gutschick, V. P. (1981). Evolved strategies in nitrogen acquisition by plants.
2272 *The American Naturalist* 118(5), 607–637.

- 2273** Hallik, L., Ü. Niinemets, and I. J. Wright (2009). Are species shade and drought
2274 tolerance reflected in leaf-level structural and functional differentiation in
2275 Northern Hemisphere temperate woody flora? *New Phytologist* 184(1), 257–
2276 274.
- 2277** Harrison, M. T., E. J. Edwards, G. D. Farquhar, A. B. Nicotra, and J. R.
2278 Evans (2009). Nitrogen in cell walls of sclerophyllous leaves accounts for
2279 little of the variation in photosynthetic nitrogen-use efficiency. *Plant, Cell*
2280 and *Environment* 32(3), 259–270.
- 2281** Harrison, S. P., W. Cramer, O. Franklin, I. C. Prentice, H. Wang,
2282 Å. Bränström, H. de Boer, U. Dieckmann, J. Joshi, T. F. Keenan,
2283 A. Lavergne, S. Manzoni, G. Mengoli, C. Morfopoulos, J. Peñuelas,
2284 S. Pietsch, K. T. Rebel, Y. Ryu, N. G. Smith, B. D. Stocker, and I. J.
2285 Wright (2021). Eco-evolutionary optimality as a means to improve vegeta-
2286 tion and land-surface models. *New Phytologist* 231(6), 2125–2141.
- 2287** Henneron, L., P. Kardol, D. A. Wardle, C. Cros, and S. Fontaine (2020). Rhizo-
2288 sphere control of soil nitrogen cycling: a key component of plant economic
2289 strategies. *New Phytologist* 228(4), 1269–1282.
- 2290** Hijmans, R. J. (2022). terra: Spatial Data Analysis.
- 2291** Hikosaka, K. and A. Shigeno (2009). The role of Rubisco and cell walls in the
2292 interspecific variation in photosynthetic capacity. *Oecologia* 160(3), 443–
2293 451.
- 2294** Hoagland, D. R. and D. I. Arnon (1950). The water culture method for growing
2295 plants without soil. *California Agricultural Experiment Station: 347* 347(2),
2296 1–32.

- 2297** Hobbie, E. A. (2006). Carbon allocation to ectomycorrhizal fungi correlates
2298 with belowground allocation in culture studies. *Ecology* 87(3), 563–569.
- 2299** Hobbie, E. A. and J. E. Hobbie (2008). Natural abundance of ^{15}N in nitrogen-
2300 limited forests and tundra can estimate nitrogen cycling through mycorrhizal
2301 fungi: a review. *Ecosystems* 11(5), 815–830.
- 2302** Hoek, T. A., K. Axelrod, T. Biancalani, E. A. Yurtsev, J. Liu, and J. Gore
2303 (2016). Resource availability modulates the cooperative and competitive na-
2304 nature of a microbial cross-feeding mutualism. *PLOS Biology* 14(8), e1002540.
- 2305** Höglberg, M. N., M. J. I. Briones, S. G. Keel, D. B. Metcalfe, C. Campbell, A. J.
2306 Midwood, B. Thornton, V. Hurry, S. Linder, T. Näsholm, and P. Höglberg
2307 (2010). Quantification of effects of season and nitrogen supply on tree below-
2308 ground carbon transfer to ectomycorrhizal fungi and other soil organisms in
2309 a boreal pine forest. *New Phytologist* 187(2), 485–493.
- 2310** Höglberg, P., M. N. Höglberg, S. G. Göttlicher, N. R. Betson, S. G. Keel, D. B.
2311 Metcalfe, C. Campbell, A. Schindlbacher, V. Hurry, T. Lundmark, S. Linder,
2312 and T. Näsholm (2008). High temporal resolution tracing of photosynthate
2313 carbon from the tree canopy to forest soil microorganisms. *New Phytolo-*
2314 *gist* 177(1), 220–228.
- 2315** Houlton, B. Z., Y.-P. Wang, P. M. Vitousek, and C. B. Field (2008). A uni-
2316 fying framework for dinitrogen fixation in the terrestrial biosphere. *Nature*
2317 454(7202), 327–330.
- 2318** Huber, M. L., R. A. Perkins, A. Laesecke, D. G. Friend, J. V. Sengers, M. J.
2319 Assael, I. N. Metaxa, E. Vogel, R. Mareš, and K. Miyagawa (2009). New
2320 international formulation for the viscosity of H₂O. *Journal of Physical and*

- 2321 *Chemical Reference Data* 38(2), 101–125.
- 2322 Hungate, B. A., J. S. Dukes, M. R. Shaw, Y. Luo, and C. B. Field (2003).
- 2323 Nitrogen and climate change. *Science* 302(5650), 1512–1513.
- 2324 IPCC (2021). *Climate Change 2021: The Physical Science Basis. Contribution of Working Group I to the Sixth Assessment Report of the Intergovernmental Panel on Climate Change*. Cambridge University Press.
- 2327 Johnson, N. C., J. H. Graham, and F. A. Smith (1997). Functioning of mycorrhizal associations along the mutualism-parasitism continuum. *New Phytologist* 135(4), 575–585.
- 2328 2329
- 2330 Kachurina, O. M., H. Zhang, W. R. Raun, and E. G. Krenzer (2000). Simultaneous determination of soil aluminum, ammonium- and nitrate- nitrogen using 1 M potassium chloride. *Communications in Soil Science and Plant Analysis* 31(7-8), 893–903.
- 2331 2332
- 2333 Kaiser, C., M. R. Kilburn, P. L. Clode, L. Fuchslueger, M. Koranda, J. B. Cliff, Z. M. Solaiman, and D. V. Murphy (2015). Exploring the transfer of recent plant photosynthates to soil microbes: mycorrhizal pathway vs direct root exudation. *New Phytologist* 205(4), 1537–1551.
- 2334 2335
- 2336 2337
- 2338 Katabuchi, M. (2015). LeafArea: An R package for rapid digital analysis of leaf area. *Ecological Research* 30(6), 1073–1077.
- 2339
- 2340 Kattge, J. and W. Knorr (2007). Temperature acclimation in a biochemical model of photosynthesis: a reanalysis of data from 36 species. *Plant, Cell and Environment* 30(9), 1176–1190.
- 2341 2342
- 2343 Kattge, J., W. Knorr, T. Raddatz, and C. Wirth (2009). Quantifying photosyn-

- 2344** thetic capacity and its relationship to leaf nitrogen content for global-scale
2345 terrestrial biosphere models. *Global Change Biology* 15(4), 976–991.
- 2346** Kayler, Z., A. Gessler, and N. Buchmann (2010). What is the speed of link
2347 between aboveground and belowground processes? *New Phytologist* 187(4),
2348 885–888.
- 2349** Kayler, Z., C. Keitel, K. Jansen, and A. Gessler (2017). Experimental evi-
2350 dence of two mechanisms coupling leaf-level C assimilation to rhizosphere
2351 CO₂ release. *Environmental and Experimental Botany* 135,
2352 21–26.
- 2353** Keeling, C. D., W. G. Mook, and P. P. Tans (1979, jan). Recent trends in the
2354 ¹³C/¹²C ratio of atmospheric carbon dioxide.
2355 *Nature* 277(5692), 121–123.
- 2356** Kenward, M. G. and J. H. Roger (1997). Small sample inference for fixed effects
2357 from restricted maximum likelihood. *Biometrics* 53(3), 983.
- 2358** Knapp, A. K., M. L. Avolio, C. Beier, C. J. W. Carroll, S. L. Collins, J. S.
2359 Dukes, L. H. Fraser, R. J. Griffin-Nolan, D. L. Hoover, A. Jentsch, M. E.
2360 Loik, R. P. Phillips, A. K. Post, O. E. Sala, I. J. Slette, L. Yahdjian, and
2361 M. D. Smith (2017). Pushing precipitation to the extremes in distributed
2362 experiments: recommendations for simulating wet and dry years. *Global
Change Biology* 23(5), 1774–1782.
- 2364** Knorr, W. (2000). Annual and interannual CO₂ exchanges of the
2365 terrestrial biosphere: process-based simulations and uncertainties. *Global
Ecology and Biogeography* 9(3), 225–252.

- 2367 Knorr, W. and M. Heimann (2001). Uncertainties in global terrestrial biosphere
2368 modeling: 1. A comprehensive sensitivity analysis with a new photosynthesis
2369 and energy balance scheme. *Global Biogeochemical Cycles* 15(1), 207–225.
- 2370 Kulmatiski, A., P. B. Adler, J. M. Stark, and A. T. Tredennick (2017). Water
2371 and nitrogen uptake are better associated with resource availability than
2372 root biomass. *Ecosphere* 8(3), e01738.
- 2373 Lavergne, A., D. Sandoval, V. J. Hare, H. Graven, and I. C. Prentice (2020).
2374 Impacts of soil water stress on the acclimated stomatal limitation of pho-
2375 tosynthesis: Insights from stable carbon isotope data. *Global Change Biol-*
2376 *ogy* 26(12), 7158–7172.
- 2377 Lawrence, D. M., R. A. Fisher, C. D. Koven, K. W. Oleson, S. C. Swen-
2378 son, G. B. Bonan, N. Collier, B. Ghimire, L. Kampenhout, D. Kennedy,
2379 E. Kluzeck, P. J. Lawrence, F. Li, H. Li, D. L. Lombardozzi, W. J. Riley,
2380 W. J. Sacks, M. Shi, M. Vertenstein, W. R. Wieder, C. Xu, A. A. Ali,
2381 A. M. Badger, G. Bisht, M. Broeke, M. A. Brunke, S. P. Burns, J. Buzan,
2382 M. Clark, A. Craig, K. M. Dahlin, B. Drewniak, J. B. Fisher, M. Flanner,
2383 A. M. Fox, P. Gentine, F. M. Hoffman, G. Keppel-Aleks, R. Knox, S. Ku-
2384 mar, J. Lenaerts, L. R. Leung, W. H. Lipscomb, Y. Lu, A. Pandey, J. D.
2385 Pelletier, J. Perket, J. T. Randerson, D. M. Ricciuto, B. M. Sanderson,
2386 A. Slater, Z. M. Subin, J. Tang, R. Q. Thomas, M. Val Martin, and X. Zeng
2387 (2019). The Community Land Model Version 5: description of new features,
2388 benchmarking, and impact of forcing uncertainty. *Journal of Advances in*
2389 *Modeling Earth Systems* 11(12), 4245–4287.
- 2390 LeBauer, D. S. and K. K. Treseder (2008). Nitrogen limitation of net primary

- 2391 productivity. *Ecology* 89(2), 371–379.
- 2392 Lefcheck, J. S. (2016). piecewiseSEM: Piecewise structural equation modelling
2393 in r for ecology, evolution, and systematics. *Methods in Ecology and Evolution*
2394 7(5), 573–579.
- 2395 Lenth, R. (2019). emmeans: estimated marginal means, aka least-squares
2396 means.
- 2397 Li, W., H. Zhang, G. Huang, R. Liu, H. Wu, C. Zhao, and N. G. McDowell
2398 (2020). Effects of nitrogen enrichment on tree carbon allocation: A global
2399 synthesis. *Global Ecology and Biogeography* 29(3), 573–589.
- 2400 Liang, J., X. Qi, L. Souza, and Y. Luo (2016). Processes regulating progressive
2401 nitrogen limitation under elevated carbon dioxide: a meta-analysis. *Biogeosciences*
2402 13(9), 2689–2699.
- 2403 Liang, X., T. Zhang, X. Lu, D. S. Ellsworth, H. BassiriRad, C. You, D. Wang,
2404 P. He, Q. Deng, H. Liu, J. Mo, and Q. Ye (2020). Global response patterns of
2405 plant photosynthesis to nitrogen addition: A meta-analysis. *Global Change
2406 Biology* 26(6), 3585–3600.
- 2407 Lu, J., J. Yang, C. Keitel, L. Yin, P. Wang, W. Cheng, and F. A. Dijkstra
2408 (2022). Belowground Carbon Efficiency for Nitrogen and Phosphorus Ac-
2409 quisition Varies Between *Lolium perenne* and *Trifolium repens* and Depends
2410 on Phosphorus Fertilization. *Frontiers in Plant Science* 13, 1–9.
- 2411 Luo, X., T. F. Keenan, J. M. Chen, H. Croft, I. C. Prentice, N. G. Smith,
2412 A. P. Walker, H. Wang, R. Wang, C. Xu, and Y. Zhang (2021). Global
2413 variation in the fraction of leaf nitrogen allocated to photosynthesis. *Nature*

- 2414** *Communications* 12(1), 4866.
- 2415** Luo, Y., W. S. Currie, J. S. Dukes, A. C. Finzi, U. A. Hartwig, B. A. Hungate,
- 2416** R. E. McMurtrie, R. Oren, W. J. Parton, D. E. Pataki, R. M. Shaw, D. R.
- 2417** Zak, and C. B. Field (2004). Progressive nitrogen limitation of ecosystem
- 2418** responses to rising atmospheric carbon dioxide. *BioScience* 54(8), 731–739.
- 2419** Maire, V., P. Martre, J. Kattge, F. Gastal, G. Esser, S. Fontaine, and J.-F.
- 2420** Soussana (2012). The coordination of leaf photosynthesis links C and N
- 2421** fluxes in C₃ plant species. *PLoS ONE* 7(6), e38345.
- 2422** Makino, A. (2003). Rubisco and nitrogen relationships in rice: leaf photosyn-
- 2423** thesis and plant growth. *Soil Science and Plant Nutrition* 49(3), 319–327.
- 2424** Markham, J. H. and C. Zekveld (2007). Nitrogen fixation makes biomass al-
- 2425** location to roots independent of soil nitrogen supply. *Canadian Journal of*
- 2426** *Botany* (9), 787–793.
- 2427** Marschner, H. and B. Dell (1994). Nutrient uptake in mycorrhizal symbiosis.
- 2428** *Plant and Soil* 159(1), 89–102.
- 2429** Matamala, R. and W. H. Schlesinger (2000). Effects of elevated atmospheric
- 2430** CO₂ on fine root production and activity in an intact tem-
- 2431** perate forest ecosystem. *Global Change Biology* 6(8), 967–979.
- 2432** Medlyn, B. E., E. Dreyer, D. S. Ellsworth, M. Forstreuter, P. C. Harley,
- 2433** M. U. F. Kirschbaum, X. Le Roux, P. Montpied, J. Strassmeyer, A. Wal-
- 2434** croft, K. Wang, and D. Loustau (2002). Temperature response of parameters
- 2435** of a biochemically based model of photosynthesis. II. A review of experimen-
- 2436** tal data. *Plant, Cell and Environment* 25(9), 1167–1179.

- 2437** Menge, D. N. L., S. A. Levin, and L. O. Hedin (2008). Evolutionary tradeoffs can
2438 select against nitrogen fixation and thereby maintain nitrogen limitation.
2439 *Proceedings of the National Academy of Sciences* 105(5), 1573–1578.
- 2440** Menne, M. J., I. Durre, R. S. Vose, B. E. Gleason, and T. G. Houston (2012).
2441 An overview of the global historical climatology network-daily database.
2442 *Journal of Atmospheric and Oceanic Technology* 29(7), 897–910.
- 2443** Meyerholt, J., K. Sickel, and S. Zaehle (2020). Ensemble projections elucidate
2444 effects of uncertainty in terrestrial nitrogen limitation on future carbon up-
2445 take. *Global Change Biology* 26(7), 3978–3996.
- 2446** Meyerholt, J., S. Zaehle, and M. J. Smith (2016). Variability of pro-
2447 jected terrestrial biosphere responses to elevated levels of atmospheric
2448 CO₂ due to uncertainty in biological nitrogen fixation. *Bio-*
2449 *geosciences* 13(5), 1491–1518.
- 2450** Minocha, R., S. Long, A. H. Magill, J. D. Aber, and W. H. McDowell (2000).
2451 Foliar free polyamine and inorganic ion content in relation to soil and soil
2452 solution chemistry in two fertilized forest stands at the Harvard Forest,
2453 Massachusetts. *Plant and Soil* 222(1-2), 119–137.
- 2454** Moore, D. J., S. Aref, R. M. Ho, J. S. Pippen, J. G. Hamilton, and E. H. De
2455 Lucia (2006). Annual basal area increment and growth duration of *Pinus*
2456 *taeda* in response to eight years of free-air carbon dioxide enrichment. *Global*
2457 *Change Biology* 12(8), 1367–1377.
- 2458** Morgan, J. A., D. E. Pataki, C. Körner, H. Clark, S. J. Del Gross, J. M.
2459 Grünzweig, A. K. Knapp, A. R. Mosier, P. C. D. Newton, P. A. Niklaus,
2460 J. B. Nippert, R. S. Nowak, W. J. Parton, H. W. Polley, and M. R. Shaw

- 2461 (2004). Water relations in grassland and desert ecosystems exposed to ele-
2462 vated atmospheric CO₂. *Oecologia* 140(1), 11–25.
- 2463 Muñoz, N., X. Qi, M. W. Li, M. Xie, Y. Gao, M. Y. Cheung, F. L. Wong, and
2464 H.-M. Lam (2016). Improvement in nitrogen fixation capacity could be part
2465 of the domestication process in soybean. *Heredity* 117(2), 84–93.
- 2466 Nadelhoffer, K. J. and J. W. Raich (1992). Fine root production estimates and
2467 belowground carbon allocation in forest ecosystems. *Ecology* 73(4), 1139–
2468 1147.
- 2469 Niinemets, Ü. and J. D. Tenhunen (1997). A model separating leaf struc-
2470 tural and physiological effects on carbon gain along light gradients for the
2471 shade-tolerant species *< i>Acer saccharum</i>*. *Plant, Cell and Environ-
2472 ment* 20(7), 845–866.
- 2473 Norby, R. J., J. Ledford, C. D. Reilly, N. E. Miller, and E. G. O'Neill
2474 (2004). Fine-root production dominates response of a deciduous forest to
2475 atmospheric CO₂ enrichment. *Proceedings of the National Academy of Sci-
2476 ences* 101(26), 9689–9693.
- 2477 Norby, R. J., J. M. Warren, C. M. Iversen, B. E. Medlyn, and R. E. Mc-
2478 Murtrie (2010). CO₂ enhancement of forest productivity constrained by
2479 limited nitrogen availability. *Proceedings of the National Academy of Sci-
2480 ences* 107(45), 19368–19373.
- 2481 Novick, K. A., D. L. Ficklin, P. C. Stoy, C. A. Williams, G. Bohrer, A. C.
2482 Oishi, S. A. Papuga, P. D. Blanken, A. Noormets, B. N. Sulman, R. L.
2483 Scott, L. Wang, and R. P. Phillips (2016). The increasing importance of
2484 atmospheric demand for ecosystem water and carbon fluxes. *Nature Climate*

- 2485 *Change* 6(11), 1023–1027.
- 2486 Noyce, G. L., M. L. Kirwan, R. L. Rich, and J. P. Megonigal (2019). Asyn-
2487 chronous nitrogen supply and demand produce nonlinear plant allocation
2488 responses to warming and elevated CO₂. *Proceedings of the*
2489 *National Academy of Sciences* 116(43), 21623–21628.
- 2490 Onoda, Y., K. Hikosaka, and T. Hirose (2004). Allocation of nitrogen to
2491 cell walls decreases photosynthetic nitrogen-use efficiency. *Functional Ecol-*
2492 *ogy* 18(3), 419–425.
- 2493 Onoda, Y., I. J. Wright, J. R. Evans, K. Hikosaka, K. Kitajima, Ü. Niinemets,
2494 H. Poorter, T. Tosens, and M. Westoby (2017). Physiological and structural
2495 tradeoffs underlying the leaf economics spectrum. *New Phytologist* 214(4),
2496 1447–1463.
- 2497 Oreskes, N., K. Shrader-Frechette, and K. Belitz (1994). Verification, vali-
2498 dation, and confirmation of numerical models in the Earth sciences. *Sci-*
2499 *ence* 263(5147), 641–646.
- 2500 Paillassa, J., I. J. Wright, I. C. Prentice, S. Pepin, N. G. Smith, G. Ethier,
2501 A. C. Westerband, L. J. Lamarque, H. Wang, W. K. Cornwell, and V. Maire
2502 (2020). When and where soil is important to modify the carbon and water
2503 economy of leaves. *New Phytologist* 228(1), 121–135.
- 2504 Parvin, S., S. Uddin, S. Tausz Posch, R. Armstrong, and M. Tausz (2020). Car-
2505 bon sink strength of nodules but not other organs modulates photosynthesis
2506 of faba bean (*i>Vicia faba</i>)) grown under elevated [CO₂] and different
2507 water supply. *New Phytologist* 227(1), 132–145.*

- 2508 Peng, Y., K. J. Bloomfield, L. A. Cernusak, T. F. Domingues, and I. C. Prentice (2021). Global climate and nutrient controls of photosynthetic capacity.
- 2509
2510 *Communications Biology* 4(1), 462.
- 2511 Perkowski, E. A., E. F. Waring, and N. G. Smith (2021). Root mass carbon
- 2512 costs to acquire nitrogen are determined by nitrogen and light availability
- 2513 in two species with different nitrogen acquisition strategies. *Journal of*
- 2514 *Experimental Botany* 72(15), 5766–5776.
- 2515 Phillips, R. P., E. R. Brzostek, and M. G. Midgley (2013). The mycorrhizal-
- 2516 associated nutrient economy: a new framework for predicting carbon-
- 2517 nutrient couplings in temperate forests. *New Phytologist* 199(1), 41–51.
- 2518 Phillips, R. P., A. C. Finzi, and E. S. Bernhardt (2011). Enhanced root ex-
- 2519 udation induces microbial feedbacks to N cycling in a pine forest under
- 2520 long-term CO₂ fumigation. *Ecology Letters* 14(2), 187–194.
- 2521 Pinheiro, J. and D. Bates (2022). nlme: linear and nonlinear mixed effects
- 2522 models.
- 2523 Poggio, L., L. M. De Sousa, N. H. Batjes, G. B. M. Heuvelink, B. Kempen,
- 2524 E. Ribeiro, and D. Rossiter (2021). SoilGrids 2.0: Producing soil information
- 2525 for the globe with quantified spatial uncertainty. *Soil* 7(1), 217–240.
- 2526 Pons, T. L. and R. W. Pearcy (1994). Nitrogen reallocation and photosynthetic
- 2527 acclimation in response to partial shading in soybean plants. *Physiologia*
- 2528 *Plantarum* 92(4), 636–644.
- 2529 Poorter, H., J. Bühler, D. Van Dusschoten, J. Climent, and J. A. Postma (2012).
- 2530 Pot size matters: A meta-analysis of the effects of rooting volume on plant

- 2531 growth. *Functional Plant Biology* 39(11), 839–850.
- 2532 Poorter, H., O. Knopf, I. J. Wright, A. A. Temme, S. W. Hogewoning, A. Graf,
2533 L. A. Cernusak, and T. L. Pons (2022). A meta-analysis of responses of C₃
2534 plants to atmospheric CO₂: dose–response curves for 85 traits ranging from
2535 the molecular to the whole-plant level. *New Phytologist* 233(4), 1560–1596.
- 2536 Prentice, I. C., N. Dong, S. M. Gleason, V. Maire, and I. J. Wright (2014).
2537 Balancing the costs of carbon gain and water transport: testing a new theo-
2538 retical framework for plant functional ecology. *Ecology Letters* 17(1), 82–91.
- 2539 Prentice, I. C., X. Liang, B. E. Medlyn, and Y.-P. Wang (2015). Reliable, ro-
2540 bust and realistic: The three R’s of next-generation land-surface modelling.
2541 *Atmospheric Chemistry and Physics* 15, 5987–6005.
- 2542 Priestley, C. H. B. and R. J. Taylor (1972). On the Assessment of Surface
2543 Heat Flux and Evaporation Using Large-Scale Parameters. *Monthly Weather
2544 Review* 100(2), 81–92.
- 2545 Querejeta, J. I., I. Prieto, C. Armas, F. Casanoves, J. S. Diémé, M. Diouf,
2546 H. Yossi, B. Kaya, F. I. Pugnaire, and G. M. Rusch (2022). Higher leaf
2547 nitrogen content is linked to tighter stomatal regulation of transpiration
2548 and more efficient water use across dryland trees. *New Phytologist* 235(4),
2549 1351–1364.
- 2550 R Core Team (2021). R: A language and environment for statistical computing.
- 2551 Raich, J. W., D. A. Clark, L. Schwendenmann, and T. E. Wood (2014). Above-
2552 ground tree growth varies with belowground carbon allocation in a tropical
2553 rainforest environment. *PLoS ONE* 9(6), e100275.

- 2554 Rastetter, E. B., P. M. Vitousek, C. B. Field, G. R. Shaver, D. Herbert, and
2555 G. I. Ågren (2001). Resource optimization and symbiotic nitrogen fixation.
2556 *Ecosystems* 4(4), 369–388.
- 2557 Reich, P. B. (2014). The world-wide ‘fast-slow’ plant economics spectrum: a
2558 traits manifesto. *Journal of Ecology* 102(2), 275–301.
- 2559 Reich, P. B., S. E. Hobbie, T. Lee, D. S. Ellsworth, J. B. West, D. Tilman,
2560 J. M. H. Knops, S. Naeem, and J. Trost (2006). Nitrogen limitation con-
2561 strains sustainability of ecosystem response to CO₂. *Na-*
2562 *nature* 440(7086), 922–925.
- 2563 Rhine, E. D., R. L. Mulvaney, E. J. Pratt, and G. K. Sims (1998). Improving
2564 the Berthelot reaction for determining ammonium in soil extracts and water.
2565 *Soil Science Society of America Journal* 62(2), 473.
- 2566 Rogers, A. (2014). The use and misuse of V_{cmax} in Earth System Models. *Pho-*
2567 *tosynthesis Research* 119(1-2), 15–29.
- 2568 Rogers, A., B. E. Medlyn, J. S. Dukes, G. B. Bonan, S. Caemmerer, M. C.
2569 Dietze, J. Kattge, A. D. B. Leakey, L. M. Mercado, Ü. Niinemets, I. C.
2570 Prentice, S. P. Serbin, S. Sitch, D. A. Way, and S. Zaehle (2017). A roadmap
2571 for improving the representation of photosynthesis in Earth system models.
2572 *New Phytologist* 213(1), 22–42.
- 2573 Saathoff, A. J. and J. Welles (2021). Gas exchange measurements in the un-
2574 steady state. *Plant Cell and Environment* 44(11), 3509–3523.
- 2575 Saleh, A. M., M. Abdel-Mawgoud, A. R. Hassan, T. H. Habeeb, R. S. Yehia,
2576 and H. AbdElgawad (2020). Global metabolic changes induced by arbuscular

- 2577 mycorrhizal fungi in oregano plants grown under ambient and elevated levels
2578 of atmospheric CO₂. *Plant Physiology and Biochemistry* 151, 255–263.
- 2579 Saxton, K. E. and W. J. Rawls (2006). Soil water characteristic estimates by
2580 texture and organic matter for hydrologic solutions. *Soil Science Society of
2581 America Journal* 70(5), 1569–1578.
- 2582 Schaefer, K., C. R. Schwalm, C. Williams, M. A. Arain, A. Barr, J. M. Chen,
2583 K. J. Davis, D. Dimitrov, T. W. Hilton, D. Y. Hollinger, E. Humphreys,
2584 B. Poulter, B. M. Racza, A. D. Richardson, A. Sahoo, P. Thornton, R. Var-
2585 gas, H. Verbeeck, R. Anderson, I. Baker, T. A. Black, P. Bolstad, J. Chen,
2586 P. S. Curtis, A. R. Desai, M. C. Dietze, D. Dragoni, C. M. Gough, R. F.
2587 Grant, L. Gu, A. K. Jain, C. Kucharik, B. E. Law, S. Liu, E. Lokipitiya,
2588 H. A. Margolis, R. Matamala, J. H. McCaughey, R. Monson, J. W. Munger,
2589 W. Oechel, C. Peng, D. T. Price, D. Ricciuto, W. J. Riley, N. Roulet,
2590 H. Tian, C. Tonitto, M. Torn, E. Weng, and X. Zhou (2012). A model-
2591 data comparison of gross primary productivity: Results from the North
2592 American Carbon Program site synthesis. *Journal of Geophysical Research:
2593 Biogeosciences* 117(G3), G03010.
- 2594 Schneider, C. A., W. S. Rasband, and K. W. Eliceiri (2012). NIH Image to
2595 ImageJ: 25 years of image analysis. *Nature Methods* 9(7), 671–675.
- 2596 Scott, H. G. and N. G. Smith (2022). A Model of C4 Photosynthetic Acclimation
2597 Based on Least-Cost Optimality Theory Suitable for Earth System Model
2598 Incorporation. *Journal of Advances in Modeling Earth Systems* 14(3), 1–16.
- 2599 Shi, M., J. B. Fisher, E. R. Brzostek, and R. P. Phillips (2016). Carbon cost
2600 of plant nitrogen acquisition: Global carbon cycle impact from an improved

- 2601 plant nitrogen cycle in the Community Land Model. *Global Change Biology*
2602 22(3), 1299–1314.
- 2603 Shi, M., J. B. Fisher, R. P. Phillips, and E. R. Brzostek (2019). Neglecting
2604 plant–microbe symbioses leads to underestimation of modeled climate im-
2605 pacts. *Biogeosciences* 16(2), 457–465.
- 2606 Smith, N. G. and J. S. Dukes (2013). Plant respiration and photosynthesis in
2607 global-scale models: incorporating acclimation to temperature and CO₂.
2608 *Global Change Biology* 19(1), 45–63.
- 2609 Smith, N. G. and T. F. Keenan (2020). Mechanisms underlying leaf photosyn-
2610 thetic acclimation to warming and elevated CO₂ as inferred from least-cost
2611 optimality theory. *Global Change Biology* 26(9), 5202–5216.
- 2612 Smith, N. G., T. F. Keenan, I. C. Prentice, H. Wang, I. J. Wright, Ü. Niinemets,
2613 K. Y. Crous, T. F. Domingues, R. Guerrieri, F. oko Ishida, J. Kattge, E. L.
2614 Kruger, V. Maire, A. Rogers, S. P. Serbin, L. Tarvainen, H. F. Togashi,
2615 P. A. Townsend, M. Wang, L. K. Weerasinghe, and S.-X. Zhou (2019).
2616 Global photosynthetic capacity is optimized to the environment. *Ecology*
2617 *Letters* 22(3), 506–517.
- 2618 Smith, N. G., D. L. Lombardozzi, A. Tawfik, G. B. Bonan, and J. S. Dukes
2619 (2017). Biophysical consequences of photosynthetic temperature acclimation
2620 for climate. *Journal of Advances in Modeling Earth Systems* 9(1), 536–547.
- 2621 Smith, N. G., S. L. Malyshev, E. Shevliakova, J. Kattge, and J. S. Dukes
2622 (2016). Foliar temperature acclimation reduces simulated carbon sensitivity
2623 to climate. *Nature Climate Change* 6(4), 407–411.

- 2624** Smith, S. E. and D. J. Read (2008). *Mycorrhizal Symbiosis*. Academic Press.
- 2625** Soil Survey Staff (2022). Web Soil Survey.
- 2626** Soudzilovskaia, N. A., J. C. Douma, A. A. Akhmetzhanova, P. M. van Bodegom, W. K. Cornwell, E. J. Moens, K. K. Treseder, and J. H. C. Cornelissen
- 2627**
- 2628** (2015). Global patterns of plant root colonization intensity by mycorrhizal fungi explained by climate and soil chemistry. *Global Ecology and Biogeography* 24(3), 371–382.
- 2629**
- 2630**
- 2631** Stocker, B. D., H. Wang, N. G. Smith, S. P. Harrison, T. F. Keenan, D. Sandoval, T. Davis, and I. C. Prentice (2020). P-model v1.0: An optimality-based light use efficiency model for simulating ecosystem gross primary production. *Geoscientific Model Development* 13(3), 1545–1581.
- 2632**
- 2633**
- 2634**
- 2635** Stocker, B. D., J. Zscheischler, T. F. Keenan, I. C. Prentice, J. Peñuelas, and S. I. Seneviratne (2018). Quantifying soil moisture impacts on light use efficiency across biomes. *New Phytologist* 218(4), 1430–1449.
- 2636**
- 2637**
- 2638** Sulman, B. N., D. T. Roman, K. Yi, L. Wang, R. P. Phillips, and K. A.
- 2639** Novick (2016). High atmospheric demand for water can limit forest carbon uptake and transpiration as severely as dry soil. *Geophysical Research Letters* 43(18), 9686–9695.
- 2640**
- 2641**
- 2642** Sulman, B. N., E. Shevliakova, E. R. Brzostek, S. N. Kivlin, S. L. Malyshev,
- 2643** D. N. L. Menge, and X. Zhang (2019). Diverse mycorrhizal associations
- 2644** enhance terrestrial C storage in a global model. *Global Biogeochemical Cycles* 33(4), 501–523.
- 2645**
- 2646** Sweet, S. K., D. W. Wolfe, A. DeGaetano, and R. Benner (2017). Anatomy

- 2647 of the 2016 drought in the Northeastern United States: Implications for
2648 agriculture and water resources in humid climates. *Agricultural and Forest*
2649 *Meteorology* 247, 571–581.
- 2650 Taylor, B. N. and D. N. L. Menge (2018). Light regulates tropical symbiotic
2651 nitrogen fixation more strongly than soil nitrogen. *Nature Plants* 4(9), 655–
2652 661.
- 2653 Terrer, C., S. Vicca, B. A. Hungate, R. P. Phillips, and I. C. Prentice (2016).
2654 Mycorrhizal association as a primary control of the CO₂ fertilization effect.
2655 *Science* 353(6294), 72–74.
- 2656 Terrer, C., S. Vicca, B. D. Stocker, B. A. Hungate, R. P. Phillips, P. B. Reich,
2657 A. C. Finzi, and I. C. Prentice (2018). Ecosystem responses to elevated CO₂
2658 governed by plant–soil interactions and the cost of nitrogen acquisition. *New*
2659 *Phytologist* 217(2), 507–522.
- 2660 Thieurmel, B. and A. Elmarhraoui (2019). suncalc: Compute sun position,
2661 sunlight phases, moon position, and lunar phase.
- 2662 Thomas, R. Q., E. N. J. Brookshire, and S. Gerber (2015). Nitrogen limita-
2663 tion on land: how can it occur in Earth system models? *Global Change*
2664 *Biology* 21(5), 1777–1793.
- 2665 Thomas, R. Q., S. Zaehle, P. H. Templer, and C. L. Goodale (2013). Global pat-
2666 terns of nitrogen limitation: confronting two global biogeochemical models
2667 with observations. *Global Change Biology* 19(10), 2986–2998.
- 2668 Thornton, P. E., J.-F. Lamarque, N. A. Rosenbloom, and N. M. Mahowald
2669 (2007). Influence of carbon-nitrogen cycle coupling on land model response

- 2670 to CO₂ fertilization and climate variability. *Global Biogeochemical Cycles* 21(4), GB4018.
- 2671
- 2672 Tingey, D. T., D. L. Phillips, and M. G. Johnson (2000). Elevated CO₂ and
2673 conifer roots: effects on growth, life span and turnover. *New Phytologist*
2674 147(1), 87–103.
- 2675 Udvardi, M. and P. S. Poole (2013). Transport and metabolism in legume-
2676 rhizobia symbioses. *Annual Review of Plant Biology* 64, 781–805.
- 2677 USDA NRCS (2022). The PLANTS Database.
- 2678 Uselman, S. M., R. G. Qualls, and R. B. Thomas (2000). Effects of increased
2679 atmospheric CO₂, temperature, and soil N availability on root exudation of
2680 dissolved organic carbon by a N-fixing tree (*Robinia pseudoacacia* L.). *Plant
2681 and Soil* 222, 191–202.
- 2682 van Diepen, L. T. A., E. A. Lilleskov, K. S. Pregitzer, and R. M. Miller (2007).
2683 Decline of arbuscular mycorrhizal fungi in northern hardwood forests ex-
2684 posed to chronic nitrogen additions. *New Phytologist* 176(1), 175–183.
- 2685 Vance, C. P. and G. H. Heichel (1991). Carbon in N₂ fixation: Limitation or
2686 exquisite adaptation. *Annual Review of Plant Physiology and Plant Molec-
2687 ular Biology* 42(1), 373–392.
- 2688 Viet, H. D., J.-H. Kwak, K.-S. Lee, S.-S. Lim, M. Matsushima, S. X. Chang,
2689 K.-H. Lee, and W.-J. Choi (2013). Foliar chemistry and tree ring δ¹³C of
2690 *Pinus densiflora* in relation to tree growth along a soil pH gradient. *Plant
2691 and Soil* 363(1-2), 101–112.
- 2692 Vitousek, P. M., K. Cassman, C. C. Cleveland, T. Crews, C. B. Field, N. B.

- 2693** Grimm, R. W. Howarth, R. Marino, L. Martinelli, E. B. Rastetter, and
2694 J. I. Sprent (2002). Towards an ecological understanding of biological nitro-
2695 gen fixation. In *The Nitrogen Cycle at Regional to Global Scales*, pp. 1–45.
2696 Springer Netherlands.
- 2697** Vitousek, P. M. and R. W. Howarth (1991). Nitrogen limitation on land and in
2698 the sea: How can it occur? *Biogeochemistry* 13(2), 87–115.
- 2699** Vitousek, P. M., S. Porder, B. Z. Houlton, and O. A. Chadwick (2010).
2700 Terrestrial phosphorus limitation: mechanisms, implications, and nitro-
2701 gen–phosphorus interactions. *Ecological Applications* 20(1), 5–15.
- 2702** Walker, A. P., A. P. Beckerman, L. Gu, J. Kattge, L. A. Cernusak, T. F.
2703 Domingues, J. C. Scales, G. Wohlfahrt, S. D. Wullschleger, and F. I. Wood-
2704 ward (2014). The relationship of leaf photosynthetic traits - V_{cmax} and J_{max}
2705 - to leaf nitrogen, leaf phosphorus, and specific leaf area: a meta-analysis
2706 and modeling study. *Ecology and Evolution* 4(16), 3218–3235.
- 2707** Wang, H., I. C. Prentice, T. F. Keenan, T. W. Davis, I. J. Wright, W. K.
2708 Cornwell, B. J. Evans, and C. Peng (2017). Towards a universal model for
2709 carbon dioxide uptake by plants. *Nature Plants* 3(9), 734–741.
- 2710** Wang, W., Y. Wang, G. Hoch, Z. Wang, and J. Gu (2018). Linkage of root mor-
2711 phology to anatomy with increasing nitrogen availability in six temperate
2712 tree species. *Plant and Soil* 425(1-2), 189–200.
- 2713** Weatherburn, M. W. (1967). Phenol-hypochlorite reaction for determination of
2714 ammonia. *Analytical Chemistry* 39(8), 971–974.
- 2715** Wellburn, A. R. (1994). The spectral determination of chlorophylls a and b, as

- 2716** well as total carotenoids, using various solvents with spectrophotometers of
2717 different resolution. *Journal of Plant Physiology* 144(3), 307–313.
- 2718** Wen, Z., P. J. White, J. Shen, and H. Lambers (2022). Linking root exuda-
2719 tion to belowground economic traits for resource acquisition. *New Phytolo-*
2720 *gist* 233(4), 1620–1635.
- 2721** Westerband, A. C., I. J. Wright, V. Maire, J. Paillassa, I. C. Prentice, O. K.
2722 Atkin, K. J. Bloomfield, L. A. Cernusak, N. Dong, S. M. Gleason, C. Guil-
2723 herme Pereira, H. Lambers, M. R. Leishman, Y. Malhi, and R. H. Nolan
2724 (2023). Coordination of photosynthetic traits across soil and climate gradi-
2725 ents. *Global Change Biology* 29(3), 1–29.
- 2726** Wieder, W. R., C. C. Cleveland, W. K. Smith, and K. Todd-Brown (2015).
2727 Future productivity and carbon storage limited by terrestrial nutrient avail-
2728 ability. *Nature Geoscience* 8(6), 441–444.
- 2729** Wieder, W. R., D. M. Lawrence, R. A. Fisher, G. B. Bonan, S. J. Cheng, C. L.
2730 Goodale, A. S. Grandy, C. D. Koven, D. L. Lombardozzi, K. W. Oleson,
2731 and R. Q. Thomas (2019). Beyond static benchmarking: using experimental
2732 manipulations to evaluate land model assumptions. *Global Biogeochemical*
2733 *Cycles* 33(10), 1289–1309.
- 2734** Wright, I. J., P. B. Reich, and M. Westoby (2003). Least-cost input mixtures
2735 of water and nitrogen for photosynthesis. *The American Naturalist* 161(1),
2736 98–111.
- 2737** Wright, I. J., P. B. Reich, M. Westoby, D. D. Ackerly, Z. Baruch, F. Bongers,
2738 J. Cavender-Bares, T. Chapin, J. H. C. Cornelissen, M. Diemer, J. Flexas,
2739 E. Garnier, P. K. Groom, J. Gulias, K. Hikosaka, B. B. Lamont, T. Lee,

- 2740** W. Lee, C. Lusk, J. J. Midgley, M.-L. Navas, Ü. Niinemets, J. Oleksyn,
2741 N. Osada, H. Poorter, P. Poot, L. Prior, V. I. Pyankov, C. Roumet, S. C.
2742 Thomas, M. G. Tjoelker, E. J. Veneklaas, and R. Villar (2004). The world-
2743 wide leaf economics spectrum. *Nature* 428(6985), 821–827.
- 2744** Xu-Ri and I. C. Prentice (2017). Modelling the demand for new nitrogen fixation
2745 by terrestrial ecosystems. *Biogeosciences* 14(7), 2003–2017.
- 2746** Zaehle, S., B. E. Medlyn, M. G. De Kauwe, A. P. Walker, M. C. Dietze, T. Hick-
2747 ler, Y. Luo, Y. P. Wang, B. El-Masri, P. Thornton, A. Jain, S. Wang,
2748 D. Warlind, E. Weng, W. Parton, C. M. Iversen, A. Gallet-Budynek, H. Mc-
2749 carthy, A. C. Finzi, P. J. Hanson, I. C. Prentice, R. Oren, and R. J. Norby
2750 (2014). Evaluation of 11 terrestrial carbon-nitrogen cycle models against
2751 observations from two temperate Free-Air CO₂ Enrichment studies. *New*
2752 *Phytologist* 202(3), 803–822.
- 2753** Zaehle, S., S. Sitch, B. Smith, and F. Hatterman (2005). Effects of parame-
2754 ter uncertainties on the modeling of terrestrial biosphere dynamics. *Global*
2755 *Biogeochemical Cycles* 19(3), GB3020.
- 2756** Zhu, Q., W. J. Riley, J. Tang, N. Collier, F. M. Hoffman, X. Yang, and G. Bisht
2757 (2019). Representing nitrogen, phosphorus, and carbon interactions in the
2758 E3SM land model: development and global benchmarking. *Journal of Ad-*
2759 *vances in Modeling Earth Systems* 11(7), 2238–2258.
- 2760** Ziegler, C., M. E. Dusenge, B. Nyirambangutse, E. Zibera, G. Wallin, and
2761 J. Uddling (2020). Contrasting Dependencies of Photosynthetic Capacity
2762 on Leaf Nitrogen in Early- and Late-Successional Tropical Montane Tree
2763 Species. *Frontiers in Plant Science* 11, 1–12.

- 2764** Ziehn, T., J. Kattge, W. Knorr, and M. Scholze (2011). Improving the pre-
2765 dictability of global CO₂ assimilation rates under climate change. *Geophysical Research Letters* 38(10), L10404.
2766